UCLA
UCLA Electronic Theses and Dissertations

Title
Electrochemical Biosensing Techniques for Detection of NADH, Estradiol and Choline

Permalink
https://escholarship.org/uc/item/8th0c8tv

Author
FENG, LILI

Publication Date
2016

Peer reviewed|Thesis/dissertation

eScholarship.org Powered by the California Digital Library
University of California

UNIVERSITY OF CALIFORNIA

Los Angeles

Electrochemical Biosensing Techniques for Detection of NADH, Estradiol and Choline

A dissertation submitted in partial satisfaction of the

requirements for the degree of Doctor of Philosophy

in Chemical Engineering

by

Lili Feng

2016

© Copyright by

Lili Feng

2016

ABSTRACT OF THE DISSERTATION

Electrochemical Biosensing Techniques for Detection of NADH, Estradiol and Choline

by

Lili Feng

Doctor of Philosophy in Chemical Engineering

University of California, Los Angeles, 2016

Professor Harold G. Monbouquette, Chair

This thesis primarily focuses on optimizing electrode behavior for sensing NADH, estradiol and a metabolite of a common neurotransmitter, choline. NADH is a crucial coenzyme involved in cellular energy metabolism and is one of the products of enzyme-catalyzed oxidation of estradiol that is used in its sensing. The sensing of estradiol is important for the prediction and prevention of ovarian hyperstimulation syndrome. Most current electrooxidation methods for detection of NADH rely on glassy carbon electrodes so as to avoid the electrode fouling observed with platinum and other noble metal electrodes. The modification of platinum electrodes with an acid-treated, carbon nanotube film was applied in this work to eliminate the electrode fouling effect and to increase the electrode sensitivity. A detection limit as low as 0.17 μM and an average sensitivity of 370 mA M^{-1} cm^{-2} were achieved. Also, a reduced potential

could be used at the sensing electrode due to the electrocatalytic properties of the carbon nanotube coating, thus less interference from electroactive species in a sample was observed.

These promising NADH sensing results suggested the feasibility of an electrochemical enzyme-multiplied immunoassay technique (EMIT) for estradiol detection. EMIT is a fast and convenient homogeneous immunoassay technology that can be practiced without much of the bulky and expensive instrumentation and tedious washing steps associated with the competing ELISA approach. EMIT relies on antibody-induced inhibition of an analyte-labeled reporter enzyme. Free analyte in solution competes for binding antibody thereby reducing reporter enzyme inhibition and resulting in increased signal with increased analyte concentration. The reporter enzyme, glucose-6-phosphate dehydrogenase, catalyzes the oxidation of glucose-6-phosphate and transfer of electrons to the β-nicotinamide adenine dinucleotide (NAD^+) coenzyme to give NADH. The NADH produced has historically been detected spectrophotometrically, however our electrochemical NADH detection technology can also be used to follow reporter enzyme activity by constant potential amperometry. Electrochemical EMIT shows a linear logit-log range from 3 nM to 30 μM stradiol and exhibits a background signal that is about two times better than with spectrophotometric EMIT.

The second major project of this thesis research was focused on sensing an important neurochemical, choline, with a microbiosensor on a microelectrode array microprobe. Choline is produced in the brain when the neurotransmitter, acetylcholine, is rapidly hydrolyzed. In fact, choline may serve as an effective surrogate for acetylcholine since it is turned over so rapidly to choline and acetate. Thus, there is great interest among the neuroscience community in a sensitive and fast choline sensor for near real time *in vivo* recording. The choline biosensor fabrication process first entails the electropolymerization of a permselective

poly-m-phenylenediamine (PPD) film on the electrode surface to provide good selectivity against electroactive interferents, such as ascorbic acid (AA) and dopamine (DA). Subsequently, Nafion dip coating is performed to improve rejection of AA due to instability of the PPD film. However, the Nafion dip coating step can be omitted if the choline sensors are used in short term (i.e., acute) applications *in vivo* as opposed to chronic studies. Finally, choline oxidase is mixed with bovine serum albumin (BSA) and glutaraldehye (GAH) in aqueous solution to give the crosslinking mixture for enzyme immobilization on the coated microelectrodes. Twelve layers of this enzyme mixture are loaded manually on two of the four-microelectrode sites on a microprobe, and the other two sites are used as controls. A high sensitivity of 390 $\mu A \cdot mM^{-1} \cdot cm^{-2}$ with a corresponding detection limit of 0.16 μM was achieved, which is good enough for applications *in vivo*. The choline sensors fabricated with the PPD coating exhibited among the highest sensitivities and lowest detection limits described in the literature to date.

The incorporation of an on-probe iridum oxide (IrOx) reference electrode was also investigated to reduce the background noise and to eliminate the necessity of a separate reference electrode. However, reference electrode with only IrOx sometimes has an issue of sudden current drop and is not stable. Platinum black was employed to increase the effective electrode surface area, which improved the IrOx reference coating. A very high sensitivity of 440 $\mu A\ mM^{-1}\ cm^{-2}$ with a corresponding low detection limit of 0.04 μM was achieved with a linear range up to156 μM. However, platinum black plating solution has cytotoxic component lead, which is not good for the *in vivo* use. A novel nanomaterial called “platinum grass” (Pt-grass) was then used to replace platinum black as the reference electrode pre-coating material. A sensitivity of 310 $\mu A\ mM^{-1}\ cm^{-2}$ and detection limit 0.07 μM were gained, which are ideal for the *in vivo* purpose.

Pt-grass was also used in modifying working electrode to reduce overpotential. Because of the background noise brought by the rough surface of Pt-grass on working electrode, the sensitivity and detection limit were affected, which were 196 μA mM^{-1} cm^{-2} and 2 μM, respectively. However, the electrocatalytic properties of Pt-grass could enable an operation of the choline biosensor at a lower working potential of 0.45 V, 0.25 V lower than that typically used, which resulted in improved selectivity. The Pt-grass all-in-one sensor, with Pt-grass on both working and reference electrode, has a sensitivity of 123 μA mM^{-1} cm^{-2} and detection limit of 3 μM under an applied potential 0.35 V. The all-in-one choline sensors are also quite promising for the *in vivo* usage since it can both minimize the electrode size and reduce the overpotential.

The dissertation of Lili Feng is approved.

Yunfeng Lu

Kate Wassum

Harold G. Monbouquette, Chair

University of California, Los Angeles

2016

TABLE OF CONTENTS

Chapter 1: Introduction..... 1
1.1 Biosensor Overview..... 1
1.2 Electrochemical sensing of NADH, Estradiol, and choline..... 3
1.2.1 Motivation..... 3
1.2.2 NADH Biosensors..... 4
1.2.3 Estradiol Biosensors..... 5
1.2.4 Choline Biosensors..... 6
1.3 References..... 8
Chapter 2: Effective NADH sensing by electrooxidation on carbon-nanotube-coated platinum electrodes..... 14
2.1 Introduction..... 15
2.2 Experimental Setup..... 17
2.2.1 Materials..... 17
2.2.2 Instrumentation..... 18
2.2.3 Procedure..... 18
2.2.3.1 Preparation of CNT-coated electrodes..... 18
2.2.3.2 Electrochemical measurements..... 19
2.3 Results and Discussion..... 19
2.3.1 Electrooxidation of NADH on metallic, SWCNT-coated Pt disk electrodes..... 19
2.3.1.1 Acid treatment after CNT deposition improved coating uniformity..... 19
2.3.1.2 Metallic SWCNT coating reduced fouling and overpotential for NADH electrooxidation..... 20
2.3.1.3 Metallic SWCNT coating improved NADH electrode sensitivity and detection limit..... 23
2.3.2 Electrooxidation of NADH on MWCNT-coated Pt disk electrodes..... 25
2.3.2.1 Dispersion of MWCNT powder in DMF enables uniform coating on Pt electrodes..... 25
2.3.2.2 MWCNT coating decreases the overpotential for NADH electrooxidation..... 27
2.3.2.3 MWCNT coating improved NADH electrode sensitivity and detection limit..... 28
2.4 Conclusion..... 31
2.5 References..... 33
Chapter 3: Estradiol detection spectrophotometrically and electrochemically with EMIT technique..... 39
3.1 Introduction..... 40
3.2 Experimental Setup..... 43
3.2.1 Materials..... 43

3.2.2 Instrumentation..... 44
3.3 Results and Discussion..... 44
3.3.1 Estradiol detection with spectrophotometer..... 44
3.3.2 Estradiol detection with potentiostat..... 45
3.4 References..... 47
Chapter 4: Implantable Microprobe with Arrayed Microsensors for Amperometric Monitoring of Choline..... 49
4.1 Introduction..... 50
4.2 Experimental Setup..... 53
4.2.1 Materials..... 53
4.2.2 Instrumentation..... 54
4.2.3 Microprobe fabrication and sensor preparation..... 54
4.3 Results and discussion..... 56
4.3.1 Effect of concentrations of bovine serum albumin on choline sensor performance..... 56
4.3.2. Amperometric response of choline sensors at the Poly(m-PPD)/Nafion-modified platinum microelectrodes..... 59
4.3.2.1 Electrochemical polymerization of PPD on platinum microelectrodes..... 59
4.3.2.2 Effect of the PPD and Nafion coating sequence on electrochemical response of Choline..... 60
4.3.3 Amperometric response of choline sensors with deposited platinum black and an on-probe IrOx on reference electrode..... 64
4.3.3.1 Choline sensing using an on-probe IrOx reference electrode..... 64
4.3.3.2 Choline sensing for the Pt-black modified electrode followed by an on-probe IrOx on reference electrode..... 65
4.3.4. Evaluation of nanostructured platinum grass on performance of choline sensors...67
4.3.4.1 Comparing structures and components of Pt-grass and PtBLK..... 67
4.3.4.2 Choline sensing for the Pt-grass modified electrode followed by an on-probe IrOx on reference electrode..... 68
4.3.5 Selectivity against electroactive interferents 70
4.3.6 Preliminary *in vivo* results..... 70
4.4 Conclusion..... 73
4.5 References..... 74
Chapter 5: An implantable electroenzymatic choline microsensor by introducing nanostructured platinum grass.....78
5.1 Introduction..... 79
5.2 Experimental Setup..... 81
5.2.1 Materials..... 81
5.2.2 Instrumentation and electrochemical measurements..... 82
5.2.3 Electrode preparation..... 83
5.3 Results and Discussion..... 84

5.3.1 Surface morphologies of Pt nanograss and Pt black.....84
5.3.2 Pt grass utilized for working electrode and Ag/AgCl as reference electrode.....86
5.3.3 IrOx as reference electrode.....88
5.3.3 Effect of interferents.....89
5.4 Conclusions.....90
5.5 References.....91
Chapter 6: Rapid glutamate signaling at AMPA receptors in the Basolateral amygdala mediates the biasing effect of reward-predictive cues on decision-making.....93
6.1 Introduction.....94
6.2 Results.....96
6.2.1 Experiment 1.....96
6.2.2 BLA AMPA and NMDA glutamate receptor involvement in the selective invigorating influence of reward-predictive stimuli over reward-seeking actions.....96
6.2.3 Experiment 2.....99
6.2.4 BLA glutamate release during instrumental conditioning.....100
6.2.5 BLA glutamate release during Pavlovian-instrumental transfer.....104
6.3 Discussion.....111
6.4 Methods.....116
6.4.1 Subjects.....116
6.4.2 Apparatus.....116
6.4.3 Behavioral training and surgery.....117
6.4.4 Pavlovian training.....117
6.4.5 Instrumental training.....118
6.4.6 Experiment 1: Outcome-specific Pavlovian-instrumental transfer tests.....118
6.4.7 Drug administration.....119
6.4.8 Experiment 2: Electroenzymatic glutamate sensing.....120
6.4.9 Reagents.....120
6.4.10 Instrumentation.....121
6.4.11 *In vitro* biosensor characterization.....121
6.4.12 Online, near-real time glutamate detection during reward seeking.....122
6.4.13 Data analysis.....122
6.4.14 Behavioral analysis.....123
6.4.15 Neurochemical recording analysis.....124
6.4.16 Histology.....124
6.5 References.....127
Chapter 7: Recommendations for future work.....137
7.1 NADH sensing.....137
7.2 Estradiol sensing.....138
7.3 Enzyme stamp printing on microelectrode.....139

7.4 References.....140
Appendix A: Microprobe Fabrication Process Traveler..... 141
Appendix B: CNT Coatings Preparation on Disk Electrode..... 147
Appendix C: Ag/AgCl Wire Reference Electrode Preparation.....149
Appendix D: Estradiol ElectroEMIT Detection-Immunoassay Preparation and Electrochemical Measurement..... 150
Appendix E: Choline Microsensor Preparation..... 154
Appendix F: IrOx/ PtBLK / Pt Grass Deposition Solution Preparation..... 160
Appendix G: Noise filtering protocol for the VMP3 potentiostat..... 162

LIST OF FIGURES

Figure 2.1 (a) Scanning electron microscope (SEM) image of H2SO4/HNO3 acid mixturetreated, 6-layer metallic SWCNT film; (b) SEM image of acetic acid-treated, 6-layer metallic SWCNT film..... 20

Figure 2.2 Cyclic voltammograms conducted with (a) bare disk Pt electrode, and (b) 6-layer(0.06 µg/mm2) SWCNT-coated Pt disk electrode in 10 mM NADH (0.1 M PBS, pH 7.4) ata scan rate of 5 mV s−1.....22

Figure 2.3 Cyclic voltammograms conducted with a bare Pt disk electrode, and 6-layer (0.06 µg/mm2) and 10-layer (0.1 µg/mm2) metallic SWCNT-coated Pt disk electrodes in 10 mM NADH (0.1 M PBS, pH 7.4) at a scan rate of 5 mV s−1..... 23

Figure 2.4 Steady-state current at fixed potential vs. NADH concentration (in 0.1 M PBS, pH 7.4) for 6-layer (0.06 µg/mm2), 8-layer (0.08 µg/mm2), and 10-layer (0.1 µg/mm2) metallic SWCNT-coated Pt disk electrodes and a bare Pt disk electrode at 0.7 V vs. Ag/ AgCl. Inset shows amperometric responses at 0.7 V vs. Ag/AgCl of a 6-layer metallic SWCNT-coated Pt disk electrode and a bare Pt electrode in PBS (0.1 M, pH 7.4) upon successive increases in NADH concentration of 0.025 µM.....24

Figure 2.5 SEM images of deposits on Pt of (a)H2SO4/HNO3-treatedMWCNTs dissolved in water at 0.5mg/mL and sonicated for 1 h, (b)MWCNTs dissolved in DMF at 0.5 mg/mL and sonicated for 1 h, (c) MWCNTs dissolved in water at 0.5 mg/mL and sonicated for 1 h, and (d) – (f) the same preparations at higher magnification.....26

Figure 2.6 Cyclic voltammograms in 10 mM NADH (0.1 M PBS, pH 7.4) at a scan rate of 5 mV s−1 obtained with Pt disk electrodes with MWCNT surface concentrations of approximately 10 µg/mm2, 1 µg/mm2, 0.1 µg/mm2 and 0.01 µg/mm2 given the electrode surface area of 2 mm2..... 28

Figure 2.7 Steady-state current at fixed potential vs. NADH concentration (in 0.1 M PBS, pH 7.4) for 0.5 µg/mm2 MWCNT-coated Pt disk electrodes at 0.5 V vs. Ag/AgCl and a bare

Pt disk electrode at 0.7 V vs. Ag/AgCl. Inset shows amperometric responses at 0.5 V vs. Ag/AgCl of a MWCNT-coated Pt disk electrode and a bare Pt electrode in PBS (0.1 M, pH 7.4) at 0.5 V vs. Ag/AgCl upon successive increases in NADH concentration of 0.025 µM..... 29

Figure 2.8 Cyclic voltammograms in 10 mM NADH (0.1 M PBS, pH 7.4) at a scan rate of 5 mV s−1 obtained with Pt disk electrodes with a MWCNT (acid treated or untreated) surface concentration of 0.5 µg/mm2..... 31

Figure 3.1 The EMIT technique of estradiol detection with G6DPH as a reporter enzyme..... 42

Figure 3.2 Estradiol detection with spectrophotometer, absorbance vs. time..... 45

Figure 3.3 (A) Current versus time data as measured by constant potential amperometry using microelectrode at different estradiol concentrations including the fully repressed state with neither antibody nor estradiol and the fully unrepressed state with no estradiol. (B) Logit of NADH generation rate versus logarithm of estradiol concentration (in nM)..... 46

Figure 4.1 Schematic diagram of the microsensor configuration..... 56

Figure 4.2 Schematic diagram of the choline sensor configuration..... 58

Figure 4.3 Sensing of choline at a constant potential of 0.7 V (vs. Ag/AgCl) when the BSA concentration was 10 mg, 20mg, and 60 mg, sequentially. The microprobe was tested with AA (250 µM), Ch (20 µM, 40 µM, 60 µM), DA (5 µM), H2O2 (20 µM), choline (100 µM), and DA (15 µM), sequentially..... 59

Figure 4.4 Sensing of choline at a constant potential of 0.7 V (vs. Ag/AgCl) with choline microbiosensors modified with PPD only and choline oxidase, sequentially. The microprobe was tested with AA (250 µM), Ch (20 µM, 40 µM, 60 µM), DA (5 µM), H2O2 (20 µM), choline (100 µM), and DA (15 µM), sequentially..... 61

Figure 4.5 Sensing of choline at a constant potential of 0.7 V (vs. Ag/AgCl) with choline

microbiosensors modified with a PPD-Nafion membrane and choline oxidase, sequentially. The microprobe was tested with AA (250 µM), Ch (20 µM, 40 µM, 60 µM), DA (5 µM), H2O2 (20 µM), choline (100 µM), and DA (15 µM), sequentially..... 61

Figure 4.6 Sensing of choline at a constant potential of 0.7 V (vs. Ag/AgCl) with choline microbiosensors modified with a Nafion -PPD membrane and choline oxidase, sequentially. The microprobe was tested with AA (250 µM), Ch (20 µM, 40 µM, 60 µM), DA (5 µM), H2O2 (20 µM), choline (100 µM), and DA (15 µM), sequentially..... 62

Figure 4.7 On-probe IrOx reference glutamate sensor calibration figure. The microprobe was tested with AA, DA, and choline (5 times) sequentially..... 65

Figure 4.8 Schematic diagram of the on-probe Pt-black/IrOx RE choline sensor configuration..... 67

Figure 4.9 Choline sensing for the Pt-black modified electrode followed by an on-probe IrOx on reference electrode. The microprobe was tested with AA (250 µM), DA (5 µM), choline (20 µM, 40 µM, 60 µM), and H2O2 (20 µM), sequentially..... 67

Figure 4.10 Schematic diagram of the choline sensor configuration..... 69

Figure 4.11 Choline sensing for the Pt-grass modified electrode followed by an on-probe IrOx on reference electrode. The microprobe was tested with AA (250 µM), DA (5 µM), choline (20 µM, 40 µM, 60 µM, 80 µM, 100 µM), and H2O2 (20 µM), sequentially..... 69

Figure 4.12 *in vivo* anesthetized recording result of choline sensor with extra Ag/AgCl reference electrode. The red line indicates the current v.s. time on control site, while the green line indicates the one on choline sensing site.....71

Figure 4.13 *in vivo* anesthetized recording result of choline sensor with on-probe IrOx reference electrode. The red line indicates the current v.s. time on control site, while the green line indicates the one on choline sensing site.....72

Figure 4.14 *in vivo* background noise comparison between Ag/AgCl and IrOx reference electrode. The red line indicates the current v.s. time for Ag/AgCl, while the black line

indicates the one for IrOx..... 73

Figure 5.1 Schematic diagram of the choline sensor configuration. The left one is the choline working electrode coated with Pt nanograss, PPD, Nafion and enzyme layers. The right one is the IrOx reference electrode coated with Pt grass (10 times concentrated Pt nanograss solution was used), IrOx and Nafion..... 83

Figure 5.2 Scanning electron microscopic (SEM) images of (a) Top view of Pt/Pt-nanograss (1X), (b) Cross section view of Pt/Pt-nanograss (1X) (c) Angled top view of Pt/Pt-nanograss (10X), (d) Cross section view of Pt/Pt-nanograss (10X), and (e, f) Angled top view of Pt black..... 86

Figure 5.3 Current response of the choline biosensor to interferents, choline, and H2O2. The biosensor response at a constant potential of 0.45 V (vs. Ag/AgCl) was monitored in stirred solution upon sequential injections to give 12.5 µM DA, 5 µM Serotonin, 12.5 µM EP, 12.5 µM NEP, 0.8 mM Glucose, 50 µM DOPAC, 50 µM DOPA, 250 µM AA, followed by 20 µM, 40 µM and 60 µM of choline (Ch), and 20 µM of hydrogen peroxide (H2O2). Control site: red, Pt grass/PPD/Nafion/BSA; Choline sensor site: blue: Pt grass/PPD/Nafion/ChOx-BSA..... 87

Figure 5.4 A calibration curve for choline sensor (Ag/AgCl as external RE). The biosensor response at a constant potential of 0.45 V (vs. Ag/AgCl) was monitored in stirred solution upon sequential injections to give 10 µM, 20 µM, 30 µM, 40 µM, 50 µM and 60 µM.....88

Figure 5.5 A calibration curve for choline sensor (IrOx as on-probe RE). The biosensor response at a constant potential of 0.35 V (vs. IrOx) was monitored in stirred solution upon sequential injections to give 10 µM, 20 µM, 30 µM, 40 µM, 50 µM and 60 µM.....89

Figure 6.1 Effect of basolateral amygdala AMPA or NMDA receptor inactivation on Pavlovian-instrumental transfer. (A) Experimental procedure (see methods). CS, conditioned stimulus; O, outcome/reward; R, instrumental lever-press response; Ø, no reward delivery. During the PIT test both levers were available, but pressing was not reinforced and each CS was presented 4 times with intervening no-cue (Pre-CS) periods

serving as a control. During CS presentation actions on the lever that, during training, earned the same outcome as the cue predicted were considered 'same' presses, while actions on the other available lever were considered 'different' (Diff) presses. (B) Schematic representation of microinfusion injector tips. Numbers to the lower right of each section represent the anterior-posterior distance (mm) from bregma of the section. Line drawings of coronal sections are taken from [73]. (C,D) The Pavlovianinstrumental transfer effect; Lever-press rate (presses/min) averaged across levers during the control Pre-CS periods compared to pressing on lever that, in training, earned the same outcome as predicted by the CS (CS-Same) relative to pressing on the opposite lever (CS-Different) for the AMPA antagonist (C) or NMDA antagonist (D) group. Error bars +1 SEM. *p < 0.05,p < 0.01, ***p < 0.001..... 97**

Figure 6.2 Experiment 2 Design. (A) Schematic representation of the placement of the microelectrode array biosensor tips. Numbers to the lower right of each section represent the anterior-posterior distance (mm) from bregma of the section. (B) Testing procedures (see methods). CS, conditioned stimulus; O, outcome/reward; R, instrumental lever-press response; Ø, no reward delivery. During the PIT test both levers were available, but pressing was not reinforced and each CS was presented 4 times with intervening no-cue (Pre-CS) periods. During the CS presentation actions on the lever that, during training, earned the same outcome as the cue predicted were considered 'same' presses, while actions on the other lever were considered 'different' (Diff) presses. BLA glutamate concentration changes were continuously monitored with constant potential amperometry at glutamate biosensors during each test.....100

Figure 6.3 Basolateral amygdala glutamate release during instrumental conditioning. (A) Representative glutamate concentration v. time trace during instrumental conditioning. Instrumental session started with lever insertion at time 0 s. Red asterisks represent significant transient glutamate concentration fluctuations above baseline (transients). Behavioral events are marked above the trace. (B) BLA glutamate transients that reached threshold were counted and averaged for each rat across the 2-min pre-test baseline period and the instrumental (inst) test sessions. (C) Glutamate transient amplitude (µM) was calculated as the peak amplitude of the transient minus the baseline concentration (first

minima 0.5–5 s before the peak). (D) Lever press and food-port entry rate collapsed across the instrumental conditioning tests. (E) Betweensubject correlation between glutamate transient frequency (Transients/min) and lever-press rate (Presses/min). Each rat is represented twice, once for each instrumental test. (F) Glutamate concentration v. time trace around initiating lever presses (occurring at time 0 s) averaged across all initiating presses in the session for a representative subject. Shading reflects +1 SEM across trials. (G) The likelihood of a glutamate transient in 10, 1-s bins, evenly distributed around presses divided by initiating presses (first press after the collection of an earned reward or after a >6 s pause in pressing, excluding presses that occurred within a pressing bout) or all lever presses combined (including both initiating and intra-bout presses), averaged across the Two instrumental tests. The press occurs at time 0 s. Likelihood of a glutamate transient is defined as the percentage of presses (or initiating presses) that had a glutamate transient in the represented 1-s time bin. Asterisks represent significance relative to the control 1-s time bin, 5 s prior to the press. The raster plot shows the corresponding raw data with each subject represented on an individual line on the y-axis, tick marks represent the peak time of each significant glutamate transient surrounding initiating presses. Error bars +1 SEM.*p < 0.05, ***p < 0.001.....101

Figure 6.4 Basolateral amygdala glutamate release during Pavlovian-instrumental transfer. (A) Average glutamate concentration change (μM) during the 2-min conditioned stimulus (CS) presentation (beginning at time 0 s) and immediately preceding 2-min pre-CS period averaged across trials during the PIT test for each rat and then averaged across rats. Dashed lines represent the between-subjects +1 SEM. (B) Glutamate transients that reached threshold were counted and averaged for each rat across the 2-min pre-test baseline period, the 2- min pre-CS periods and the 2-min CS periods. (C) Glutamate transient the amplitude (μM) was calculated as the peak amplitude of the transient minus the baseline glutamate concentration. (D) Lever-press rate (Presses/min) averaged across levers during the control Pre-CS periods compared to pressing during CS presentation distinguished by whether it was on lever that, in training, earned the same outcome as predicted by the presented CS (CS-Same Actions) relative to pressing on the opposite lever (CS-Diff Actions). Main effect of CS: $F_{2,14} = 8.85$, $p = 0.003$. (E) Glutamate transient frequency (Transients/min) v. lever-press rate (Presses/min) betweensubjects correlation.

(F) Glutamate concentration v. time traces for the 5 s prior to and after initiating presses (occurring at time 0 s) during the CS averaged across all initiating presses for a representative subject. Shading reflects +1 SEM across trials. (G) The likelihood of a glutamate transient distributed in 1-s bins, 5 s prior to and after initiating presses (occurring at time 0 s; first press after a >6 s pause in pressing). Glutamate transient likelihood is defined as the percentage of initiating presses with a glutamate transient in the represented 1-s time bin. Asterisks represent significance relative to the first 1-s time bin. Raster plot displays corresponding raw data; each subject is represented on an individual line on the y-axis with tick color reflecting trial type. Tick marks represent the peak time of each glutamate transient that reached threshold surrounding initiating presses. Error bars +1 SEM. *p < 0.05, **p < 0.01, ***p < 0.001..... 105

Figure 6.5 Outcome specificity of basolateral amygdala glutamate release during Pavlovian-instrumental transfer. (A) Between-subjects correlation between glutamate transient frequency (Transients/min) and elevation [CS pressing/(CS + Pre-CS pressing)] v. response [CSSame/(CS-Same + CS-Different)] ratio. (B) Glutamate concentration v. time traces for the 5 prior to and after initiating presses (occurring at time 0 s) was averaged across all CS-Same initiating presses during the PIT test for the same representative subject as in 4F. Traces are divided by the type of outcome the action earned. Shading reflects the +1 SEM across trials. (C) The likelihood of a glutamate transient distributed in 1-s bins, 5 s prior to and after CS-Same initiating presses (occurring at time 0 s). Data are divided by the two CS-Same trial types. O1: Outcome 1 is defined as the outcome earned by the action that was exclusively (for 6/8 subjects) or preferentially (for 1/8 subjects) preceded by transient glutamate release. For the single subject in which he glutamate signal did not distinguish between outcome types outcome 1 was randomly assigned to the grain pellet outcome. Likelihood of a glutamate transient is defined as the percentage of initiating presses that had a glutamate transient in the represented 1-s time bin. Asterisks represent significance relative to the control 1-s time bin 5 s prior to the press. *p < 0.05, ***p < 0.001..... 109

LIST OF TABLES

Table 2.1 NADH sensing performance of Pt disk electrodes with varied SWCNT coatings at 0.7 V vs. Ag/AgCl..... 24

Table 2.2 NADH sensing performance at varied potential (vs. Ag/AgCl) of Pt disk electrodes with untreated MWCNT coating at 0.5 µg/mm^2..... 30

Table 3.1 The regression equations of different concentration of free estradiol assay..... 46

Table 4.1 Comparison of performance the PPD, PPD-Nafion, Nafion- PPD and OPPy-Nafion membranes deposited on choline sensors in terms of current responses of H2O2, choline, AA, and DA, response time, consistency, selectivity, and detection limit, respectively..... 63

Table 6.1 Pavlovian-instrumental transfer test lever pressing bouts. As in the instrumental conditioning test, rats organized their reward seeking in bouts of lever pressing during the PIT test. Because no rewards were delivered during this test an initiating press was defined as the first press after a pause in pressing of >6 s. Pressing bout information is presented in this table. Numbers represent average values, with values in italics below representing the between-subject SEM. During the PIT test rats showed significantly more lever-pressing bouts on the CS- Same action relative to both the CS-Different action and to the pre-CS period (*p < 0.05, in both cases; main effect of CS period F2,4 = 5.81, p = 0.01). Main effects for all other measures were non-significant..... 107

ACKNOWLEDGMENTS

It could be impossible for me to complete my Ph.D. work without the guidance and encouragement from many individuals. I really appreciate all of them.

First of all, I would like to give my greatest thankfulness and gratefulness to my Ph.D. advisor Professor Harold G. Monbouquette who provided me tremendous help during my five years Ph.D. life. I will never forget the first year of my Ph.D. when I could not communicate with others about research fluently in English and often felt awkward and embarrassing. He is the one who is always patient to listen to me and taught me some basic principles on whiteboard step by step in very slow pace. What's more, he always put forward some novel ideas to help develop my research and point out my mistakes directly which helped me avoid wasting a lot of time. He is very responsible for all his students and spent lot of time in helping students revising their papers and reports. He is a great mentor not only cares about my Ph.D. research but also cares about my future career path and offers me plenty of opportunities for my career development. From him, I learnt how to be a good person, to be nice to students, colleagues, to family members and others with a tolerable and generous heart. I will be grateful to his kindness forever.

I extend my gratitude to the other three professors in my dissertation committee. I would like to thank professor Kate Wassum who I worked with for over five years and also invited me to work at her lab during summer quarter 2016. She gave me a lot of guidance and encouragement when I got bad experiment results. She is patient to help me solve problems and troubleshoot various issues, as well as teaching me some new techniques. I would also like to thank professor Lu and professor Segura for their precious suggestions and valuable time. I

would like to acknowledge NIH funding R01NS087494 and UCLA graduate division for financially supporting me during past five years.

In addition, I would like to thank my senior and current labmates, as well as our collaborators. Dr Tina Tseng is my first supervisor ever since 2010 and she taught me every basic lab skills which is significant for my later Ph.D. research. Dr. Vanessa Tolosa provided me some useful protocols and helped me troubleshoot some tricky issues. Dr. Allison Yorita spent lots of her time in helping us fabricate wafers which saves me a lot of time in my own research. Bonhye Koo, Bo Wang, Brenda Huang, Mac Clay are also my dear labmates who always support me when I feel depressed and we all helped each other in our research. I like the lab environment we built which is harmonious and full of love. Xiaona Wen and Willy Li are two undergraduates who I worked with me during my Ph.D. time. They helped me with some experiments and contribute a lot to my papers. I would also thank my collaborators, all the Ph.D. students and postdocs from Wassum Lab and Nigel Lab, Dr. Huaping Li, Dr. Kosmos Galatsis for their help in my research.

Last but not least, I would like to give my thankfulness to my family and friends for their consistent support and love. Thanks to my Mom for her everyday call which help me go through the most difficult time. Thanks to my other family members who support me and care about me. Special thanks to my fiancé Tianwu Zang, a very smart physics PhD who faces every challenges together with me and always be my biggest support in my research and daily life. I am lucky to have him as my loyal family member, my best friend, my patient mentor in PhD career and my soul mate for the rest of my life.

Chapter 2 is a version of **L. Feng**, H. Li, K. Galatsis, H.G. Monbouquette, "Effective NADH Sensing by Electrooxidation on Carbon-Nanotube-Coated Platinum Electrodes", *Journal*

of Electroanalytical Chemistry, 773 (2016) 7–12. This work was supported by a subcontract to HM from Aneeve Nanotechnologies to fulfill work on DARPA contract no. HR0011-10-9-0003. Bonhye Koo helped in taking SEM figures and Willy Li helped in doing some of the experiments. Thanks to all of them.

Half of Chapter 3 is based on the work of Tina Tseng and May Chiu on the project "A convenient homogeneous enzyme immunoassay for estradiol detection", which had been published on Biotechnology and Applied Biochemistry, 2011. The other half of Chapter 3 was completed by Xiaona Wen and me. Xiaona helped me finish half of the experiments and data processing.

Chapter 4 is a version of the manuscript **L. Feng**, A. Collins, K.M. Wassum, H.G. Monbouquette, "Implantable Microprobe with Arrayed Microsensors for Amperometric Monitoring of Choline". I will acknowledge Xiaona Wen in helping prepare the manuscript and Annie Collins in helping with the recording in the anesthetized rat brain. The work is supported by NIH funding R01NS087494.

Chapter 5 is a version of the manuscript B. Wang †, **L. Feng** †, B. Koo, H.G. Monbouquette, "An electroenzymatic choline microsensor based on a nanostructured platinum microelectrode". Bo and I are equally in contributing in finishing this project. Thanks to Bo Wang for collaborating with me.

Chapter 6 is a version of Malvaez, M.; Greenfield, V. Y.; Wang, A. S.; Yorita, A. M.; **Feng, L**.; Linker, K. E.; Monbouquette, H. G.; Wassum, K. M. "Rapid glutamate sensing at AMPA receptors in the basolateral amygdala mediates the biasing effect of reward-predictive cues on decision-making," Sci. Rep. 2015, 5, 12511 doi:10.1038/srep12511.

M.M. did most of the experiments, analyzed the data, and wrote the manuscript. K.M.W. guided this project, analyzed the data and revised the manuscript. V.Y.G., K.E.L. and A.S.W. assisted with the experiments and data collection. M.M., A.M.Y. and **L.F.** prepared the glutamate biosensors which was used for the *in vivo* recording. H.G.M. designed the glutamate biosensors and revised the manuscript. All authors contributed to manuscript preparation.

VITA

2008-2010	Undergraduate Student Researcher Polymer Science and Engineering Sichuan University, China
2007-2011	Wu Yuzhang Honor College Sichuan University, China
2010	Visiting Student Material Science and Engineering National Cheng Kung University, Taiwan
2010-2011	Undergraduate Student Researcher Chemical and Biomolecular Engineering University of California, Los Angeles
2011	B.S., Polymer Science and Engineering Department Sichuan University, China
2011-2013	University Fellowship Recipient UCLA Graduate Division
2011-2016	Graduate Student Researcher Chemical and Biomolecular Engineering University of California, Los Angeles
2013-2016	Teaching Assistant Chemical and Biomolecular Engineering University of California, Los Angeles
2016	Technical Consulting Fellowship Recipient Calbiotech, Inc San Diego, CA

PUBLICATIONS AND PRESENTATIONS

L. Feng, H. Li, K. Galatsis, H.G. Monbouquette, "Effective NADH Sensing by Electrooxidation on Carbon-Nanotube-Coated Platinum Electrodes"*, Journal of Electroanalytical Chemistry*, 773 (2016) 7–12

L. Feng, A. Collins, K.M. Wassum, H.G. Monbouquette, "Implantable Microprobe with Arrayed Microsensors for Amperometric Monitoring of Choline". (In preparation)

B. Wang†, **L. Feng†**, B. Koo, H.G. Monbouquette, "An implantable electroenzymatic choline microsensor by introducing nanostructured platinum grass". (In preparation, † co-first authors)

M. Malvaez, V.Y. Greenfield, A. S.Wang, A. M. Yorita, **L. Feng**, K. Linker, H.G. Monbouquette, K.M. Wassum, "Basolateral amygdala rapid glutamate release encodes an outcome-specific representation vital for reward-predictive cues to selectively invigorate reward-seeking actions", *Scientific Reports* 5. 12511 (2015)

L. Feng, B. Wang, H.G. Monbouquette, "Micromachined multielectrode microprobes for choline sensing with an on-probe iridium oxide reference", *251st ACS National Meeting and Exposition*, 2016

L. Feng, H. Li, K. Galatsis, H.G. Monbouquette, "CNT Coated Platinum Electrodes for NADH sensing", *UCLA Engineering Tech Forum*, 2014

L. Feng, T. Tseng, V. Tolosa, H.G. Monbouquette, K.M. Wassum, "Implantable Microprobe with Microelectrode Array Sensors for Real-Time Monitoring of Glutamate and Dopamine", *UCLA Engineering Tech Forum*, 2013

L. Feng, T. Tseng, V. Tolosa, H.G. Monbouquette, K.M. Wassum, *"*On-probe IrOx Reference Electrode Biosensor for Glutamate Detection*", UCLA CSST Poster Presentation*, 2010

Chapter 1: Introduction

1.1 Biosensor Overview

A biosensor is a sensing device that utilizes a biological recognition element to bind an analyte and includes some transduction mechanism to convert this recognition event into a measurable signal [1]. Biosensing technologies driven by the requirements of disease diagnosis [2], food safety assessment[3], and environmental contamination[4] are used for identifying, monitoring, and controlling biological phenomena currently. Medical diagnostics incorporating biosensing technologies is one of the most intensely studied research topics in recent decades.

Among many current types of biosensor, four of them are commonly used for measuring the concentration of chemicals. In calorimetric biosensors[5], the concentration of a chemical (such as enzyme) is measured by the temperature change of an exothermic reaction. While it is the most generally applicable biosensor, the sensitivity of such biosensors is relatively low due to the difficulty of maintaining the temperature in the solution stream. In optical biosensors[6], a change in fluorescence or absorbance is used to measure the concentration of chemical reactants. The optical sensor can be used in catalytic or affinity reactions in living cells[7]. The third type of biosensor is called a potentiometric biosensor[8], which typically use ion-selective electrodes to detect the pH change in reactions that generate protons. Similar to potentiometric biosensors, amperometric biosensors[9] also transduce chemical signals to electrical signals. In this kind of biosensor, the amplitude of current is measured after a potential is applied at the sensing electrode. The biggest advantage of amperometric biosensors is that the electrochemical reactions at the electrode surface can be controlled by the applied potential.

In recent years, the rapid development of bio-MEMS technique enabled the detection of small amounts of chemicals on microchips[10]. Because the devices usually have small size (e.g., several hundreds of micrometers) and electrode materials can be made non-toxic, MEMS biosensors can be easily implanted into the living body to detect the chemical species *in vivo*[11]. Therefore, there are broad prospects to use MEMS-fabricated amperometric biosensors to perform real-time monitoring of important chemicals related to metabolic processes, even diseases.

The working mechanism of amperometric biosensors is based on electrochemical principles. In three-electrode experiments[12], the working electrode (WE) is the electrode where the chemical reaction happens. For example, the oxidation reaction of NADH happens on the platinum WE with according to the following reaction

$$\mathrm{NADH} \rightarrow \mathrm{NAD^+} + \mathrm{H^+} + 2e^-$$

The reference electrode (RE) is the electrode with a well-known, stable, and fixed potential. RE is used for precise control of WE potential based on the potential difference between RE and WE. For example, the reaction of Ag/AgCl reference is as follows.

$$\mathrm{Ag^+} + \mathrm{Cl^+} \leftrightarrow \mathrm{AgCl_{(s)}} + \mathrm{e^-}$$

The standard potential of Ag/AgCl electrode against SHE is 0.230V$\pm$10mV. The counter electrode (CE), usually made of platinum, is to balance the charge and form an electrical circuit. Compared to two-electrode system where CE and RE is the same electrode[13], the potential control in three-electrode system is more stable unless the current density at the RE is very small in a two-electrode system. Thus, two-electrode system are used most commonly with very small WEs where the currents are very low.

1.2 Electrochemical sensing of NADH, Estradiol, and choline

1.2.1 Motivation

NADH is an important coenzyme that widely exists in the human body, with the major role of accepting and donating electrons in cellular respiration[14]. For example, NADH serves as a donor of ADP-ribose moieties in ADP-ribosylation reactions and a precursor of cyclic-ADP-ribose in redox reactions[15]. The sensing of NADH concentration in living cells not only is crucial for understanding certain metabolic processes, but also has shown some potential in the treatment of several diseases such as Alzheimer's and Parkinson disease[16]. Real-time monitoring of NADH can greatly help design drugs such as enzyme inhibitors and activators, and in particular, it would greatly benefit the sensing of estradiol as NADH is one of the products of the enzyme catalyzed oxidation in estradiol detection. Therefore, it is desirable to develop robust detection methods for NADH.

Efficient detection of estradiol has been one of the major interests and a long-term goal in the field of biosensing. With the increasing demand of infertility services and rapid development of assisted reproductive techniques (ART) in the past decades, the risk of ovarian hyperstimulation syndrome (OHSS)[17] should also be taken seriously. OHSS, with symptoms of obvious multiple follicular enlargement, hemoconcentration, and intravascular volume depletion, is usually associated with assisted reproductive techniques (ARTs)[18]. It has been observed that nearly all the at-risk patients have elevated estradiol levels[19]. Most patients who develop OHSS have an estradiol level above 11 nM as compared with 6 nM for normal patients on the 11th day of ovarian stimulation[20]. Therefore, biosensing the concentration of estradiol of the patients will help in predicting and preventing of OHSS.

As a biosynthetic precursor of the neurotransmitter, acetylcholine (ACh), and a product of the rapid hydrolysis of ACh in the brain, choline is an important physiological component related to the learning and memory formation in the central nervous system[21]. A variety of neurological and psychological behaviors, such as addiction, as well as lots of neurological and psychiatric disorders, such as Parkinson disease and epilepsy, can be studied using biosensors to detect the concentration change of neurotransmitters under stimulation. It is also reported that choline acetyltransferase activity is essential to understanding the behavior of Alzheimer's disease and Parkinson's disease[22], as abnormal release of neurotransmitters plays a vital role in causing these diseases. Accordingly, real-time detection of choline, particularly as a surrogate for ACh, in living systems will definitely contribute to understanding the etiology of mental diseases.

The thesis focuses on novel techniques for NADH, estradiol, and choline sensing with platinum disk electrodes and microsensors fabricated by MEMS techniques. In Chapter 2, NADH sensing with platinum disk electrodes with high sensitivity and low detection limit are developed. In Chapter 3, estradiol sensing with enzyme-multiplied immunoassay technique (EMIT) is used for fast and accurate detection. Chapters 4 and 5 are about choline sensing. In Chapter 4, an implantable microprobe with arrayed microsensors with ChOx WE and IrOx RE are introduced with optimized sensitivity, selectivity and detection limit. In Chapter 5, high performance microsensors with nanostructured platinum grass are developed for non-toxic, biocompatible choline sensing *in vivo*.

1.2.2 NADH Biosensors

As mentioned before, the electrochemical oxidation reaction on a working electrode for NADH sensing is:

$$NADH \rightarrow NAD^+ + H^+ + 2e^-.$$

Currently, the biggest challenge for effectively sensing NADH is the high overpotential at bare, untreated or unmodified classical solid electrodes[23]. The common solution to this problem is to add nanostructured carbon materials such as pyrolytic graphite[24], carbon nanofibers[25] or carbon microparticles[26] for reducing the overpotential. Over the years, carbon-nanotube-modified glassy carbon electrode (GCE) is widely used as the working electrode of a NADH sensor[27]. As a nanomaterial with excellent electron transfer properties, carbon nanotube (CNT) can be coated onto the electrode and significantly decrease the overpotential of electrochemical reactions. M. Wooten and W. Gorski have reported an overpotential of 0.4 V and detection limit of 4.0 μM and 2.0 μM, respectively, for boiled CNTs in water and microwaved CNTs in concentrated nitric acid on glassy carbon electrode for NADH sensing[28].

On the other hand, the progress of using noble metal electrodes as WE in NADH sensing is quite slow since the 1980s, due to high overpotential of the NADH•+/NADH couple. In addition, the fouling effect[29] on platinum electrode also reduces the lifetime of NADH sensor. The usage of CNT coating technique might provide the possibility of using metal electrodes, such as platinum, to sense NADH. Compared with glassy carbon, Pt-based sensors usually have much higher sensitivity, as demonstrated in other systems such as glutamate sensing[30]. Therefore, Pt-based sensors are expected to be the next generation NADH sensor if the fouling effect and high overpotential issues are overcome.

1.2.3 Estradiol Biosensors

While optical sensing of estradiol has been developed for years, it is desirable to have more portable and less expensive sensors for the fast detection of estradiol. Enzyme-multiplied immunoassay technique (EMIT)[31, 32] is an immunoassay approach where the key component is a reporter enzyme responsible for signal generation. EMIT relies on antibody-induced inhibition of the reporter enzyme conjugated to analyte. EMIT was first invented by Svya Company in 1973 for the detection of morphine[32]. Nowadays, it has become a widely used technique in research institutes, hospitals and clinic labs for the quantification of drugs and other small molecules in urine and serum. The advantages of EMIT include the fact that it is a homogeneous assay unlike ELISA, low detection limits, simple protocols and rapid assay time.

1.2.4 Choline Biosensors

The electrochemical method is the mainstream approach for choline sensing because of the small size and high sensitivity of electrodes. Although various methods such as liquid chromatography [33], enzymatic-spectrophotometric method [34], chemiluminescence [35], and electrochemiluminescence [36] have been developed for the choline determination, investigation of amperometric choline oxidase (ChOx)-based biosensors is of particular interest because of its high sensitivity, rapid response, low detection limit, and low cost [37]. In the ChOx-based biosensors, the enzymatic conversion of choline to betaine aldehyde by choline oxidase (ChOx) produces hydrogen peroxide (H_2O_2) that can be detected electrochemically. Chemical reactions on the working electrode are shown as follows:

$$\text{Choline} + 2O_2 \xrightarrow{\text{ChOx}} \text{Betaine} + 2H_2O_2 \quad (1)$$

$$2H_2O_2 \rightarrow 2O_2 + 4H^+ + 4e^- \quad (2)$$

While the ChOx electrode is very efficient in sensing choline *in vitro*, there are several problems in using unmodified electrodes *in vivo*. First, amperometric signals arising from oxidation of the endogenous electroactive biogenic amines and interferents such as ascorbic acid (AA) in brain extracellular fluid (ECF) can affect H_2O_2 oxidation. Without the elimination of AA, the choline sensors would lose their selectivity. Second, while iridium oxide (IrOx) is a stable and biocompatible material for a reference electrode[38], the linear range for choline detection using an IrOx on polished platinum RE in two-electrode mode is limited due to the instability of this IrOx potential at even modest current levels. Therefore, a material called platinum black (Pt-black) with a rough surface is used to increase the IrOx deposition on electrode surface and the linear range of choline sensors[39]. Nevertheless, the preparation of Pt-black involves the use of the toxic heavy metal, lead, and is toxic to living body. This hinders the usage of Pt-black-based electrode in *in vivo* experiments.

We will focus on addressing the above issues in this thesis. On one hand, several modifications are introduced to eliminate interfering signals caused by non-choline chemicals in brain extracellular fluid. Nafion is used to exclude AA and polypyrrole (PP) films are used to exclude dopamine (DA). On the other hand, a non-toxic nanomaterial, called Pt-grass[40], is used to replace Pt-black on IrOx reference electrode. It is demonstrated that our microsensors have higher sensitivity and lower detection limit than previous work. The details of choline sensing protocols will be discussed in Chapter 4 & 5.

1.3 References

[1] T. Anthony,W George, K Isao. (1987) Biosensors: Fundamentals and Applications, Oxford, UK: Oxford University Press. pp. 770.

[2] M.L. Sin, K. E. Mach, P.K. Wong, and J.C. Liao. (2014) Advances and challenges in biosensor-based diagnosis of infectious diseases, *Expert Rev Mol Diagn*., vol. 14(2): 225–244.

[3] M. S. Thakur and K. V. Ragavan. (2013) Biosensors in food processing, *J Food Sci Technol.*, vol. 50(4): 625–641.

[4] J. Wang, et al. (1997) DNA electrochemical biosensors for environmental monitoring. A review, *Anaytica Chimica Acta,* vol. 347, pp. 1-8.

[5] B. Danielsson, U. Hedberg, M. Rank, B. Xie. (1992) Recent investigations on calorimetric biosensors, *Sensors und Actuators B,* vol. 6, pp. 138-142.

[6] A.J. Haes and R.P. Van Duyne. (2002) A Nanoscale Optical Biosensor: Sensitivity and Selectivity of an Approach Based on the Localized Surface Plasmon Resonance Spectroscopy of Triangular Silver Nanoparticles, *J. Am. Chem. Soc.*, vol. 124 (35), pp. 10596–10604.

[7] X. Gao, G. Tang, X. Su. (2012) Optical detection of organophosphorus compounds based on Mn-doped ZnSe d-dot enzymatic catalytic sensor, *Biosensors and Bioelectronics*, vol. 36-1, pp. 75–80.

[8] A.A. Karyakin, O. A. Bobrova, L.V. Lukachova, E.E. Karyakina. (1996) Potentiometric biosensors based on polyaniline semiconductor films*, Sensors and Actuators B:Chemical*, vol. 33(1–3), pp. 34-38.

[9] B.A. Gregg, A. Heller. (1990) Cross-linked redox gels containing glucose oxidase for amperometric biosensor applications, *Anal. Chem.,* vol. 62 (3), pp. 258–263.

[10] R. Bashir. (2004) BioMEMS: state-of-the-art in detection, opportunities and prospects, *Advanced Drug Delivery Reviews,* vol. 56(11), pp. 1565–1586.

[11] A.C.R. GRAYSON et al. (2004) A BioMEMS review: MEMS technology for physiologically integrated devices, *Proceedings of the IEEE*, vol. 92(1).

[12] A.J. Bard, L.R. Faulkner. (2000) Electrochemical Methods: Fundamentals and Applications (2 ed.). Wiley. ISBN 0-471-04372-9.

[13] P. Wang et al. (2008) Ag@AgCl: A Highly Efficient and Stable Photocatalyst Active under Visible Light, *Angewandte Chemie International Edition*, vol. 47(41), pp. 7931–7933.

[14] D.H. Williamson, P. Lund, H.A. Krebs (1967) The redox state of free nicotinamide-adenine dinucleotide in the cytoplasm and mitochondria of rat liver, *Biochem. J.* , vol. 103 (2): 514–27.

[15] A.H. Guse. (2004) Biochemistry, biology, and pharmacology of cyclic adenosine diphosphoribose (cADPR), *Curr. Med. Chem.,* vol. 11 (7): 847–55

[16] P. Belenky, K.L. Bogan, C. Brenner. (2007), NAD^+ metabolism in health and disease, *Trends Biochem. Sci.,* vol.32 (1): 12–9.

[17] D. Shmorgun, P. Claman (2011) The diagnosis and management of ovarian hyperstimulation syndrome, *Journal of Obstetrics and Gynaecology*, vol. 33 (11): 1156–62.

[18] Abma, J., Chandra, A., Mosher, W., Peterson, L., and Piccinino, L. (1997) Fertility, family planning, and women's health: New data from the 1995 National Survey of Family Growth. National Center for Health Statistics.*Vital Health Stat.,* vol. 23, 6–7. Forman, R. G., Frydman, R., Egan, D., Ross, C., and Barlow, D. H. (1990) *Fertil. Steril.,* vol.53, 502–509, Rabau, E., David, A., Serr, D. M.,Mashiach, S., and Lunenfeld, B. (1967) *Am. J. Obstet. Gynecol*., vol. 98, pp. 92–98.

[19] Haning, R. V. J., Austin, C. W., Carlson, I. H., Kuzma, D. L., Shapiro, S. S., and Zweibel, W. J. (1983) *Fertil. Steril.,* vol. 40, 31–36. Navot, D., Reclou, A., Birkenfeld, A., Rabinowitz, R., Brzezinski, A., and Margalioth, E. J. (1988) *Am. J. Obstet. Gynecol.*, vol. 159, pp. 210–215.

[20] D'Angelo, A., Davies, R., Salah, E., Nix, B. A., and Amso, N. N. (2004) *Fertil. Steril.,* vol. 81, pp. 332–336.

[21] L.M. Fischer, K.A. da Costa, L. Kwock; J. Galanko, S.H. Zeisel (2010) Dietary choline requirements of women: effects of estrogen and genetic variation, *American Journal of Clinical Nutrition.*, vol. 92 (5): 1113–1119.

[22] A.H. Van Beek, J.A. Claassen (2010) The cerebrovascular role of the cholinergic neural system in Alzheimer's disease, *Behavioural Brain Research*, vol. 221 (2): 537–542.

[23] H. Jaegfeldt. (1980) *J. Electroanal. Chem.*, vol. 110, pp. 295. J. Moiroux, P. J. Elving. (1978) *Anal. Chem.,* vol. 50, pp. 1056.

[24] R. R. Moore, C. E. Banks, R. G. Compton, (2004) *Anal. Chem.*, vol. 76, pp. 2677.

[25] L. N. Wu, X. J. Zhang, H. X. Ju. (2007) *Anal.Chem.*,vol. 79, pp. 453. A. Arvinte, F. Valentini, A. Radoi, F. Arduini, E. Tamburri, L. Rotariu, G. Palleschi, C. Bala. (2007) *Electroanalysis*, vol. 19, pp. 1455.

[26] B. Pérez, M. del Valle, S. Alegret, A. Merkoçi, (2007) *Talanta*, vol.74, pp. 398.

[27] M. Musameh, J. Wang, A. Merkoci, Y. Lin, (2002) Low-potential stable NADH detection at carbon-nanotube-modified glassy carbon electrodes, (2002) *Electrochemistry Communications,* vol. 4(10), pp. 743–746.

[28] M. Wooten and W. Gorski. (2010) Facilitation of NADH Electro-oxidation at Treated Carbon Nanotubes, *Anal. Chem.*, vol. 82 (4), pp. 1299–1304.

[29] D.P. Manica , Y. Mitsumori and A.G. Ewing. (2003) Characterization of Electrode Fouling and Surface Regeneration for a Platinum Electrode on an Electrophoresis Microchip, *Anal. Chem.*, vol. 75 (17), pp. 4572–4577.

[30] R.D. O'Neill, S.C Chang, J.P. Lowry, C.J. McNeil. (2004) Comparisons of platinum, gold, palladium and glassy carbon as electrode materials in the design of biosensors for glutamate, *Biosensors and Bioelectronics*, vol. 19(11), pp. 1521–1528.

[31] E. Engvall. (1980) Enzyme immunoassay ELISA and EMIT, *Methods in Enzymology,* vol. 70, pp. 419–439.

[32] S. J. Mulé, M. L. Bastos, D. Jukofsky, (1974) Evaluation of Immunoassay Methods for Detection, in Urine, of Drugs Subject to Abuse, *Clin. Chem.*, vol. 20(2), pp. 243-248.

[33] Li, J., and El Rassi, Z. (2002) High Performance Liquid Chromatography of Phenolic Choline Ester Fragments Derived by Chemical and Enzymatic Fragmentation Processes:

Analysis of Sinapine in Rape Seed, *Journal of Agricultural and Food Chemistry*, vol. 50, pp. 1368-1373.

[34] Campanella, L., Tomassetti, M., and Sammartino, M. P. (1988) Enzyme sensor for the determination of choline-containing phospholipids in some biological fluids, *Analyst*, vol. 113, pp. 77-80.

[35] Tsafack, V. C., Marquette, C. A., Pizzolato, F., and J. Blum, L.C. (2000) Chemiluminescent choline biosensor using histidine-modified peroxidase immobilised on metal-chelate substituted beads and choline oxidase immobilised on anion-exchanger beads co-entrapped in a photocrosslinkable polymer, *Biosensors and Bioelectronics*, vol. 15, pp. 125-133.

[36] Leca-Bouvier, B. D., Sassolas, A., and Blum, L. J. (2014) Polyluminol/hydrogel composites as new electrochemiluminescent-active sensing layers, *Analytical and Bioanalytical Chemistry*, vol 406, pp. 5657-5667.

[37] Zhang, H., Yin, Y., Wu, P., and Cai, C. (2012) Indirect electrocatalytic determination of choline by monitoring hydrogen peroxide at the choline oxidase-prussian blue modified iron phosphate nanostructures, *Biosens. Bioelectron*., vol. 31, pp. 244-250.

[38] H. Yang, S.K. Kang, C.A. Choi, H. Kim, D.H. Shin, Y.S. Kim and Y.T. Kim. (2004) An iridium oxide reference electrode for use in microfabricated biosensors and biochips, *Lab on Chip*, vol. 4, pp. 42-46.

[39] H.K. Seo, D.J. Park, J.Y. Park, (2008) Fabrication and characterization of platinum black and mesoporous platinum electrodes for in-vivo and continuously monitoring electrochemical sensor applications, *Thin Solid Films*, vols 516(16), pp.5227–5230. K. W. Johnson, (1991) Reproducible electrodeposition of biomolecules for the fabrication of

miniature electroenzymatic biosensors, *Sensors and Actuators B: Chemical*, vol. 5(1–4), pp. 85-89.

[40] C. Boehler, T. Stieglitz, M. Asplund, (2015) Nanostructured platinum grass enables superior impedance reduction for neural microelectrodes, *Biomaterials*, vol. 67, pp. 346–353.

Chapter 2: Effective NADH sensing by electrooxidation on carbon-nanotube-coated platinum electrodes

Abstract

Coatings of carbon nanotubes (CNTs) on conventional Pt electrodes enable sensing of NADH by fixed-potential amperometry without fouling and with high sensitivity and low detection limit. Effective electrochemical oxidation of NADH has been pursued aggressively for many years due to the utility of NAD+-dependent dehydrogenases in sensing, diagnostics, and chemical synthesis. Pt electrodes have not been explored for electrochemical NADH sensing in recent years due to reported problems with fouling. In this work, acid-treated, metallic, single-wall carbon nanotubes (SWCNTs) and untreated multiwall carbon nanotubes (MWCNTs) were explored as coatings for Pt disk electrodes to reduce fouling and to enhance electrochemical detection of NADH. The electrodes with CNT coatings were characterized by scanning electron microscopy (SEM), cyclic voltammetry (CV) and fixed-potential amperometry. A detection limit as low as 0.17μM was observed with the SWCNT coating at 0.7V (vs. Ag/AgCl) and 0.19μM with the MWCNTs at 0.5V. Average sensitivities of both preparations were ~ 370 mA M^{-1} cm^{-2}. However, similar results were obtained with the MWCNT-coated electrodes at the much reduced potential of 0.3V, which suggests a significant advantage of the MWCNT preparation that is worthy of further investigation. This study demonstrates the utility of relatively inert, conventional Pt electrodes with a simple CNT coating for effective NADH sensing at reduced potential without fouling.

2.1 Introduction

The efficient electrochemical oxidation of NADH has been pursued for decades due to the role of NAD+ as coenzyme and charge carrier or many dehydrogenase-catalyzed reactions important for organic chemical synthesis, diagnostics, and electroenzymatic sensing [1–12]. For example, NAD+ regeneration generally is required for the synthetically useful, dehydrogenase-catalyzed oxidations of alcohols, aldehydes, and acids [10,13–15]. Although schemes have been employed for enzymatic regeneration of NAD+ to support the synthetic reaction, such strategies obviously require additional reagents that add expense [13]. Dehydrogenases also are useful for electroenzymatic sensing of, for example, certain sugars, alcohols and amino acids [1,12,15–18]; yet for most such sensor designs, efficient electrooxidation of the NADH produced by the dehydrogenase-catalyzed oxidation of the analyte is necessary to give the desired current signal. Thus, a strong driving force has persisted for simple and efficient electrooxidation of NADH to NAD+.

Unfortunately electrochemical oxidation of NADH commonly occurs only at high overpotentials on conventional electrodes due to the high potential of the NADH•+/NADH couple, which makes this step rate limiting for the overall electrooxidation reaction [10]. Although the dimerization of the intermediate radical species has been reported, it is readily oxidized yielding enzymatically active NAD+ [10]. However, NAD+ itself can adsorb to glassy carbon electrode surfaces thereby hindering electron transfer [3,15]. Also, the required high overpotentials frequently lead to undesired side reactions, which can be reflected in reduced sensor selectivity and can result in electrode fouling. Electrode fouling diminishes the efficiency of NADH electrooxidation and leads to lower sensitivity, reproducibility and stability of dehydrogenase based biosensors [15,19]. Thus, there is a need for electrode constructs for

NADH electrooxidation at low overpotentials that also show resistance to fouling. One approach to ameliorate this problem is to increase electrode surface area, and mesoporous carbon coatings, nanoporous metals and films of graphene sheets, for example, have been explored for this purpose [18,20,21].

In more direct attempts to reduce overpotentials and fouling, a general preference for carbon electrodes has emerged; and electron transfer mediators, such as quinone [22,23], diamines [24], ferrocene [25], phenazine [26] and L-glutamate [27] derivatives, have been widely investigated. Such mediators may be present free in solution or may be immobilized on the electrode surface by various means. Among the many mediator chemistries explored, quinones and diaminobenzenes that facilitate NADH oxidation via hydride or hydrogen atom transferhave exhibited appealing kinetics at relatively low overpotentials [8,28]. Although some impressive NADH electrooxidation results have been obtained with these mediators, low stability remains a common problem and immobilization processes can be cumbersome. In this regard, modification of carbon electrodes with other materials such as conducting polymers and carbon nanotubes [29], which also can mediate electron transfer, has shown promise.

Members of the sp2 carbon family, carbon nanotubes (CNTs) exhibit a special sidewall curvature and possess a π-conjugated structure with a hydrophobic surface [30]. Importantly, CNTs can exhibit high electrical conductivity and chemical stability [29,30]. Further, evidence has emerged that CNTs with oxygenated functional groups on the exterior sidewall and/or on the ends give improved performance as an electrode modifier for electron transfer to redox species in solution [31]. Introduction of defect sites and oxygenated species on the CNT surface, including quinone species, may be accomplished by a variety of means including boiling in water, strong acid treatment, and electrochemical oxidation [31–33]. Similar to observations with lower

molecular weight quinone mediators mentioned above, glassy carbon electrodes, coated with treated CNTs, exhibited sensitive, relatively low-potential amperometric detection of NADH [32,33].

Due to the fouling and high overpotential issues associated with noble metal electrodes [3], publications describing the use of such electrodes for NADH sensing have been relatively rare since the 1980s.Most investigators use a carbon electrode as the basis for their sensors as described above. However, we hypothesized that coatings of CNT preparations on Pt might provide a simple and efficient route to effective NADH-sensing electrodes. In particular, we surmised that CNT coatings on Pt would lower the potential for NADH oxidation and reduce fouling as compared to bare Pt. Recent success with CNT-coated gold electrodes for NADH sensing supported pursuit of our study [34–37].

2.2 Experimental Setup

2.2.1 Materials

Single-walled, metallic carbon nanotubes (SWCNTs) of 1.2–1.7 nm in diameter and 0.3–5 μm in length (IsoNanotube-M) were purchased from NanoIntegris, Inc. These SWCNTs were obtained as solutions in purified water with a proprietary combination of ionic surfactants and some iodixanol, a non-ionic, water-soluble iodine derivative. Multiwalled carbon nanotube (MWCNT) powder of 95% purity, consisting of nanotubes 11 nm in diameter and 10 μm in length, were obtained from Cnano, Inc. (FloTube™ 9000). N,N-dimethylformamide (DMF) was purchased from Sigma Aldrich (USA). B Nicotinamide adenine dinucleotide (NADH), reduced disodium salt hydrate, ≧97%, was purchased from Sigma Life Science (USA). Phosphate buffer solution (PBS; pH 7.4), prepared with 50 mM sodium phosphate dibasic (Sigma) and 100 mM

sodium chloride (Fisher), was used as the supporting electrolyte for electrochemical experiments. Ultra pure water (resistivity ~ 18 MΩ cm) from a Millipore-MilliQ system was used for the preparation of all aqueous solutions. Argon was used to dry electrode surfaces and beakers. Acetic acid, 99.7%; sulfuric acid, 73–98%; and nitric acid, 50%–70%, were purchased from Fisher (ACS certified reagent grade).

2.2.2 Instrumentation

Electrochemical experimentswere performed using a VersatileMultichannel Potentiostat (VMP3, Bio-Logic) equipped with a 'p' low current option and N'Stat box driven by EC-LAB software (Bio-Logic, LLC, Knoxville, TN). A standard three-electrode system, consisting of a Pt disk working electrode (1.6 mm dia.) (BASi, W. Lafayette, IN), a Pt wire auxiliary electrode, and a Ag/AgCl glass-bodied reference electrode (BASi, W. Lafayette, IN), was used in a Faraday cage. SEM images were obtained with Nova 600 SEM/FIB System (FEI, Hillsboro, OR).

2.2.3 Procedure

2.2.3.1 Preparation of CNT-coated electrodes

Bare platinum electrodes were cleaned chemically with isopropyl alcohol and then treated electrochemically in 1 M sulfuric acid by cycling from−0.25 V to 1.65 V at a scan rate of 50 mV s−1 for 3 cycles. Following cleaning, the electrodes were dried with Ar. The metallic SWCNT coated electrodes were prepared by casting 2 μL aliquots of a 0.1 mg SWCNT in 10 mL aqueous suspension on the surfaces of 1.6-mm-diameter Pt disk electrodes and by drying for 30 min in air at room temperature between applications. Each SWCNT layer consisted of ~0.02 μg of metallic SWCNTs. After application and drying of each layer, three droplets (50–100 μL) of a nitric and sulfuric acid mixture (1:3 ratio, of 70% and 98% acid, respectively) were applied to the

electrode surfaces. After 10 min, the electrodes were rinsed with ultrapure water and dried with Ar.

The MWCNT powder (various amounts ranging from 0.01 mg to 10 mg) was dispersed in 1 mL DMF solvent and sonicated for 1 h. Two microliter volumes of these multiwall MWCNT-DMF solutions were cast on Pt disk electrodes and dried for 1 h at room temperature. Acid treatments were also applied to some of these electrodes as described above.

2.2.3.2 Electrochemical measurements

Cyclic voltammetry (CV) was performed in 10 mM NADH (in PBS, pH 7.4), over a potential range of−0.4–1.0 V (vs. Ag/AgCl) at a potential sweep rate of 5 mV s−1.Most prior work has been conducted at or near neutral pH, so this work was performed at near neutral pH for comparison purposes. Electrodes also were evaluated for NADH sensing by constant potential amperometry in stirred solutions. Current was recorded at 0.7 V upon successive additions of 10 μL of 25 mM NADH stock solution into 10 mL of PBS for metallic SWCNT-coated electrodes or at potentials corresponding to peak currents (from cyclic voltammograms) for MWCNT-coated electrodes.

2.3 Results and discussion

2.3.1 Electrooxidation of NADH on metallic, SWCNT-coated Pt disk electrodes

2.3.1.1 Acid treatment after CNT deposition improved coating uniformity

Acid treatment of CNTs is known to introduce oxygen-containing groups onto the surface and to improve dispersion in aqueous media [30,33,38]. The effects of acetic acid treatment of metallic SWCNTs after deposition on Pt disk electrodes was compared with treatment by a

H2SO4/HNO3 acid mixture, and the latter was found to improve the distribution of SWCNTs on the electrodes (Fig. 2.1). Treatment with the H2SO4/HNO3 acid mixture also gave coated electrodes that exhibited lower baseline noise when used in detecting NADH by fixed potential amperometry (see below).

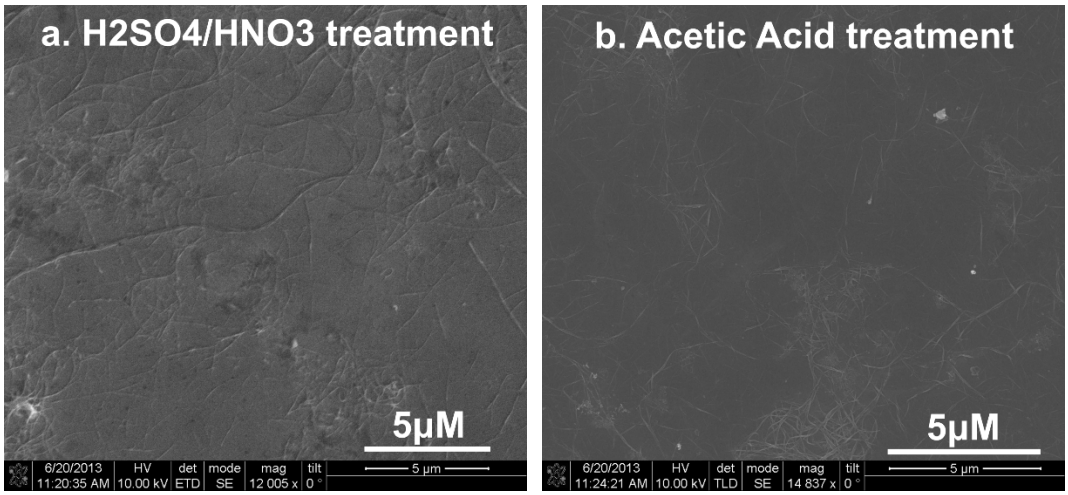

Figure 2.1 (a) Scanning electron microscope (SEM) image of H2SO4/HNO3 acid mixturetreated,6-layer metallic SWCNT film; (b) SEM image of acetic acid-treated, 6-layer metallic SWCNT film.

2.3.1.2 Metallic SWCNT coating reduced fouling and overpotential for NADH electrooxidation

It has been reported widely that NADH electrooxidation on Pt electrodes causes fouling [1,3,15,39], however we have found that a coating of either metallic SWCNTs or MWCNTs on Pt reduces fouling significantly. For example in Fig. 2.2, cyclic voltammograms in 10 mM NADH conducted with a bare Pt electrode and a Pt electrode coated with 6 layers of metallic SWCNTs are compared. Fouling occurs quite quickly on the bare electrode as evidenced by a readily observable 0.07 V shift in the voltammogram in the first two cycles, whereas no significant change in the CV results was observed for the CNT coated electrode for the next several cycles. Reduced fouling is one important feature of the CNT-coated Pt electrodes. This

result is consistent with that achieved with both CNT-coated glassy carbon and gold electrodes [32, 34,36]. Note that the small reduction peak evident on the CVs of Fig. 2.2 correspond to reduction of platinum oxide [40], whereas the corresponding Pt oxidation peak is masked by the current due to NADH oxidation.

The SWCNT-coated electrodes also exhibited NADH electrooxidation at reduced overpotential as compared to bare Pt. Thus, these CNT treated electrodes may be used at lower potential for NADH sensing thereby reducing current signal interference from other electrooxidizable species that may be present in a real sample [41]. As shown in Fig. 2.3, the NADH oxidation peak potential decreases with increasing CNT surface concentration from 0.77 V for bare Pt to 0.69 V for a 10-layer metallic CNT coating (0.1 μg CNT/mm2). A consensus is emerging in the literature that the lower NADH oxidation potential achieved with CNT coated electrodes is due to the electrocatalytic properties of the nanotube ends where the material properties are more like those of the edge-plane face of graphite [42–44] There also is evidence that defects in the CNT walls, particularly when derivatized with oxygen-containing functional groups, may play an important role in electrocatalysis [31–33]. The reduction in overpotential observed here is modest compared to reports of 0.4 V and 0–0.36 V peak potentials for NADH reduction on Au and glass carbon electrodes coated with CNTs (and no other modifiers) [32,33,35,42,45]. However, these published studies were conducted with MWCNTs [32,33,42] or SWCNT preparations that likely were mixtures of conducting (metallic) and semiconducting CNTs [35,45]. Nevertheless, we continued work with metallic SWCNTs and compared results with those we obtained with MWCNTs (see below).

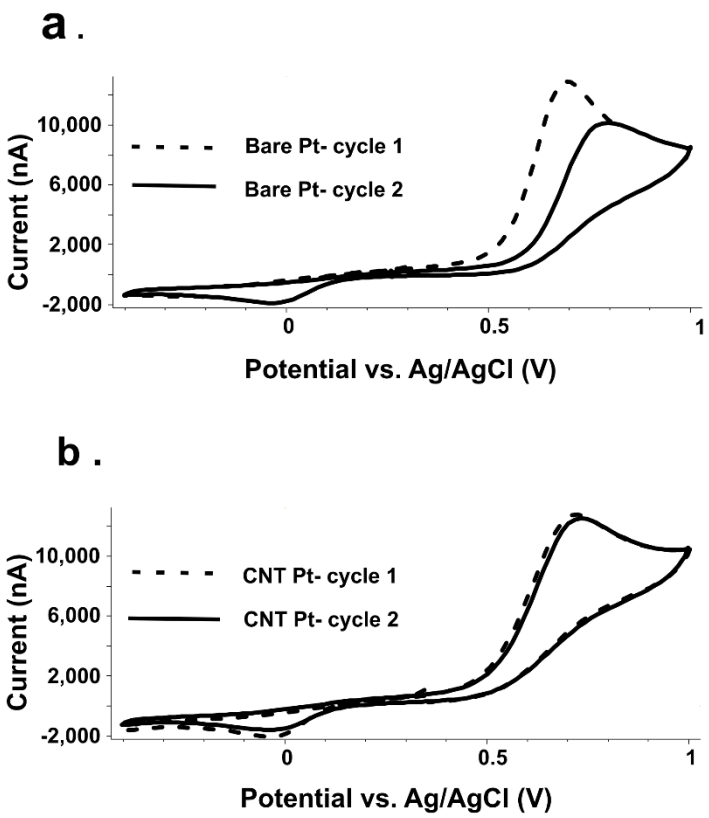

Figure 2.2 Cyclic voltammograms conducted with (a) bare disk Pt electrode, and (b) 6-layer(0.06 µg/mm2) SWCNT-coated Pt disk electrode in 10 mM NADH (0.1 M PBS, pH 7.4) ata scan rate of 5 mV s−1.

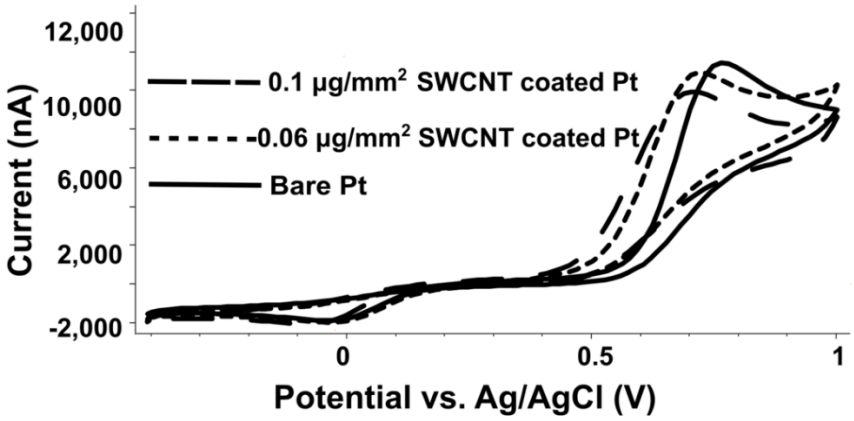

Figure 2.3 Cyclic voltammograms conducted with a bare Pt disk electrode, and 6-layer (0.06 μg/mm2) and 10-layer (0.1 μg/mm2) metallic SWCNT-coated Pt disk electrodes in 10 mM NADH (0.1 M PBS, pH 7.4) at a scan rate of 5 mV s−1.

2.3.1.3 Metallic SWCNT coating improved NADH electrode sensitivity and detection limit

The steady-state current signals at fixed potential from Pt disk electrodes with multiple SWCNT coatings and H2SO4/HNO3 treatments are shown in Fig. 2.4. For the electrodes coated with less than or equal to 10 layers of metallic SWCNTs, the response to NADH increased with the number of CNT layers. A 20-layer,metallic CNT-coated Pt disk electrode exhibited an unstable response and low sensitivity, perhaps due to physical instability of the CNT coating, poor conductance through the thick deposit, and/or hindered transport of NADH [8]. In all cases shown, Pt electrodes with metallic SWCNT coating showed a significant increase in the sensing current compared to the bare Pt electrode (Fig. 2.4). The standard deviation of baseline noise, sensitivity, and detection limit (at 3-fold the baseline noise) exhibited by the NADH electrodes were used for further quantitative evaluation and comparison purposes (Table 2.1) [46]. The Table 2.1 data reflect the observed increase in sensitivity with number of SWCNT layers, however the lowest noise levels were attained at 6 SWCNT layers, which contributed to the lowest NADH detection limit observed, 0.17 μM, among 10 electrodes tested. These results suggest that a coating of 6 metallic SWCNT layers, corresponding to an electrode surface concentration of ~0.06 μg/mm2, may be near optimal. A detection limit of 0.35 μM±0.04μM and a sensitivity of 366±44 mAM−1 cm−2was obtained from several repeated tests of metallic SWCNT coated Pt electrodes (n =10).

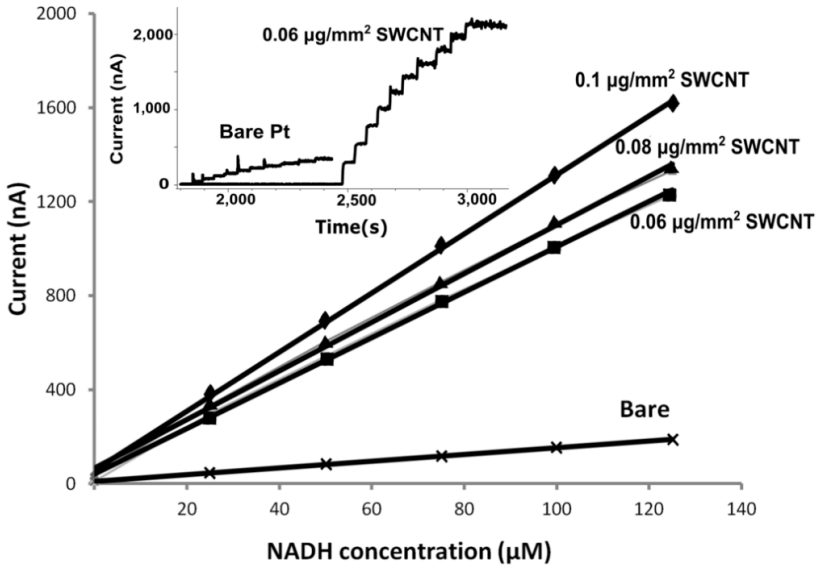

Figure 2.4 Steady-state current at fixed potential vs. NADH concentration (in 0.1 M PBS, pH 7.4) for 6-layer (0.06 μg/mm2), 8-layer (0.08 μg/mm2), and 10-layer (0.1 μg/mm2) metallic SWCNT-coated Pt disk electrodes and a bare Pt disk electrode at 0.7 V vs. Ag/ AgCl. Inset shows amperometric responses at 0.7 V vs. Ag/AgCl of a 6-layer metallic SWCNT-coated Pt disk electrode and a bare Pt electrode in PBS (0.1 M, pH 7.4) upon successive increases in NADH concentration of 0.025 μM.

Sensitivity		Baseline Noise (nA)	Detection Limit (μM)	(mA M^{-1} cm^{-2})
Bare Pt1.55±0.2	5.8±0.52	75±4.8		
6-Layers	0.56±0.08	0.35±0.043	366±44.5	
8-Layers	1.85±0.2	0.86±0.1	380±46	
10-Layers	2.80±0.32	1.2±0.18	594±52	

Table 2.1 NADH sensing performance of Pt disk electrodes with varied SWCNT coatings at 0.7 V vs. Ag/AgCl.

The combination of detection limit and sensitivity achieved with the SWCNT-coated Pt electrodes compares well with the literature. In particular, the high sensitivity (on an electrode area basis) appears to be matched uncommonly [45,47–49], except through the construction of unusual or complicated electrodes such as boron-doped diamond [47], poly(phenosafranin)-functionalized SWCNTs on edge-plane pyrolytic graphite [48], and poly(luminol) and poly(neutral red) with MWCNTs and graphene oxide on glassy carbon [49]. Yet, these more exotic preparations gave detection limits more than an order of magnitude lower than achieved here and at significantly lower potential in the cases of Saleh et al. [48] and Lin et al. [49]. The lower detection limits described in these reports at similar sensitivities suggests that our detection limit could be reduced if noise could be suppressed or filtered effectively. We moved on to a study with MWCNTs in an attempt to lower the optimal operating potential for NADH detection as well.

2.3.2 Electrooxidation of NADH on MWCNT-coated Pt disk electrodes

2.3.2.1 Dispersion of MWCNT powder in DMF enables uniform coating on Pt electrodes

The MWCNTs were supplied as a powder, so it was necessary to disperse these CNTs in solution to enable coating on Pt electrodes. Pretreatment of MWCNTs with the H2SO4/HNO3 acid mixture prior to dispersion in water was explored as was direct dispersion (no pretreatment) in aqueous solution and in DMF. It was anticipated that the acid treatment would introduce oxygen-containing groups onto the CNTs, which would result in improved dispersion in water and a better coating on Pt. However, this proved not to be the case. As shown in Fig. 2.5a, the acid treatment resulted in a deposit consisting of large bundles of entangled MWCNTs unevenly distributed on the surface. A similar result was observed with the MWCNTs dispersed in water without pretreatment (Fig. 2.5c). The best results were obtained using DMF as solvent with no

acid pretreatment (Fig. 2.5b). Subsequently, Pt electrodes with a MWCNT coating were prepared using a CNT solution in DMF [50].

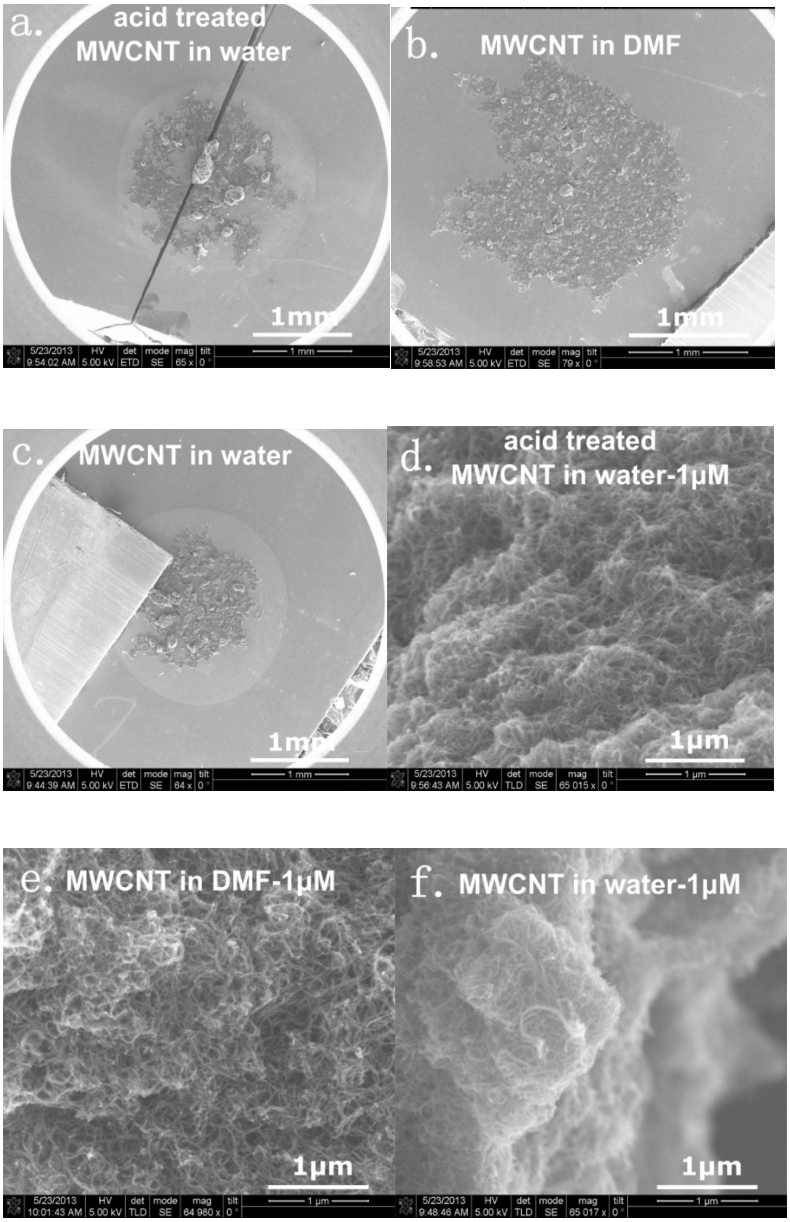

Figure 2.5 SEM images of deposits on Pt of (a)H2SO4/HNO3-treatedMWCNTs dissolved in water at 0.5mg/mL and sonicated for 1 h, (b)MWCNTs dissolved in DMF at 0.5 mg/mL and sonicated for 1 h, (c) MWCNTs dissolved in water at 0.5 mg/mL and sonicated for 1 h, and (d) – (f) the same preparations at higher magnification.

2.3.2.2 MWCNT coating decreases the overpotential for NADH electrooxidation

Based on the results with the metallic SWCNTs, the obvious question arose concerning the performance of Pt electrodes with a MWCNT deposit for NADH electrooxidation. Solutions of MWCNTs dissolved in DMF were prepared with concentrations ranging from 0.01 mg/mL to 10mg/mL, which subsequently were used to create coatings on Pt electrodes with CNT surface concentration ranging from ~0.01 μg/mm2 to ~10 μg/mm2. As with the work with metallic SWCNTs, cyclic voltammetry was used to compare the NADH oxidation peak potentials as a function of CNT surface concentration. As can be seen in Fig. 2.6, the peak potential decreases from 0.68 V to 0.26 V as the surface concentration of MWCNT increases. This result is in good agreement with the literature results mentioned earlier that show NADH electrooxidation at significantly reduced overpotential on CNT-coated Au and glassy carbon electrodes [32,33,35,42,45]. Since for the same loading (0.2 μg) of metallic SWCNTs and MWCNTs on a Pt electrode the shorter SWCNTs provide more edge-plane sites, the lower oxidation peak potential observed for the MWCNT-coated electrode at 0.55 V (versus 0.69 V for SWCNTs) cannot be explained by differences in availability of edge-plane sites. Rather, since as described earlier the literature results were obtained with MWCNTs or with SWCNTs that likely were a mixture of metallic and semiconducting CNTs, our results and those in the literature suggest that it may be the semiconducting CNTs that best facilitate NADH electrooxidation at reduced potential. This issue goes beyond the scope of this study, which is focused on a demonstration that CNT coatings on Pt electrodes enable effective NADH sensing, yet clearly is worthy of further investigation.

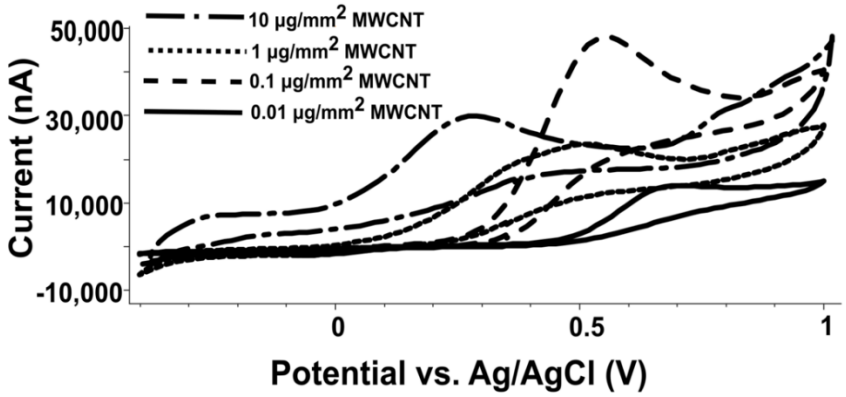

Figure 2.6 Cyclic voltammograms in 10 mM NADH (0.1 M PBS, pH 7.4) at a scan rate of 5 mV s−1 obtained with Pt disk electrodes with MWCNT surface concentrations of approximately 10 µg/mm2, 1 µg/mm2, 0.1 µg/mm2 and 0.01 µg/mm2 given the electrode surface area of 2 mm2.

2.3.2.3 MWCNT coating improved NADH electrode sensitivity and detection limit

Once again, constant potential amperometry was used with the MWCNT-coated electrodes in assessing performance for NADH sensing. Electrodes with the same four surface concentrations used in the CV work were prepared and were operated at their respective peak potentials determined by voltammetry. The electrodes with surface CNT concentrations of 0.1 µg/mm2 and 1 µg/mm2 showed better detection limits than those with 0.01 µg/mm2 and 10 µg/mm2. Further research was conducted to optimize the surface concentration of CNTs between 0.1 µg/ mm2 and 1 µg/mm2. The best sensing result was found at a concentration of 0.5 µg/mm2. Potentials from 0.3 V to 0.6 V were used in the fixed potential amperometry studies with electrodes treated with the optimal MWCNT concentration of 0.5 µg/mm2 (Table 2.2). At a working potential of 0.5 V vs. Ag/AgCl, a relatively low standard deviation of baseline noise of

0.41 nA was observed, with a lowest recorded detection limit of 0.19 µM and corresponding sensitivity of 369mAM−1cm−2.

The baseline noise varied significantly at different working potentials, which caused large differences in detection limits (Table 2.2). However, the sensitivities were similar at different working potentials. The mean detection limit and sensitivity were in the ranges of 0.5 ± 0.1 µM and 359 ± 10 mAM−1 cm−2 for the 0.5 µg/mm2MWCNT loading (n = 4). The steady-state current signal at fixed potential from Pt disk electrodes coated with 0.5 µg/mm2 MWCNTs is shown in Fig. 2.7. To put these results in perspective, the sensitivity (on a per electrode surface area basis) of our MWCNT-coated Pt electrodes is nearly an order of magnitude larger than that obtained with CNT-coated Au electrodes at the same potential [34,36].

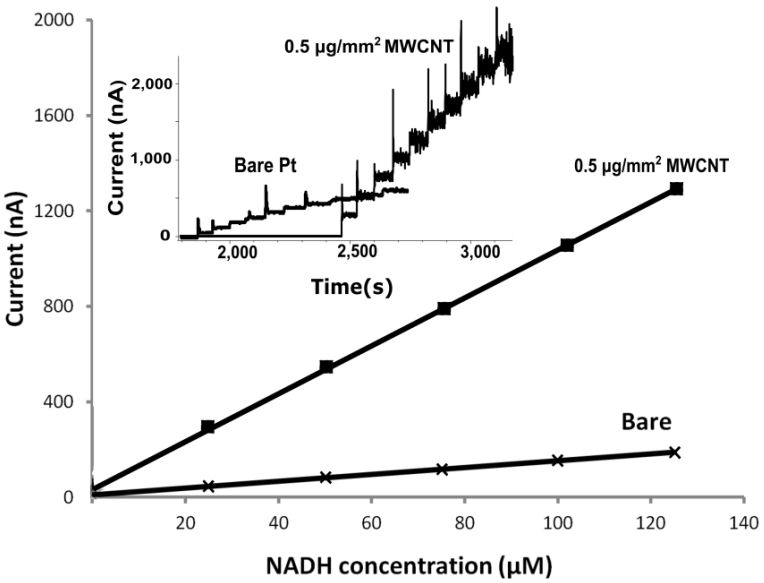

Figure 2.7 Steady-state current at fixed potential vs. NADH concentration (in 0.1 M PBS, pH 7.4) for 0.5 µg/mm2 MWCNT-coated Pt disk electrodes at 0.5 V vs. Ag/AgCl and a bare Pt disk electrode at 0.7 V vs. Ag/AgCl. Inset shows amperometric responses at 0.5 V vs. Ag/AgCl of a MWCNT-coated Pt disk electrode and a bare Pt electrode in PBS (0.1 M, pH 7.4) at 0.5 V vs. Ag/AgCl upon successive increases in NADH concentration of 0.025 µM.

Potential (V)	Baseline Noise (nA)	Detection Limit (μM)	Sensitivity (mA M^{-1} cm^{-2})
0.3	0.86±0.2	0.98±0.18	315±9.8
0.4	1.33±0.4	1.44±0.21	333±12.2
0.5	0.41±0.12	0.5±0.12	359±10
0.6	1.89±0.45	1.88±0.68	380±36.2

Table 2.2 NADH sensing performance at varied potential (vs. Ag/AgCl) of Pt disk electrodes with untreated MWCNT coating at 0.5 μg/mm^2.

The acid mixture treatment used with SWCNTs (see above) was explored after MWCNT loading and drying as a means to improve electrode performance. The cyclic voltammograms of electrodes with and without acid treatment were compared (Fig. 2.8). Due to the poor adhesion of MWCNTs to Pt, the acid treatment caused loss of MWCNTs from the surface, which led to a small increase in peak potential. Thus, acid treatment was not pursued with MWCNTs.

The MWCNT-coated electrodes gave similar performance to the metallic SWCNT-coated electrodes, but at lower working potential. Although the optimal working potential was ~0.5 V, good performance also was achieved at 0.3 V (Table 2.2), which is more in line with that reported in the literature for CNT-coated carbon electrodes [32,33,35,42,45]. Further improvement in NADH detection performance at lower potential with the MWCNTs may be had if better adhesion of acid-treated MWCNTs to Pt can be achieved. Also, it is interesting that the electrodes coated with the acid-treated, metallic SWCNTs showed similar performance to those with MWCNTs (albeit at higher potential) at nearly an order of magnitude lower surface concentration. This difference may be due to the acid treatment, to differences in

the density of the coatings due to the significant differences in both the average diameter and length of the two CNT preparations, to the greater proportion of edge plane sites for the SWCNT coating, or to the metallic nature of the SWCNTs used versus the more variable characteristics of the MWCNTs. Among these factors, a less dense CNT coating that enables less restricted penetration of NADH to the underlying electrode may be most readily understood as a possible contributor to better sensor performance. The differences in performance that one might attribute to the metallic versus semiconducting nature of the CNTs used are more difficult to address. We are aware of no other attempts to use purely metallic SWCNTs in the construction of electrochemical NADH sensors, and the conducting nature of CNTs may be a fruitful topic for further study in this context.

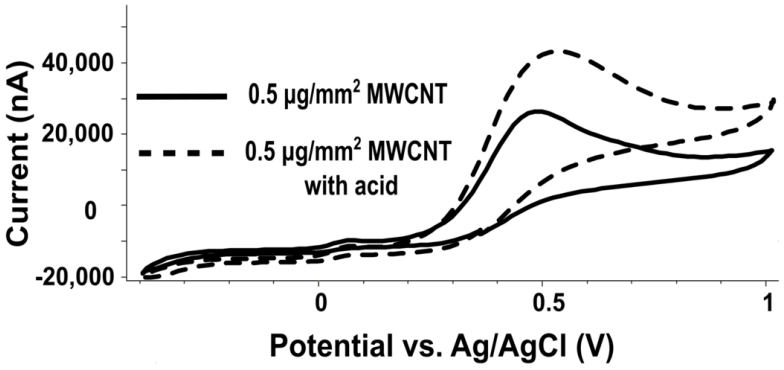

Figure 2.8 Cyclic voltammograms in 10 mM NADH (0.1 M PBS, pH 7.4) at a scan rate of 5 mV s−1 obtained with Pt disk electrodes with a MWCNT (acid treated or untreated) surface concentration of 0.5 µg/mm2.

2.4 Conclusion

This study demonstrates the utility of conventional Pt elefctrodes for NADH sensing, when coated with CNTs, contrary to the widely held belief that noble metal electrodes are less suitable for this application. Both metallic SWCNT and MWCNT coatings inhibit electrode fouling and enable NADH sensing at reduced potential. Acid treatment enhanced the performance of the SWCNT-coated electrodes, but the untreated MWCNT-coated electrodes exhibited similar limit of detection and sensitivity at significantly lower potential. The limits of detection achieved compare well with the literature, however the very high sensitivities are uncommon, are indicative of the advantages of Pt as an electrode material for this application, and suggest that improvements to the detection limit can be achieved if noise can be suppressed further or filtered effectively. Also, some enhancement in performance at lower potentials may be attained if a means to improve adhesion of acid treated MWCNTs to Pt can be found. Thus, CNT-coated Pt electrodes may provide an attractive, relatively simple route to high performance NADH sensors.

2.5 References

[1] A. Radoi, D. Compagnone, Recent advances in NADH electrochemical sensing design, *Bioelectrochemistry* 76 (2009) 126–134.

[2] J. Moiroux, P.J. Elving, Effects of adsorption, electrode material, and operational variables on the oxidation of dihydronicotinamide adenine dinucleotide at carbon electrodes, *Anal. Chem.* 50 (1978) 1056–1062.

[3] Z. Samec, P.J. Elving, Anodic oxidation of dihydronicotinamide adenine dinucleotide at solid electrodes; mediation by surface species, *J. Electroanal. Chem.* 144 (1983) 217–234.

[4] W.J. Blaedel, R.A. Jenkins, Study of the electrochemical oxidation of reduced nicotinamide adenine dinucleotide, *Anal. Chem.* 47 (1975) 1337–1343.

[5] W.J. Blaedel, R.A. Jenkins, Steady-state voltammetry at glassy carbon electrodes, *Anal. Chem.* 46 (1974) 1952–1955.

[6] H. Jaegfeldt, A. Torstensson, G. Johansson, Electrochemical oxidation of reduced nicotinamide adenine dinucleotide directly and after reduction in an enzyme reactor, *Anal. Chim. Acta* 97 (1978) 221–228.

[7] H. Jaegfeldt, Adsorption and electrochemical oxidation behaviour of NADH at a clean platinum electrode, *J. Electroanal. Chem.* 110 (1980) 295–302.

[8] P.N. Bartlett, E. Simon, C.S. Toh, Modified electrodes for NADH oxidation and dehydrogenase-based biosensors, *Bioelectrochemistry* 56 (2002) 117–122.

[9] M. Aizawa, R.W. Coughlin,M. Charles, Electrochemical regeneration of nicotinamide adenine dinucleotide, *Biochim. Biophys. Acta* 385 (1975) 362–370.

[10] F. Hollman, A. Schmid, Electrochemical regeneration of oxidoreductases for cell-free biocatalytic redox reactions, *Biocatal. Biotransfor.* 22 (2004) 63–88.

[11] E.-S. Jeong, M. Sathishkumar, R. Jayabalan, S.-H. Jeong, S.-Y. Park, S.-P. Mun, S.-E. Yun, Immobilization of a mediator onto carbon cloth electrode and employment of themodified electrode to an electroenzymatic bioreactor, *J. Microbiol. Biotechnol*. 22 (2012) 1406–1411.

[12] H. Li, K.E. Worley, S.C. Barton, Quantitative analysis of bioactive NAD+ regenerated by NADH electro-oxidation, *ACS Catal.* 2 (2012) 2572–2576.

[13] H.K. Chenault, G.M. Whitesides, Regeneration of nicotinamide cofactors for use in organic synthesis, *Appl. Biochem. Biotechnol*. 14 (1987) 147–197.

[14] F. Hollman, K. Bühler, B. Bühler, Oxidation of alcohols, aldehydes, and acids, in: K. Drauz, H. Gröger, O. May (Eds.), Enzyme Catalysis in Organic Synthesis, third ed.Wiley-VCH, New York 2012, pp. 1325–1437.

[15] S. Kochius, A.O. Magnusson, F. Hollman, J. Schrader, D. Holtmann, Immobilized redox mediators for electrochemical NAD(P)+ regeneration, *Appl. Microbiol. Biotechnol.* 93 (2012) 2251–2264.

[16] J. Wang, M. Musameh, A reagentless amperometric alcohol biosensor based on carbon-nanotube/Teflon composite electrodes*, Anal. Lett.* 36 (2003) 2041–2048.

[17] S. Chakraborty, C.R. Raj, Amperometric biosensing of glutamate using carbon nanotube based electrode, Electrochem. Commun. 9 (2007) 1323–1330.

[18] H. Qiu, L. Xue, G. Ji, G. Zhou, X. Huang, Y. Qu, P. Gao, Enzyme-modified nanoporous gold-based electrochemical biosensors, *Biosens. Bioelectron.* 24 (2009) 3014–3018.

[19] M.A. Hayes, W.G. Kuhr, Preservation of NADH voltammetry for enzyme-modified electrodes based on dehydrogenase, *Anal. Chem.* 71 (1999) 1720–1727.

[20] W.-J. Lin, C.-S. Liao, J.-H. Jhang, Y.-C. Tsai, Graphene modified basal and edge plane pyrolytic graphite electrodes for electrocatalytic oxidation of hydrogen peroxide and β-nicotinamide adenine dinucleotide, *Electrochem. Commun.* 11 (2009)

2153–2156.

[21] Y. Wang, C. You, S. Zhang, J. Kong, J.-L. Marty, D. Zhao, B. Liu, Electrocatalytic oxidation of NADH at mesoporous carbon modified electrodes, *Microchim. Acta* 167

[22] F. Pariente, F. Tobalina, M. Darder, E. Lorenzo, H.D. Abruña, Electrodeposition of redox-active films of dihydroxybenzaldehydes and related analogs and their electrocatalytic activity toward NADH oxidation, *Anal. Chem.* 68 (1996) 3135–3142.

[23] D.C.-S. Tse, T. Kuwana, Electrocatalysis of dihydronicotinamide adenosine diphosphate with quinones and modified quinone electrodes, *Anal. Chem.* 50 (1978) 1315–1318.

[24] A. Kitani, Y.-H. So, L.L.Miller, An electrochemical study of the kinetics of NADH being oxidized by diimines derived from diaminobenzenes and diaminopyrimidines, *J. Am. Chem. Soc.* 103 (1981) 7636–7641.

[25] T. Matsue, M. Suda, I. Uchida, T. Kato, U. Akiba, T. Osa, Electrocatalytic oxidation of

NADH by ferrocene derivatives and the influence of cyclodextrin complexation, *J. Electroanal. Chem. 234* (1987) 163–173.

[26] A. Torstensson, L. Gorton, Catalytic oxidation of NADH by surface-modified graphite electrodes*, J. Electroanal. Chem.* 130 (1981) 199–207.

[27] P. Norouzi, F. Faridbod, H. Rashedi, M.R. Ganjali, Flow injection glutamate biosensor based on carbon nanotubes and Pt-nanoparticles using EFT continuous cyclic voltammetry, *Int. J. Electrochem. Sci*. 5 (2010) 1713–1725.

[28] A. Pinczewska, M. Sosna, S. Bloodworth, J.D. Kilburn, P.N. Bartlett, High-throughput synthesis and electrochemical screening of a library of modified electrodes for NADH oxidation, *J. Am. Chem. Soc.* 134 (2012) 18022–18033.

[29] S.A. Kumar, S.-M. Chen, Electroanalysis of NADH using conducting and redox active polymer/carbon nanotubes modified electrodes-a review, *Sensors* 8 (2008) 739–766.

[30] L. Hu, D.S. Hecht, G. Grüner, Carbon nanotube thin films: fabrication, properties, and applications, *Chem. Rev.* 110 (2010) 5790–5844.

[31] M. Tominaga, S. Sakamoto, H. Yamaguchi, Jungle-gym structured films of single walled carbon nanotubes on a gold surface: oxidative treatment and electrochemical properties, *J. Phys. Chem. C* 116 (2012) 9498–9506.

[32] M. Musameh, J. Wang, A. Merkoci, Y. Lin, *Electrochem. Commun.* 4 (2002) 743–746.

[33] M. Wooten, W. Gorski, Facilitation of NADH electro-oxidation at treated carbon nanotubes, *Anal. Chem.* 82 (2010) 1299–1304.

[34] X. Tu, Q. Xie, Z. Huang, Q. Yang, S. Yao, Synthesis and characterization of novel quinone-amine polymer/carbon nanotubes composite for sensitive electrocatalytic detection of NADH, *Electroanal*. 19 (2007) 1815–1821.

[35] H.Muguruma, S. Yoshida, M. Urata, K. Fujisawa, Y.Matsui, An amperometric biosensor for glucose based on a composite electrode of glucose dehydrogenase, carbon nanotubes, and plasma-polymerized thin films, *Electrochemistry* 76 (2008), pp. 545–548.

[36] B. Ge, Y. Tan, Q. Xie, M. Ma, S. Yao, Preparation of chitosan-dopamine-multiwalled carbon nanotubes nanocomposite for electrocatalytic oxidation and sensitive electroanalysis of NADH, *Sensors Actuators B Chem.* 137 (2009) 547–554.

[37] T. Hoshino, H. Muguruma, *Electrochemistry* 80 (2012) 85–87.

[38] C.Y. Hu, F.Y. Li, L. Hua, R.B. Zhang, , *J. Serb. Chem. Soc.* 71 (2006) 1153–1160.

[39] L. Gorton, E. Domínguez, Electrocatalytic oxidation of NAD(P)H at mediatormodified electrodes, *Rev. Mol. Biotechnol.* 82 (2002) 371–392.

[40] S.F. Cogan, Neural stimulation and recording electrodes, *Annu. Rev. Biomed. Eng*. 10 (2008) 275–309.

[41] H.C. Yoon, H.-S. Kim, Electrochemical characteristics of a carbon-based thick-film Llactate biosensor using L-lactate dehydrogenase, *Anal. Chim. Acta* 336 (1996) 57–65.

[42] C.E. Banks, R.G. Compton, *Analyst* 130 (2005) 1232–1239.

[43] R.R. Moore, C.E. Banks, R.G. Compton, Basal plane pyrolytic graphite modified electrodes: comparison of carbon nanotubes and graphite powder as electrocatalysts, *Anal. Chem.* 76 (2004) 2677–2682.

[44] A.F. Holloway, G.G.Wildgoose, R.G. Compton, L. Shao, M.L.H. Green, The influence of edge-plane defects and oxygen-containing surface groups on the voltammetry of acid-treated, annealed and "super-annealed" multiwalled carbon nanotubes, *J. Solid State Electrochem*. 12 (2008) 1337–1348.

[45] J.M. Goran, C.A. Favela, K.J. Stevenson, Electrochemical oxidation of dihydronicotinamide adenine dinucleotide at nitrogen-doped carbon nanotube electrodes, *Anal. Chem.* 85 (2013) 9135–9141.

[46] Analytical Methods Committee, Recommendations for the definition, estimation and use of the detection limit, *Analyst* 112 (1987) 199–204.

[47] T.N. Rao, I. Yagi, T. Miwa, D.A. Tryk, A. Fujishima, Electrochemical oxidation of NADH at highly boron-doped diamond electrodes, *Anal. Chem*. 71 (1999) 2506–2511.

[48] F.S. Saleh, T. Okajima, F. Kitamura, L. Mao, T. Ohsaka, Poly(phenosafranin)-functionalized single-walled carbon nanotube as nanocomposite electrocatalysts: fabrication and electrocatalysis for NADH oxidation, *Electrochim. Acta* 56 (2011) 4916–4923.

[49] K.C. Lin, S.Y. Lai, S.M. Chen, A highly sensitive NADH sensor based on a myceliumlike nanocomposite using graphene oxide and multi-walled carbon nanotubes to co-immobilize poly(luminol) and poly(neutral red) hybrid films, *Analyst* 139 (2014) 3991–3998.

[50] T.T. Nguyen, S.U. Nguyen, D.T. Phuong, D.C. Nguyen, A.T. Mai, Dispersion of denatured carbon nanotubes by using a dimethylformamide solution, *Adv. Nat. Sci.: Nanosci. Nanotechnol*. 2 (2011) 035015 (4pp).

Chapter 3: Estradiol detection spectrophotometically and electrochemically with EMIT technique

Abstract

Enzyme-multiplied immunoassay technique (EMIT) is used to detect estradiol *in vitro*. It is a convenient homogeneous enzyme immunoassay which does not require time-consuming separation steps or expensive automated systems since all reagents are freely suspended in bulk solution and it can be simple and fast without costly instrumentation. The key component of this assay system, an estradiol-reporter enzyme conjugate, was prepared by covalently binding β-estradiol-6-(O-carboxymethyl)oxime to glucose-6-phosphate dehydrogenase (G6PDH) by an N-hydroxysuccinimide-enhanced, carbodiimide-mediated coupling reaction. The estradiol-G6PDH activity can be repressed up to 46% upon anti-estradiol antibody binding. The lower detection limit of the assay is 1 nM estradiol in aqueous solution, and the standard curve is linear on logit-log scale-up to 6.7 μM estradiol. A detection limit of 11.5 nM in estradiol-spiked human serum samples suggests the feasibility of applying this assay to monitor estradiol levels for the prediction and prevention of ovarian hyperstimulation syndrome. In order to produce a small, portable, low-cost, and easy to use hormone meter that can be commercialized, an electrochemical EMIT to monitor estradiol levels is of interest. The estradiol level can be derived from the NADH versus time data obtained electrochemically, which is a reflection of the reporter enzyme activity and therefore, the concentration of estradiol. The NADH versus time slopes obtained with a novel carbon nanotube coated Pt electrode at different concentrations of free estradiol lie between the unrepressed state and repressed state of the reporter enzyme conjugate

and are in a nearly linear range. These results suggest that electrochemical EMIT may be an attractive alternative to the standard EMIT approach with spectrophotometric detection of NADH.

3.1 Introduction

Estradiol is derived from cholesterol, and is one of three molecules called “estrogen” produced mostly in the ovaries of women in reproductive years. Estradiol can easily diffuse into cells and interacts with a cytoplasmic target estrogen receptor (binds well to both), which can then allow entrance to the cell nucleus regulating gene transcription for production of specific proteins in target cell [1] .Estradiol level is used as an evaluation measure for patients at risk of developing ovarian hyperstimulation syndrome (OHSS). These at risk patients are usually engaged in assisted reproductive techniques (ARTs). Studies show 85% of patients who developed OHSS had estradiol levels above 11 nM (compared to normal 6 nM) [2], [3]. Declining estrogen levels in aging women are associated with a wide array of symptoms that deteriorate quality of life (e.g., hot flashes, night sweats). Hormone replacement therapy is used to limit these symptoms, however, this can lead to increased risk of breast cancer, heart disease, stroke, and other side effects. [4]

Radioimmunoassay (RIA) is the primary method for estradiol detection due to its high sensitivity and selectivity, but a major drawback is the required use of radioactive materials [5]. Alternatives, such as enzyme-linked immunosorbent assays (ELISA), [6], [7], fluoroimmunoassay, [8], [9], chemiluminescent immunoassay [10], [11], [12] are heterogenous assays requiring several time consuming and lab intensive steps. [7] In comparison, the

enzyme-multiplied immunoassay technique (EMIT), a homogeneous enzyme immunoassay (EIA) method [13], is fast and convenient and requires no washing steps or expensive instrumentation [14].

The enzyme-multiplied immunoassay technique (EMIT) is a homogeneous enzyme immunoassay technique dependent on a reporter enzyme for signal generation. Different from other enzyme immunoassays (EIA), EMIT relies on antibody-induced inhibition of the analyte-labeled reporter enzyme. A key feature of this homogenous enzyme immunoassay is the activity of a reporter enzyme. Although there are a few possibilities for reporter enzyme, glucose-6-phosphate dehydrogenase (G6PDH) is used most commonly for its ability to serve as a reporter in serum and for its insensitivity to common interferents. This reporter enzyme performs its catalytic action on glucose-6-phosphate and requires a β-nicotinamide adenine dinucleotide (NAD^+) as coenzyme. NADH is produced with reporter enzyme catalysis, which is typically detected spectrophotometrically at a wavelength of 340 nm, to quantify reporter enzyme activity. [2]

The working principle of EMIT for detection of estradiol with G6DPH as a reporter enzyme is illustrated in Fig. 3.1.

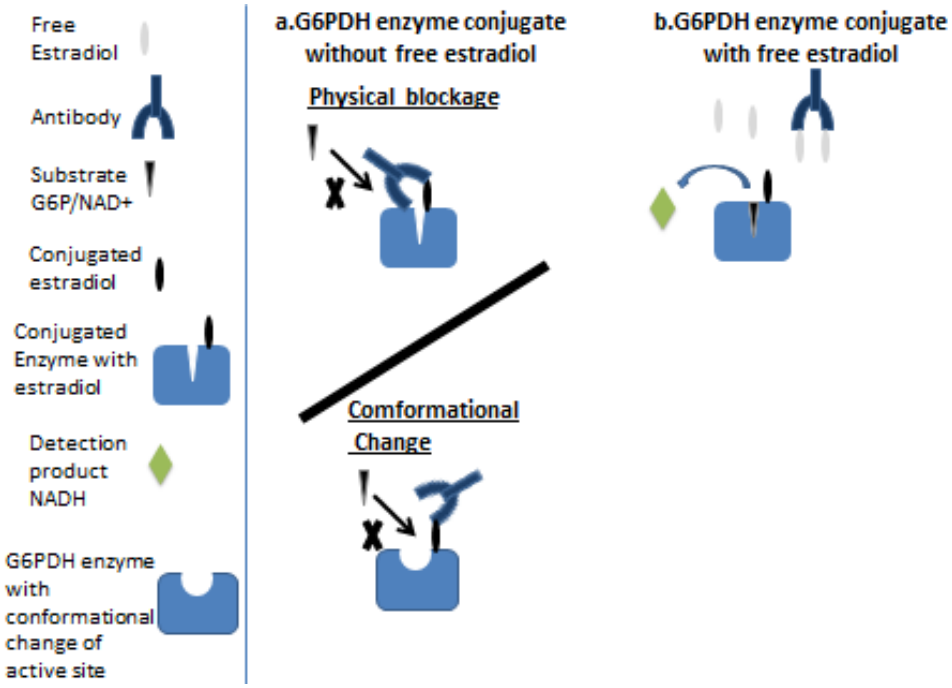

Figure 3.1 The EMIT technique of estradiol detection with G6DPH as reporter enzyme

To achieve detection of free estradiol, the reporter enzyme, G6DPH, is conjugated to an estradiol derivative. When anti-estradiol antibody (Ab) is added to the system, it will bind conjugated estradiol. The binding of Ab causes a physical blockage and/or conformational change resulting in a reduction in catalytic activity or a repression of the reporter enzyme activity. The system is then able to detect free estradiol, because once Ab is added in the presence of free estradiol, there will be competition for the Ab binding, resulting in less binding to reporter enzyme and reduced enzyme repression. According to this method, the concentration of free estradiol will determine the available sites of Ab binding for inhibition of the enzyme (depending on its probability of binding and concentration) such that activity of reporter enzyme is correlated with the concentration of free analytes. [13]

Spectrophotometric analysis of estradiol detection has been studied by May Chiu and Tina Tseng [2] in Monbouquette lab to report a repression rate of 46% upon anti-estradiol antibody binding. The lower detection limit of the assay is 1 nM estradiol in aqueous solution, and the standard curve is linear on a logit-log scale-up to 6.7 μM estradiol. A detection limit of 11.5 nM is achieved in estradiol-spiked human serum samples.

The estradiol detection method requires spectrophotometric analysis, which requires optics that can be bulky. My research focuses on proving the feasibility of applying electrochemical EMIT to monitor estradiol levels for the prediction and prevention of ovarian hyperstimulation syndrome by producing a small, portable, low-cost, and easy to use hormone meter that can be commercialized. This can be done through electrochemical detection of NADH with designed circuit electronics on a device similar to that of a potentiostat that must simply apply a voltage and measure the current response over time.

3.2 Experimental Setup

3.2.1 Materials

The following materials were used as received: β-Ethyl-6-one 6-(O-carboxymethyloxime) (E2-6-CMO, Sigma K2126), N-hydroxysuccinimide (NHS, Pierce 24500), 1-ethyl-3-[3-dimethylaminopropyl]carbodiimide hydrochloride (EDC, Pierce 22980), glucose-6-phosphate dehydrogenase from *Leuconostoc mesenteroides* (G6PDH, Sigma G5885), N,N-dimethylformamide, anhydrous, 99.8% (DMF, Sigma 227056), Zeba^{TM} desalt spin columns, 0.5mL, (Pierce 89883), Microcon Y-M30 (Millipore 42410), β-estradiol (E2, Sigma E8875), D-glucose 6-phosphate sodium salt, (G6P, Sigma G7879), nicotinamide adenine dinucletide

hydrate (NAD^+, Sigma N7004), filtered PBS buffer (pH = 7.3), trizma, gelatin, sodium chloride (Fisher), 9V battery, silver wire (AM Systems). Deionized water was generated using a Millipore Milli-Q Water System and was used for preparation of all solutions.

3.2.2 Instrumentation

Spectroscopic analyses were performed with a UV-visible spectrophotometer (model DT-1000-BT-CE; Analytical Instrument Systems, Flemington, NJ, USA). Sensor development and electrode deposition were conducted with a Versatile Multichannel Potentiostat (model VMP3) equipped with the 'p' low current option and N'Stat box driven by EC-LAB software (Bio-Logic USA, LLC, Knoxville, TN) in a three-electrode system consisting of the sensing electrode (working electrode), a Pt wire auxiliary electrode, and a Ag/AgCl reference electrode wire.

3.3 Results and Discussion

For the estradiol detection, the repression could be used to evaluate the concentration of free estradiol in aqueous solution.

Repression:

$$\%\text{Repression} = \frac{activity_{unrepressed} - activity_{repressed}}{activity_{repressed}} * 100$$

3.3.1 Estradiol detection with spectrophotometer

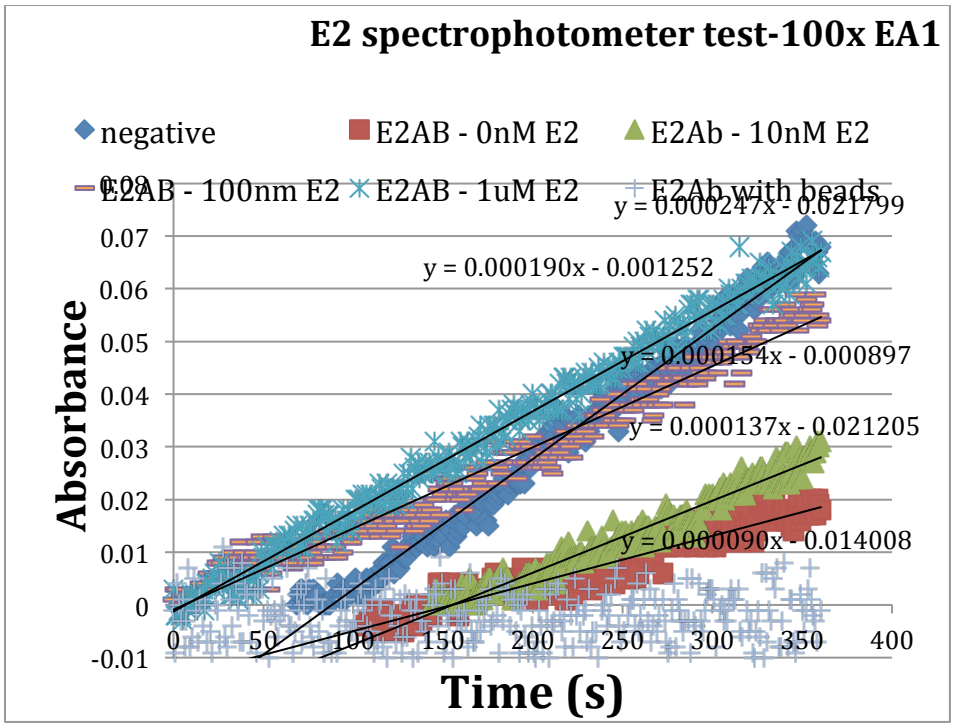

Figure 3.2 Estradiol detection with spectrophotometer, absorbance vs. time

As shown in Fig. 3.2, the solution with antibody without any free estradiol has the highest repression of 63.56%. As the concentration of free estradiol increases, the repression effect becomes smaller. The result above is consistent with T. Tseng and M. Chiu' work.

3.3.2 Estradiol detection with potentiostat

50X Estradiol	**Regression**
Fully unrepressed	y=0.0005x-0.6727
Fully repressed	y=0.000008x+0.0998
3 nM	y=0.00003x-0.0129
300 nM	y=0.00004x-0.0389
30 µM	y=0.00008x-0.0551

Table 3.1 The regression equations fitting current versus time for different concentrations of free estradiol.

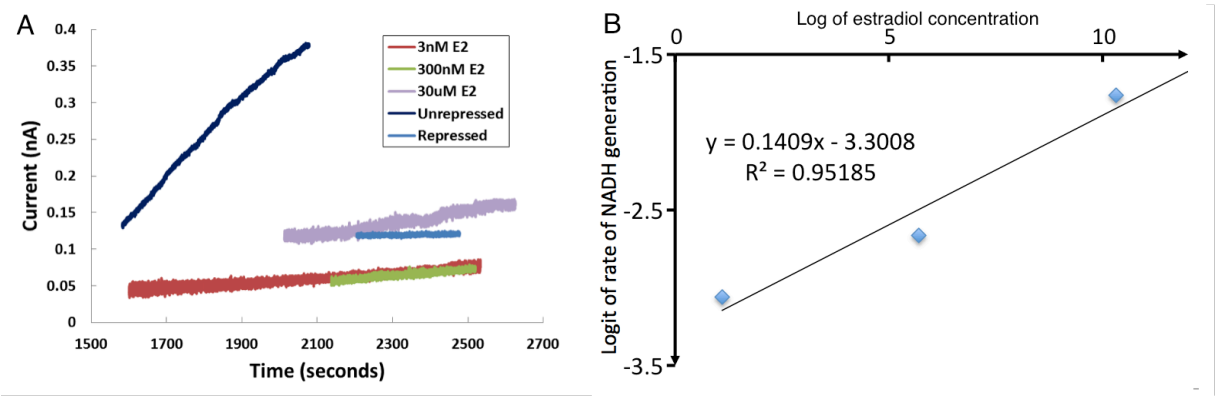

Figure 3.3 (A) Current versus time data as measured by constant potential amperometry using microelectrode at different estradiol concentrations including the fully repressed state with neither antibody nor estradiol and the fully unrepressed state with no estradiol. (B) Logit of NADH generation rate versus logarithm of estradiol concentration (in nM).

It is showed that the repression without free estradiol is over 90% which is larger than that observed with spectrophotometric method (Fig.3.3A). Since the fully repressed state constitutes the background against which estradiol concentration is assay, this result suggests that the electrochemical approach is promising. There is an approximately linear logit-log scale (Fig. 3.3B) relationship over the full estradiol concentration range corresponding to the fully repressed to the fully unrepressed states using electrochemical NADH detection, which suggest that this is a viable approach.

3.4 References

[1] Wu CH, Motohashi T, Abdel-Rahman HA, Flickinger GL, Mikhail G (August 1976). Free and protein-bound plasma estradiol-17 beta during the menstrual cycle. *J. Clin. Endocrinol. Metab.* 43 (2): 436–45.doi:10.1210/jcem-43-2-436. PMID 950372

[2] May Chiu, Tina Tseng, Harold Monbouquette, A convenient homogeneous enzyme immunoassay for estradiol detection, *Biotechnology and Applied Biochemistry,* Volume 58, Number 1, January/February 2011, Pages 75–82

[3] D'Angelo, A., Davies, R., Salah, E., Nix, B. A., and Amso, N. N. (2004) *Fertil.Steril.* 81, 332–336.

[4] Rossouw JE, Anderson GL, Prentice RL, LaCroix AZ, Kooperberg C, Stefanick ML, et al.. *JAMA: the journal of the American Medical Association.* 2002; 288(3):321.

[5] Yalow, R. S. and Berson, S. A. (1959) *Nature* 184, 1648–1649.

[6] Butler, J. E. (2000) *J. Immunoassay Immunochem.* 21, 165–209.

[7] Engvall, E. and Perlmann, P. (1971) *Immunochemistry* 8, 871–874.

[8] Meltola, N., Jauria, P., Saviranta, P., and Mikola, H. (1999) *Bioconjugate Chem.* 10, 325–331.

[9] Hemmila, I. (1985) *Clin. Chem.* 31, 359–370.

[10] Woodhead, J. S. and Weeks, I. (1985) *Pure Appl. Chem*. 57, 523–529.

[11] Taieb, J., Benattar, C., Diop, R., Birr, A. S., and Lindenbaum, A. (2003) *Clin. Chem.* 49, 183–186.

[12] De Boever, J., Mares, A., Stans, G., Bosmans, E., and Kohen, F. (1995) *Anal Chim. Acta.* 303, 143–148.

[13] Rubenstein, K. E., Schneider, R. S., and Ullman, E. F. (1972) *Biochem. Biophys. Res. Commun.* 47, 846–851.

[14] Deshpande, S. S. (1996) Enzyme Immunoassays: From Concept to Product Development, pp. 244–247, Chapman & Hall, NY

Chapter 4: Implantable Microprobe with Arrayed Microsensors for Amperometric Monitoring of Choline

Abstract

An implantable microprobe with a microsensor array for monitoring of the neurotransmitter, choline (Ch), by constant potential potential amperometry has been created and characterized. Oxidized polypyrrole (OPPy) or poly-m-phenylenediamine (PPD) and Nafion were used as permselective barrier films to prevent access to the electrode surface by electroacitve interfering species present in brain extracellular fluid such as biogenic amines, ascorbic acid and uric acid. In this study, we first evaluated the optimal concentration of bovine serum albumin (BSA) that was used to immobilize choline oxidase using a cross-linking method. The optimal ChOx solution consisted of ChOx (0.33 unit/μL), BSA (20 μg /μL) and glutaraldehyde (5×10^{-3} μL /μL). A choline current response of 0.32 nA at 20 μM choline chloride was achieved. Second, we investigated the effect of PPD electrodeposition time, potential and coating sequence with Nafion on the performance of choline biosensors. We found that the best *in vitro* performance was accomplished with biosensors that were protected by a PPD film formed from 5 mM PPD deposited on the platinum electrode at 0.85 V for 5 min combined with a subsequently applied 1% Nafion layer. The choline biosensor exhibited a high sensitivity of 390 $\mathrm{mA \cdot M^{-1} \cdot cm^{-1}}$ with a detection limit of 0.09 μM. No responses from AA and DA over their respective physiological concentration ranges were detected. Third, we investigated the performance of a choline biosensor by electrochemically depositing platinum black (Pt-black), iridium oxide (IrOx), and Nafion on reference electrode, sequentially.

Microprobe studies *in vitro* revealed choline biosensor sensitivity of 440 $\mathrm{mA \cdot M^{-1} \cdot cm^{-1}}$ with corresponding detection limits of 0.04 μM, over a linear range up to 156 μM. Also, the microbiosensor showed no detectable response to either AA or DA. Finally, in order to reduce the cytotoxic effect of Pt-black, we then reported the performance of choline biosensors by electrochemically depositing Pt-grass and on-probe IrOx reference electrode, the sensitivity was 310 $\mathrm{mA \cdot M^{-1} \cdot cm^{-1}}$ with a detection limit of 0.07 μM over a linear range of up to 172 μM. These fabricated choline biosensors were attracted due to their low detection limit and high sensitivity. The choline sensors fabricated with the PPD coating exhibited among the highest sensitivities and lowest detection limits described in the literature to date. They will be one of the best choline sensors that could be used as research tools for neuroscientist on neuroscience research.

4.1 Introduction

Choline is a biosynthetic precursor of the neurotransmitter acetylcholine (ACh) and a product of its rapid hydrolysis in the brain that is involved in learning and memory formation in the central nervous system [1]. It also is an integral component of some phospholipids that maintain the structural integrity of cell membranes and facilitate transmembrane signaling [2]. Finally, it is a source of methyl groups via one of choline's metabolites, betaine [3]. Therefore, analytical tools for monitoring of choline in near real time as a surrogate for ACh would be very useful in the study of Parkinson and Alzheimer diseases [4,5]. Although various methods such as liquid chromatography [6], enzymatic-spectrophotometric method [7], chemiluminescence [8], and electrochemiluminescence [9] have been developed for choline determination, investigation of amperometric choline oxidase (ChOx)-based biosensors is of particular interest because of their high sensitivity, rapid response, low detection limit, and low cost [10]. In these

electrochemical biosensors, the enzymatic conversion of choline to betaine aldehyde by choline oxidase (ChOx) produces hydrogen peroxide (H_2O_2) that can be detected electrochemically. Quantification of choline can be achieved by monitoring the H_2O_2 generation at the surface of an electrode where ChOx has been immobilized. The overall enzymatic reaction is shown in Reaction (1) [11] and the current generating electrochemical step is shown in Reaction (2) [12]:

$$\text{Choline} + 2O_2 \xrightarrow{ChOx} \text{Betaine} + 2H_2O_2 \quad (1)$$

$$2H_2O_2 \rightarrow 2O_2 + 4H^+ + 4e^- \quad (2)$$

However, the efficient oxidation of H_2O_2 on unmodified electrodes requires a relatively high anodic potential (~0.7 V vs. Ag/AgCl) at which the amperometric signal arising from oxidation of the endogenous electroactive biogenic amines and interferents such as ascorbic acid (AA) in brain extracellular fluid (ECF) can mask the current signal from H_2O_2 electrooxidation [13]. Sensor selectivity against interferents can be achieved by coating electrode surfaces with suitable permselective polymers prior to ChOx immobilization. Nafion, which is a perfluoronated ionomer, is commonly used to exclude anionic interferents such as AA [14]. Polypyrrole (PP) has also been commonly deposited on electrodes as a cation-exchange film. Polypyrrole films are formed by electropolymerizing pyrrole to polypyrrole at a high oxidizing potential. Such films are useful for the rejection of positively charged dopamine (DA) [15]. Moreover, glutaraldeyde (GAH) and bovine serum albumin (BSA) are commonly used in enzyme immobilization. Glutaraldeyde, which is a bifunctional compound, links covalently to the amine groups of lysine in the protein molecules to create a stable structure [16]. Also, when the protein concentration in the enzyme preparation is low, addition of bovine serum albumin (BSA) facilitates enzyme cross-linking [17]. In this regard, choline oxidase can be immobilized

by cross-linking with glutaraldehyde (GAH) in the presence of bovine serum albumin (BSA) on the surface of a platinum electrode coated with PP and Nafion.

Poly-m-phenylenediamine (PPD) can also be integrated into the design of electrochemical sensors to function as the permselective polymer. PPD is created by electrosynthesizing the monomer, m-phenylenediamine (mPD), to PPD at oxidizing potential [18]. A PPD film confers selectivity by limiting access of larger molecules such as AA and DA to the electrode surface [19] while allowing smaller molecules such as H_2O_2 to pass through. A number of previous works have detailed the permselective properties of electrochemical sensors that incorporate both Nafion and PPD layers deposited on the electrode surface [20]. However, results obtained by repeating those protocols do not display any advantages over those of OPPy/Nafion-modified microsensors. In this regard, optimization of PPD deposition by modifying Nafion concentrations, the number of Nafion coating layers, and the PPD and Nafion coating sequence is necessary.

Our previous work has reported that using iridium oxide (IrOx) as an on-probe reference electrode material is expected to reduce noise arising from external sources, which then can lower the detection limit, and to be stable over a range of potentials and in the presence of other components [21]. However, the IrOx-coated microelectrode that is tested as an on-probe RE for choline biosensing microelectrondes exhibits an unstable potential at higher currents that is manifested as a sharp drop in current signal at the choline sensor at higher choline concentrations. To solve this problem, the electrode surface is modified by depositing platinum black (Pt-black) that provides a highly roughened surface resulting in more IrOx deposition [22]. Pt-black can also reduce the impedance more than one order of magnitude, but practical applicability is limited because Pt-black involves the use of the toxic heavy metal, lead, as an electrolyte in the

electrodeposition process [23]. A similar approach using non-toxic components has been introduced by Boehler 2015, known as platinum grass (Pt-grass) [24]. In comparison to the Pt-black deposition, the formation of Pt-nanograss is simple, cost-efficient, and free from cytotoxic components.

In this chapter, we investigated the amounts of BSA and GAH added to OPPy/Nafion-modified platinum microsensors to establish a high and reliable response to choline. We also described the optimization of PPD deposition by mainly optimizing the PPD deposition time, potential and PPD/Nafion coating sequence. Separate wire Ag/AgCl REs were used for the both PPY and PPD electrochemical systems. We evaluated the performance of OPPy/Nafion-modified and PPD/Nafion-modified Pt microsensors based on their sensitivity, detection limit, and response time. We further optimized the electrochemical system by using an on-probe IrOx reference electrode on a choline biosensor where the IrOx reference site was created on a platinum black deposit. We then electrochemically deposited Pt-grass instead of Pt-black for creation of the on-probe IrOx reference electrode and compared the baseline noise with a separate Ag/AgCl reference choline sensor. Finally, *in vivo* optogenetics choline recording was conducted with a choline biosensor on a microbe with an on probe IrOx reference.

4.2 Experimental Setup

4.2.1 Materials

Choline oxidase (Alcaligenes), glutaraldehyde solution (25%), bovine serum albumin (BSA) lyophilized powder, m-phenylenediamine, Nafion® (5%), hydrogen peroxide solution (30%), formic acid, chloroplatinic acid hexahydrate, chloroplatinic acid, and lead acetate, Argon, iridium tetrachloride hydrate, anhydrous potassium carbonate, oxalic acid dehydrate (99%),

choline hydrochloride, L-ascorbic acid, dopamine hydrochloride, 3,4-dihydroxyphenylacetic acid, 3,4-dihydroxy-DL-phenylalanine, and uric acid were purchased from Sigma-Aldrich (St. Louis, MO). Isopropyl alcohol and hydrochloric acid were obtained from Fisher Scientific (Pittsburgh, PA). Ag/AgCl glass-bodied reference electrodes with 3 M NaCl electrolyte and a 0.5 mm diameter platinum (Pt) wire auxiliary electrode were purchased from BASi (West Lafayette, IN). Sodium phosphate buffer (PBS) was composed of 50 mM sodium phosphate (dibasic) and 100 mM sodium chloride (pH 7.4). Deionized water was generated using a Millipore Milli-Q Water System and was used for preparation of all solutions.

4.2.2 Instrumentation

Sensor development and electrode deposition were conducted with a Versatile Multichannel Potentiostat (model VMP3) equipped with the 'p' low current option and N'Stat box driven by EC-LAB software (Bio-Logic USA, LLC, Knoxville, TN) in a three-electrode system consisting of the sensing electrode (working electrode), a Pt wire auxiliary electrode, and a Ag/AgCl glass-bodied reference electrode. Multichannel FAST-16 potentiostat (Quanteon, LLC, Lexington, KY) in a two-electrode mode system was used for sensor calibration.

4.2.3 Microprobe fabrication and sensor preparation

Our microelectrodes were fabricated at UCLA nanolab with microelectro-mechanical-system (MEMS) technologies. The fabrication process was described in previous work [25]. Each site was modified accordingly, to act either as a working or reference electrode. Selective electrodeposition of PPy films (200 mM Py in stirred PBS, 0.85 V, ~5 min and 2% Nafion dip coating, baking at 180°C, repeat dip coating and baking once) or PPD films (5 mM PD in stirred PBS, 0.85 V, 10 min without Nafion or 0.85 V, 5 min and 1 layer 1%

Nafion dip coating, baking at 175°C) was carried out to make working electrode, both choline sensing site and control site. Choline sensing site was selectively immobilized with ChOx solution on the two sites at the tip (site 3 and 4) using a microsyringe under the microscope. The ChOx solution was prepared by mixing 4 μL ChOx (0.5 unit/μL) with 2 μL BSA solution (60 mg/mL) containing glutaraldehyde (15 μL /mL). The final solution consisted ChOx (0.33 unit/μL), BSA (20 μg/μL) and glutaraldehyde (5 × 10-3 μL /μL). The control site (site 2 or site 1 and 2) was loaded with only BSA and GAH. The resulting choline sensor microprobe was left to dry at least 48 h in a dessicator at 4 °C. During calibration, over 30 min of equilibrium time in PBS buffer was required to approach a constant baseline, followed by AA, DA, Ch, H_2O_2 or interferent injections.

The platinum nanograss plating solution consisted 2.5 mM H_2PtCl_6 and 1.5 mM formic acid. Pt-grass deposition was conducted at a potential of -0.1 V vs Ag/AgCl for 300 s in the plating solution (Boehler et al. 2015) [26]. For Pt black deposition, Pt black layer was deposited at cycling potential between 1.4 and 2.0 V at 500 mV/s for a total of 15 cycles in a vigorously stirred plating solution. The plating solution consisted 1% chloroplatinic acid, 0.0025% HCl, and 0.01% lead acetate in water, which was Ar-purged for 15 min [13].

The on probe reference electrode was made by Pt-grass or Pt-black deposition first and then followed by IrOx deposition. IrOx was electrodeposited following the method described by Yamanaka [21].

For just choline sensor, sites 3 and 4 were coated with PPD, Nafion and ChOx+BSA/GAH. Sites 1 and 2 were coated with PPD, Nafion and BSA/GAH without ChOx. For on probe reference choline sensor, sites 3 and 4 were coated with PPD, Nafion and

ChOx+BSA/GAH. Site 2 was coated with PPD, Nafion and BSA/GAH without ChOx. Site 1 was coated with Pt-grass or Pt-black and IrOx.

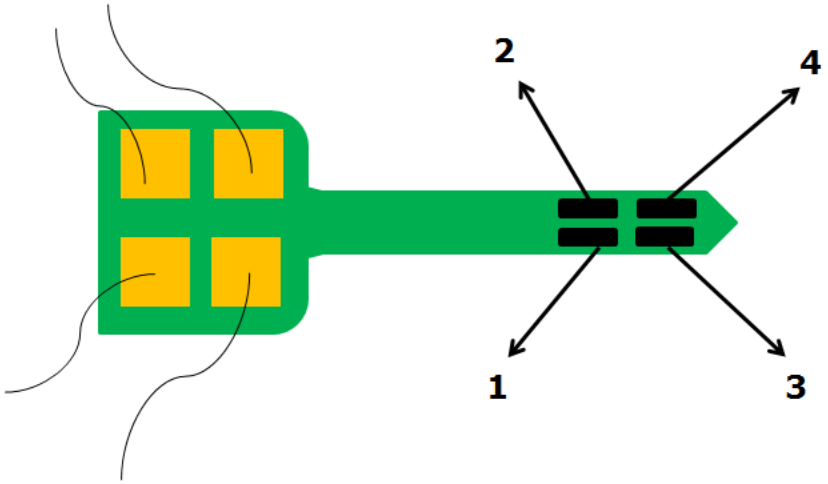

Figure 4.1 Schematic diagram of the microsensor configuration.

4.3 Results and discussion

4.3.1 Effect of concentrations of bovine serum albumin on choline sensor performance

To immobilize an active enzyme into a permeable membrane to maximize the signal, the microelectrode Pt surface was modified by overoxidized polypyrrole and Nafion coating followed by immnobilization of ChOx by using bovine serum albumin (BSA) as the stabilizing agent and glutaraldeyde (GAH) as the crosslinker. The scheme in Fig. 4.1 illustrates the biosensor design, as described in the methods section. The extent of enzyme crosslinking is mainly controlled by the amount of crosslinker employed [26]. Hence, the BSA concentration can influence diffusivity through the enzyme layer and the amount of enzyme immobilized by crosslinking.

The resulting choline sensor was first tested *in vitro* at 0.7 V (vs. Ag/AgCl) in stirred SPB buffer solution when the BSA concentration is 10 mg, 20 mg, and 60 mg, respectively. First, as shown in Fig. 4.2, no detectable response was observed in the presence of the negatively charged electroactive interferent, ascorbic acid (AA), at 250 μM and positively charged interferent, dopamine (DA). These promising results suggested that the modified sensors that combined OPPy, Nafion, ChOx, BSA, and GAH repelled AA, DA at physiological concentrations. Fig. 4.2 also shows the sensitivity in terms of current response at 20 μM Ch correlated to BSA amount. As it can be seen, choline current response was ~0.1 nA when 10 mg BSA was added; choline current response was ~ 0.2 nA when 20 mg BSA was added; and choline current response was 0.32 nA when 60 mg BSA was added. Thus, the higher the BSA concentration caused the higher choline sensitivity and the higher the calibration factor.

The upper limit of BSA concentrations was determined to be 60 mg, resulting in 0.32 nA Ch response, such as to ensure a reasonable gelation time because the increased BSA amount decreased the crosslinking time. For example, 90 mg BSA would result in only about 10 sec crosslinking time, which was not reasonable for the manual deposition technique used.

In summary, (1) the combination of OPPy, Nafion, ChOx, BSA, and GAH could discriminate the small neutral H_2O_2 molecule from anionic and cationic electroactive species (i.e., AA and DA, respectively) as expected, (2) the detected current responses of the choline sensor upon varying the BSA concentration showed that the increased BSA amount increased choline current responses and also decreased the calibration factor and the crosslinking time, (3) the optimal BSA amount was 60 mg at 15 μL GAH concentration, (4) and the optimal final ChOx solution consisted ChOx (0.33 unit/μL), BSA (20 μg/μL) and glutaraldehyde (5×10^{-3} μL/μL).

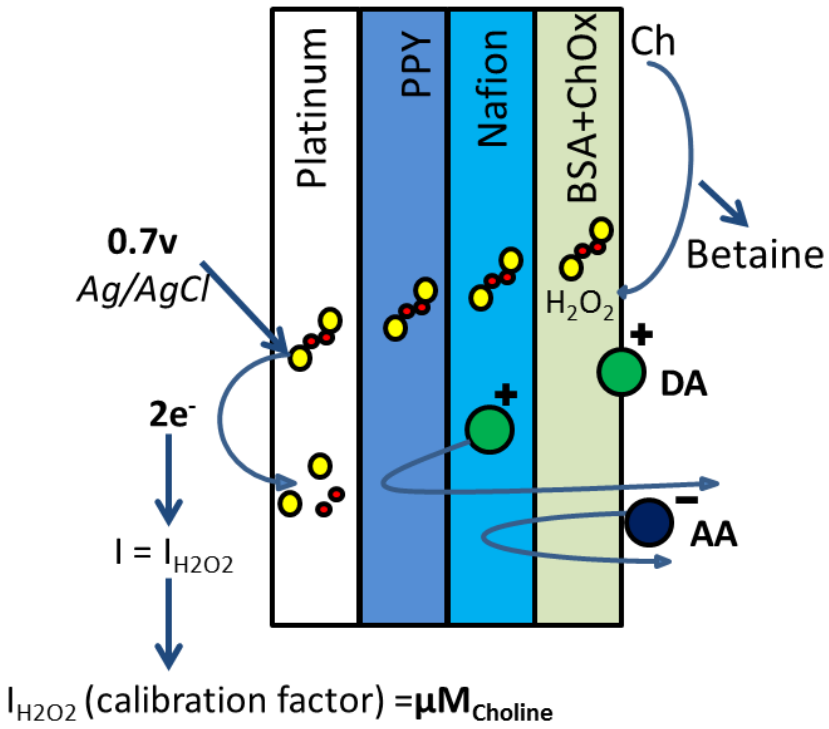

Figure 4.2 Schematic diagram of the choline sensor configuration.

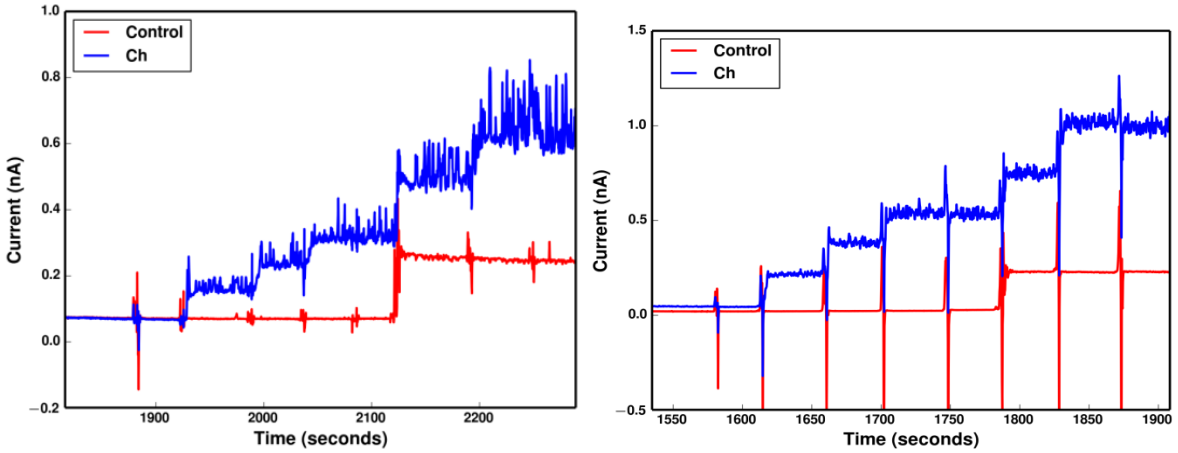

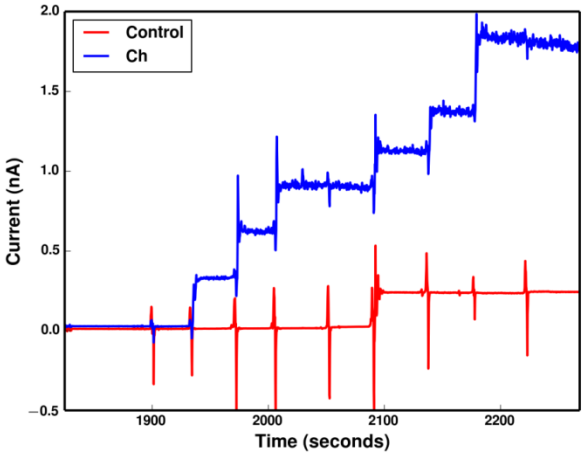

Figure 4.3 Sensing of choline at a constant potential of 0.7 V (vs. Ag/AgCl) when the BSA concentration was 10 mg, 20mg, and 60 mg, sequentially. The microprobe was tested with AA (250 µM), Ch (20 µM, 40 µM, 60 µM), DA (5 µM), H_2O_2 (20 µM), choline (100 µM), and DA (15 µM), sequentially.

4.3.2. Amperometric response of choline sensors at the Poly(m-PPD)/Nafion-modified platinum microelectrodes

4.3.2.1 Electrochemical polymerization of PPD on platinum microelectrodes

The permselectivity of ions or molecules through the polymer films was strongly controlled by the assemblrd structure of the films. The Pt surface was modified prior to immobilization of the enzyme layer by electropolymeriztion of PPD. The selectivity of PPD was reported to be improved significantly compared to other membranes, such as OPPy. Moreover, several authors have reported that Nafion improved the biocompatibility during *in vivo* implantation. The choline sensor was constructed by following the protocol of baking Nafion at 175 °C for 4 min first and then depositing PPD with cyclic voltammetry for 20 min [27]. However, about 0.15 nA current response was observed in the presence of AA and DA, respectively, which was not desirable. Also, the sensor resulted in a 0.2 nA current response for

choline, which did not display the advantages of utilizing PPD deposition. To improve the performance of choline sensors formed with electrodeposited by PPD, we optimized the process of PPD deposition (time interval and potential) and changed the PPD and Nafion coating sequence.

4.3.2.2 Effect of the PPD and Nafion coating sequence on electrochemical response to choline

This study investigated PPD deposition only without Nafion, PPD-Nafion, and Nafion-PPD films, respectively, for a choline sensor. When the microprobe was constructed with PPD and ChOx, sequentially, as shown in Fig. 4.4, the electrode showed no detectable response to AA or DA. Also, the current response of 0.6 nA to choline at 20uM was detected. In another experiment, we tested *in vitro* Pt microelectrodes modified with PPD, Nafion and ChOx. As shown in Fig. 4.5, excellent rejection of AA and DA was detected and about 0.5 nA choline response was detected. Finally, we tested the performance of choline sensor with the Nafion-PPD membrane. As shown in Fig. 4.6, no AA and DA response was detected. Also, about 0.45 nA response for choline was detected. However, this coating caused an inconsistent sensing result and also showed occasional responses to AA.

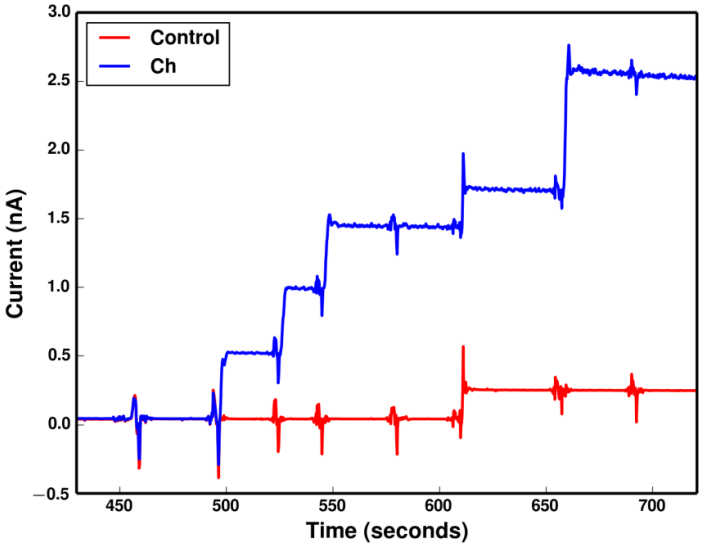

Figure 4.4 Sensing of choline at a constant potential of 0.7 V (vs. Ag/AgCl) with choline microbiosensors modified with PPD only and choline oxidase, sequentially. The microprobe was tested with AA (250 µM), Ch (20 µM, 40 µM, 60 µM), DA (5 µM), H_2O_2 (20 µM), choline (100 µM), and DA (15 µM), sequentially.

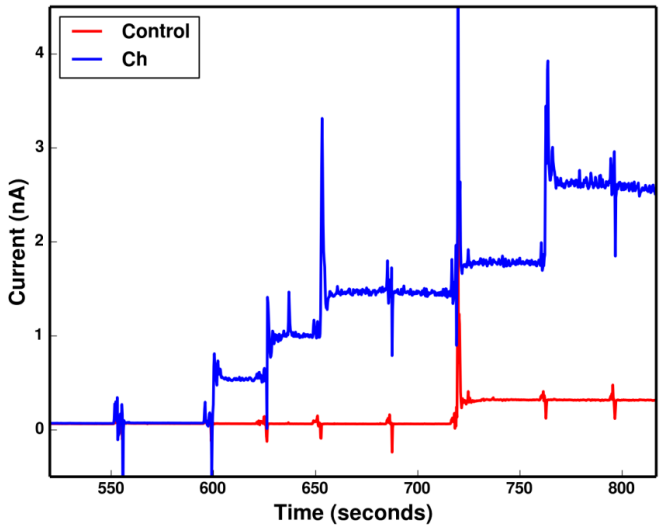

Figure 4.5 Sensing of choline at a constant potential of 0.7 V (vs. Ag/AgCl) with choline microbiosensors modified with a PPD-Nafion film and choline oxidase, sequentially. The

microprobe was tested with AA (250 µM), Ch (20 µM, 40 µM, 60 µM), DA (5 µM), H_2O_2 (20 µM), choline (100 µM), and DA (15 µM), sequentially.

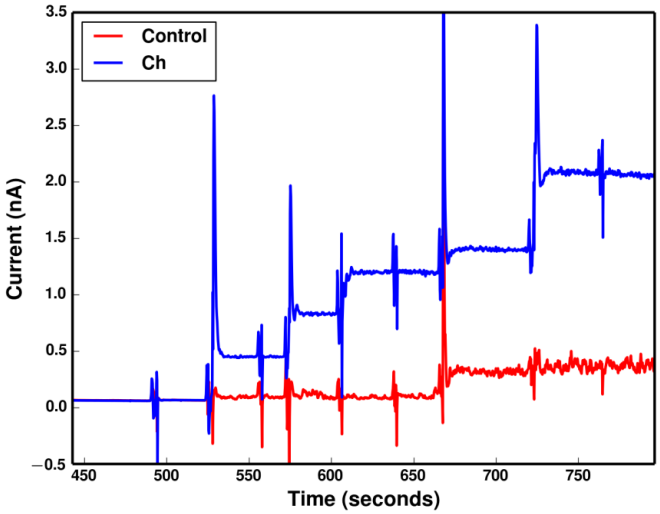

Figure 4.6 Sensing of choline at a constant potential of 0.7 V (vs. Ag/AgCl) with choline microbiosensors modified with a Nafion -PPD film and choline oxidase, sequentially. The microprobe was tested with AA (250 µM), Ch (20 µM, 40 µM, 60 µM), DA (5 µM), H_2O_2 (20 µM), choline (100 µM), and DA (15 µM), sequentially.

Table 4.1 compared the PPD, PPD-Nafion, Nafion- PPD and OPPy-Nafion membranes in terms of response time, consistency, selectivity, and detection limit. The PPD only membrane showed the highest sensitivity and detection limit among four membranes. We concluded that the PPD only membrane was promising in acute *in vivo* test. The PPD-Nafion membrane displayed the desirable sensitivity and detection limit, and good consistency. Then we concluded that the PPD-Nafion was most promising for chronic *in vivo* tests. The Nafion- PPD membrane was not recommended for *in vivo* tests because the results were not consistent and the sensor displayed a low selectivity performance again interfering species, AA. One possible explanation for this

phenomenon might be the changing of the PPD structure, since some of phenylenediamine molecular growth on top of Nafion membrane (due to Nafion as conducting polymer), leading to a layer that is less permeable to interferents. Thus, the PPD-Nafion membrane followed by immobilization of ChOx by using BSA and GAH as cross-linkers was chosen to deposit on working electrodes for later investigations.

	PPD Only	**PPD + Nafion**	**Nafion + PPD**	**PPY + Nafion**
H_2O_2 (nA)	~0.3	~0.3	~0.3	~0.25
Choline (nA)	~0.6	~0.5	~0.45	~0.35
AA, DA	No	No	Sometimes AA	No
Response Time (sec)	~1.8	~ 2	~3.2	~3
Consistancy	OK	Good	Not good	Good
Sensitivity/ $mA \cdot M^{-1} \cdot cm^{-2}$	~ 400	~ 390	~ 320	~ 250
Detection Limit/ µM	~ 0.16	~ 0.09	~ 0.05	~ 0.12

Table 4.1 Comparison of performance the PPD, PPD-Nafion, Nafion- PPD and OPPy-Nafion membranes deposited on choline sensors in terms of current responses of H_2O_2, choline, AA, and DA, response time, consistency, selectivity, and detection limit, respectively.

The above results were compared to work done by Gerhardt *et al* to assess the performance of our proposed choline sensor deposited by PPD and Nafion sequentially. Gerhardt *et al* utilized the biosensor that had four 15 × 333 μm platinum (Pt) recording sites arranged in pairs [28]. Based on his *in vitro* calibration recordings, the microprobe was tested with AA (250 μM), ACh (20 μM, 40 μM, 60 μM), Ch (20 μM), DA (20 μM) and NE (2 μM), sequentially [28]. At an applied potential of 0.7 V vs. a Ag/AgCl reference electrode, the biosensor sensitivity was 39.3 ± 3.9 pA/μM, which is equivalent to 186 ± 78 $mA \cdot M^{-1} \cdot cm^{-2}$ given the electrode size used, and the detection limit was 0.08 μM [28]. However, our fabricated biosensors had similar Pt recording sites area (40 × 100 μM) and we also added Ch progressively in 20 μM increment. Based on our data shown in Table 4.1, the sensitivity of the choline sensor deposited with PPD-Nafion membranes was 390 $mA \cdot M^{-1} \cdot cm^{-2}$ and the limit of detection was 0.09 μM. Although our fabricated choline sensors showed similar detection limit with that of Gerhardt *et al*, our sensors increased the sensitivity about 2 orders of magnitude. Thus, our proposed choline sensor was promising to use.

4.3.3 Amperometric response of choline sensors with deposited platinum black and an on-probe IrOx on reference electrode

4.3.3.1 Choline sensing using an on-probe IrOx reference electrode

Using iridium oxide (IrOx) as the reference electrode material makes it attractive for *in vivo* neurosceience applications, because IrOx is stable, biocompatible, and nontoxic over a range of potentials and in the presence of the ions and other components of brain extracellular fluid [21]. Our previous work has demonstrated that by placing the RE on the same platform as the working electrode, baseline RMS noise at the working electrode was found to be diminished by 61 ± 8% (95% confidence interval, n=23) [21]. This noise reduction greatly improved the

sensing electrode detection limit, especially in freely-moving rodent studies where noise was increased due to animal movement. Sensors using on-probe IrOx can also selectively detect choline and reject common electroactive species in brain extracellular fluid, of which AA and DA are most important. However, as shown in Fig. 4.7, an IrOx film on a Pt microelectrode used as an on-probe RE for amperometric sensing systems encountered the sharp current drop issue sometimes at a high current level in choline sensor calibration, where the linear range was 20-80 μM.

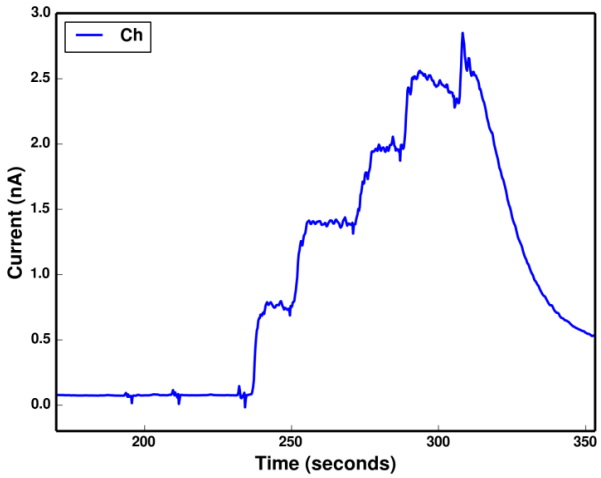

Figure 4.7 On-probe IrOx reference glutamate sensor calibration figure. The microprobe was tested with AA, DA, and choline (5 times) sequentially.

4.3.3.2 Choline sensing for the Pt-black modified electrode followed by an on-probe IrOx on reference electrode

In an attempt to combine improved selectivity and response time in a single, easy-to-assemble probe, we constructed a choline microbiosensor by electrochemically depositing Pt-black, IrOx, and Nafion sequentially on reference electrode. Pt-black, a "spongy" electrodeposit of platinum, leaded more IrOx deposition due to its large effective surface area.

Two working electrode sites were deposited with PPD, Nafion, and ChOx and the control site was deposited without ChOx. The scheme in Fig. 4.8 illustrates the biosensor design, as described in the methods section. The microbiosensor detection limit at a given potential was estimated based on an analysis of signal to noise ratio. The background noise was 2 to 5 times smaller than that of separate Ag/AgCl reference electrode. The detection limit was estimated at 0.04 µM at operating potential of 0.6 V.

Fig. 4.9 shows representative microbiosensor response to sequential injections of choline in SPB buffer solution. At 0.6 V, average microbiosensor sensitivity was 440 $\text{mA} \cdot \text{M}^{-1} \cdot \text{cm}^{-1}$ over a linear range of 20 to 156 µM choline. The detection limit was 0.04 µM. As important as it is for the microbiosensor to be sensitive to choline, it is equally important for it to be insensitive to electroactive interferents, especially AA and DA in brain extracellular fluid (ECF). Fig. 4.9 also shows that the microbiosensor gave no detectable response to either AA or DA. In summary, we introduced Pt-black in terms of an add-on functionalization process to increase the electrode roughness at significantly reduced costs and enhanced IrOx deposition.

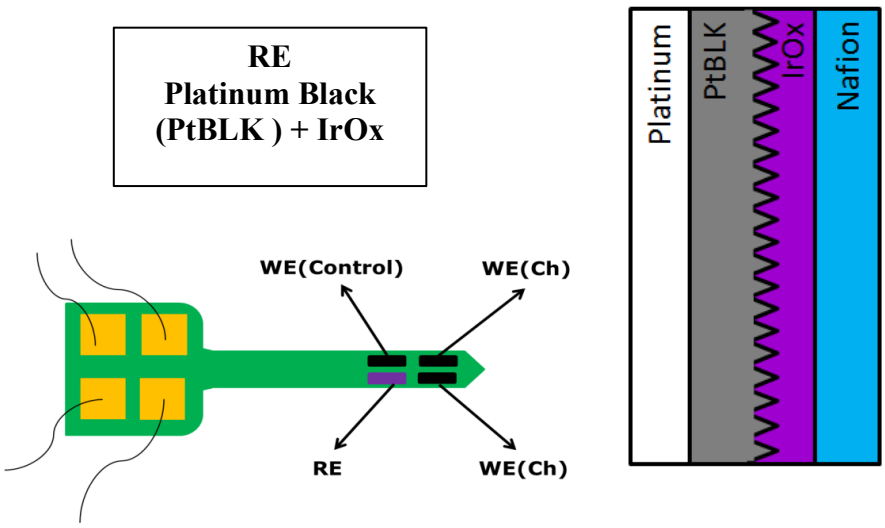

Figure 4.8 Schematic diagram of the on-probe Pt-black/IrOx RE choline sensor configuration.

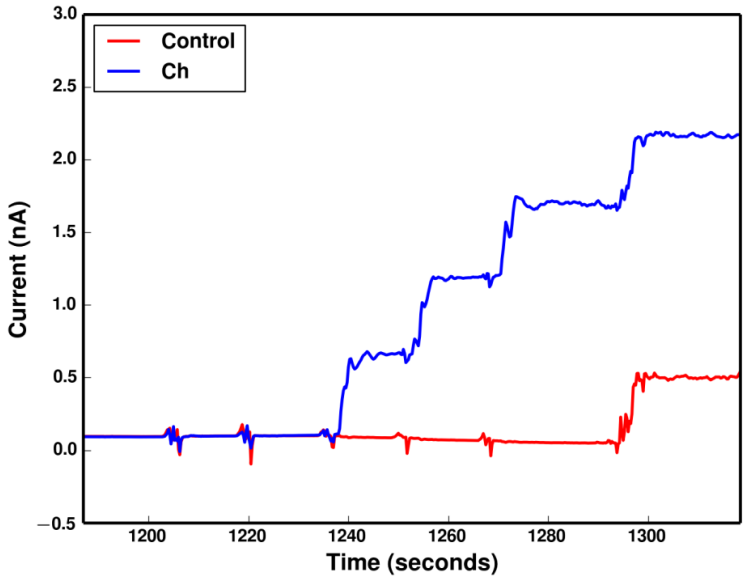

Figure 4.9 Choline sensing for the Pt-black modified electrode followed by an on-probe IrOx on reference electrode. The microprobe was tested with AA (250 µM), DA (5 µM), choline (20 µM, 40 µM, 60 µM), and H_2O_2 (20 µM), sequentially.

4.3.4. Evaluation of nanostructured platinum grass on performance of choline sensors

4.3.4.1 Comparing structures and components of Pt-grass and PtBlk

Pt-black is a good material to improve IrOx deposition, but Pt-black has been reported to involve the use of toxic heavy metal lead as an electrolyte ingredient and traces of lead that elute from the final coating *in vivo* cause cytotoxic reaction. Although acute *in vivo* experiments were feasible, using Pt-black for chronic *in vivo* tests was not recommended [29]. A new material called nanostructured platinum grass was used to replace Pt-black [24]. In comparison to the

platinum black deposition, all chemicals used for the Pt-grass formation were free of cytotoxic components. (More about Pt-grass will be discussed in Chapter 5)

4.3.4.2 Choline sensing for the Pt-grass modified electrode followed by an on-probe IrOx on reference electrode

As reported in previous sections, an on-probe IrOx reference electrode reduced noise and fastened the response time, so we constructed a choline microbiosensor by electrochemically depositing Pt-grass, IrOx, and Nafion sequentially on reference electrode. Similar to the Pt-black modified electrode, two working electrode sites of the Pt-grass modified electrode were also deposited with PPD, Nafion, and ChOx and the control site was deposited without ChOx. The scheme in Fig. 4.10 illustrated the biosensor design, as described in the methods section. The choline biosensor displayed a detection limit of 0.07 μM at an operating potential of 0.6 V. At 0.6 V, and the average microbiosensor sensitivity was 310 $\mathrm{mA \cdot M^{-1} \cdot cm^{-1}}$ over a linear range of 20 to 172 μM choline. Fig. 4.11 also did not show detectable response to either AA or DA. Thus, when Pt-grass was deposited on the top of bare Pt microsensor in order to increase the amount of deposition of IrOx, the application of our proposed choline sensor *in vivo* was valid because values of sensitivity and detection limit were desirable.

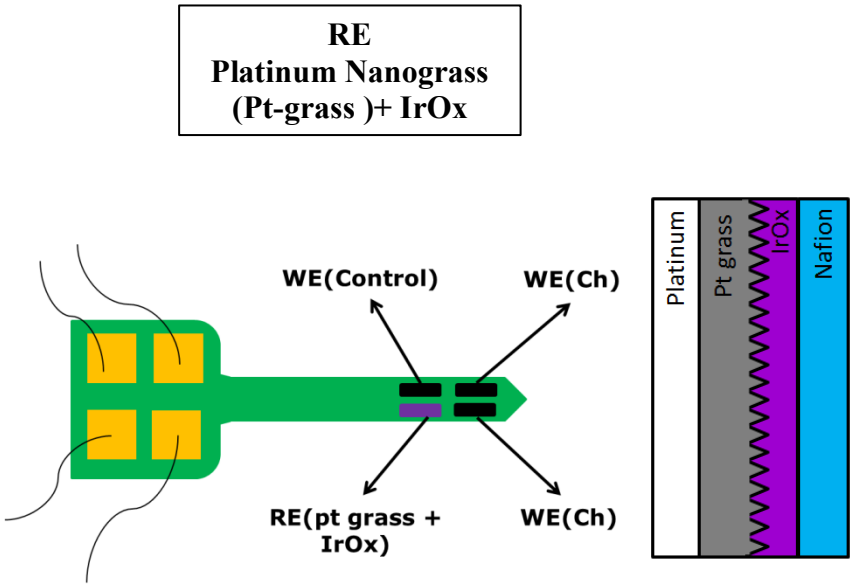

Figure 4.10 Schematic diagram of the choline sensor configuration.

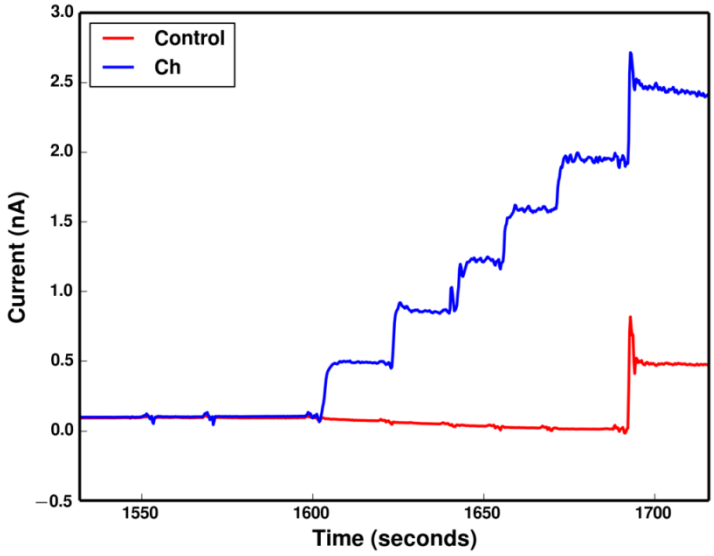

Figure 4.11 Choline sensing for the Pt-grass modified electrode followed by an on-probe IrOx on reference electrode. The microprobe was tested with AA (250 µM), DA (5 µM), choline (20 µM, 40 µM, 60 µM, 80 µM, 100 µM), and H_2O_2 (20 µM), sequentially.

4.3.5 Selectivity against electroactive interferents

The choline biosensors selectivity against interferents was tested, including AA, DA, DOPAC, DOPA, and uric acid (UA) in brain extracellular fluid at typical physiological concentrations. The selectivity was defined here as the ratio of sensitivity to the choline by that for the interferent. The choline biosensors showed excellent selectivity for choline against the interferents. Average selectivity ratios of choline to AA (250 μM), DA (12.5 μM), DOPAC (50 μM), and UA (250 μM) were all more than at least 1000:1 for the choline biosensors. This indicates that permselective polymers deposited at the electrode surface of our proposed choline biosensors *in vivo* effectively exclude interferents.

4.3.6 Preliminary in vivo results

Following are the preliminary *in vivo* anesthetized recording results of our choline sensor. The Fig 4.12 shows the *in vivo* anesthetized recording result of choline sensor with extra Ag/AgCl reference electrode. It is obviously found that when the 450 nm blue light laser illuminates the nac regions of the rat brain with optogenetics, choline is released and the concentration of choline is increased in brain. This is indicated by the increase of difference between the current on working site and on control site.

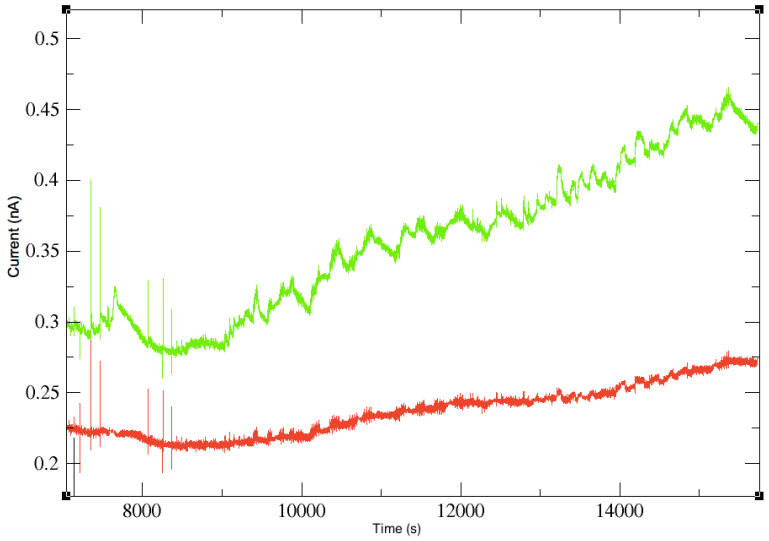

Figure 4.12 *in vivo* anesthetized recording result of choline sensor with separate Ag/AgCl reference electrode. The red line indicates the current versus time on control site, while the green line indicates the one on choline sensing site.

Fig 4.13 shows the *in vivo* anesthetized recording result of choline sensor with on-probe IrOx reference electrode. It is shown in the figure that two light signals stimulated are brain at ~600 s and ~1750 s, respectively. After the second signal, the current difference between green line and red line increase as expected. However, the difference actually decreases after the first signal, which is totally unexpected. This is the first and only *in vivo* experiment of our IrOx choline sensor, so more work should be done to give the final conclusion.

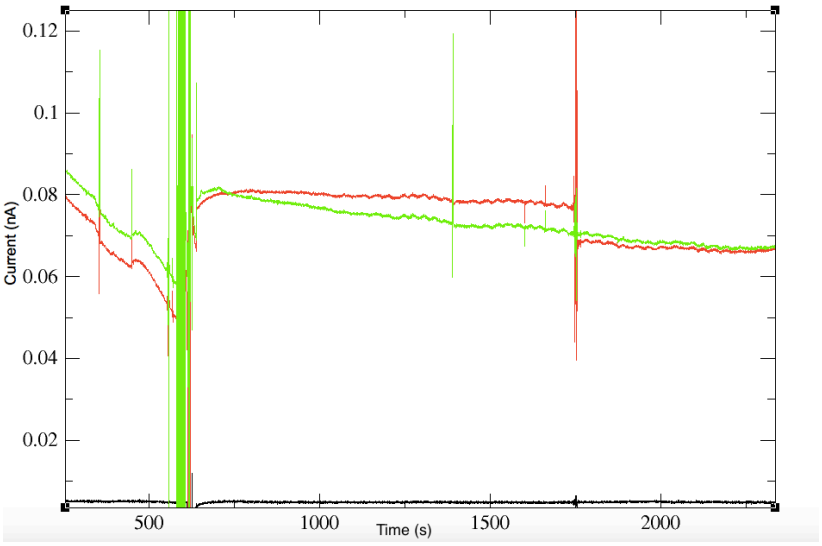

Figure 4.13 *in vivo* anesthetized recording result of choline sensor with on-probe IrOx reference electrode. The red line indicates the current versus time on control site, while the green line indicates the one on choline sensing site.

Fig 4.14 shows the in vivo noise comparison between Ag/AgCl and IrOx reference electrode. It can be obviously found that Ag/AgCl has much greater background noise (over 5 times greater than IrOx). The lower background noise could lead to lower detection limit.

To summarize, positive results of Ag/AgCl reference electrode is observed *in vivo*. Compared with Ag/AgCl, IrOx has lower background noise that could bring lower detection limit. However, only limited results are present to verify the effectiveness of IrOx in the *in vivo* anesthetized recording experiments. In the future, more *in invo* experiment should be done to verify the feasibility of using IrOx reference electrode.

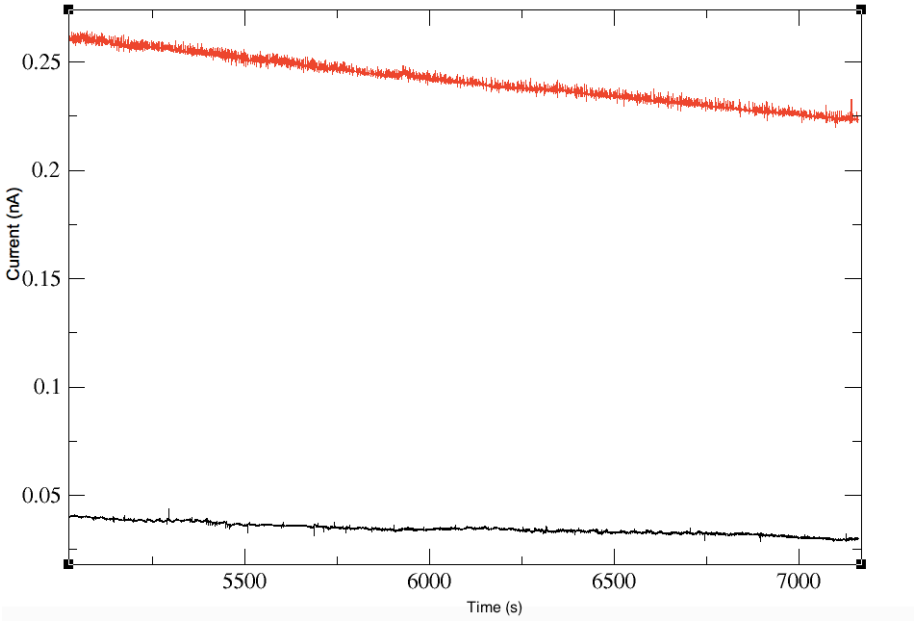

Figure 4.14 *in vivo* background noise comparison between Ag/AgCl and IrOx reference electrode. The red line indicates the current v.s. time for Ag/AgCl, while the black line indicates the one for IrOx.

4.4 Conclusions

A high sensitivity amperometric choline biosensor was developed with PPD and Nafion coating, as well as ChOx/BSA/GAH loading. The results showed that the permselective PPD film can successfully be employed as a suitable matrix for choline detection without responses to AA and DA. In comparison with other studies, better sensitivity and lower detection limit were achieved. Our sensor also had relatively broad linear range, good selectivity against interferents and stability. The Pt-black or Pt-grass that enhanced on probe IrOx reference choline sensor made the baseline noise much smaller than that of separate Ag/AgCl reference electrode and made the sensor size smaller for the *in vivo* surgery. All these good features suggest that the choline biosensor is a promising candidate for applications *in vivo*.

4.5 References

[1] Misgeld, T., Burgess, R. W., Lewis, R. M., Cunningham, J. M., Lichtman, J. W., and Sanes, J. R. Roles of Neurotransmitter in Synapse Formation, *Neuron 36*, 635-648.

[2] Panfili, G., Manzi, P., Compagnone, D., Scarciglia, L., and Palleschi, G. (2000) Rapid Assay of Choline in Foods Using Microwave Hydrolysis and a Choline Biosensor, *Journal of Agricultural and Food Chemistry 48*, 3403-3407.

[3] Zeisel, S. H. (2006) Choline: Critical Role During Fetal Development and Dietary Requirements in Adults, *Annual review of nutrition 26*, 229-250.

[4] Khan, A., Khan, A. A. P., Asiri, A. M., Rub, M. A., Azum, N., Rahman, M. M., Khan, S. B., and Ghani, S. A. (2013) A New Trend on Biosensor for Neurotransmitter Choline/Acetylcholine—an Overview, *Applied Biochemistry and Biotechnology 169*, 1927-1939.

[5] Rinne, J. O., Myllykyla¨, T., Lo¨nnberg, P., and Marjama¨ki, P. i. (1991) A postmortem study of brain nicotinic receptors in Parkinson's and Alzheimer's disease, *Brain Research 547*, 155-158.

[6] Li, J., and El Rassi, Z. (2002) High Performance Liquid Chromatography of Phenolic Choline Ester Fragments Derived by Chemical and Enzymatic Fragmentation Processes: Analysis of Sinapine in Rape Seed, *Journal of Agricultural and Food Chemistry 50*, 1368-1373.

[7] Campanella, L., Tomassetti, M., and Sammartino, M. P. (1988) Enzyme sensor for the determination of choline-containing phospholipids in some biological fluids, *Analyst 113*, 77-80.

[8] Tsafack, V. C., Marquette, C. A., Pizzolato, F., and J. Blum, L. c. (2000)

Chemiluminescent choline biosensor using histidine-modified peroxidase immobilised on metal-chelate substituted beads and choline oxidase immobilised on anion-exchanger beads co-entrapped in a photocrosslinkable polymer, *Biosensors and Bioelectronics 15*, 125-133.

[9] Leca-Bouvier, B. D., Sassolas, A., and Blum, L. J. (2014) Polyluminol/hydrogel composites as new electrochemiluminescent-active sensing layers, *Analytical and Bioanalytical Chemistry 406*, 5657-5667.

[10] Zhang, H., Yin, Y., Wu, P., and Cai, C. (2012) Indirect electrocatalytic determination of choline by monitoring hydrogen peroxide at the choline oxidase-prussian blue modified iron phosphate nanostructures, *Biosens. Bioelectron. 31*, 244-250.

[11] Keihan, A. H., Sajjadi, S., Sheibani, N., and Moosavi-Movahedi, A. A. (2014) A highly sensitive choline biosensor based on bamboo-like multiwall carbon nanotubes/ionic liquid/Prussian blue nanocomposite, *Sensors and Actuators B: Chemical 204*, 694-703.

[12] Baker, K. L., Bolger, F. B., and Lowry, J. P. (2015) A microelectrochemical biosensor for real-time in vivo monitoring of brain extracellular choline, *Analyst 140*, 3738-3745.

[13] Hamdi, N., Wang, J., and Monbouquette, H. G. (2005) Polymer films as permselective coatings for H2O2-sensing electrodes, *J. Electroanal. Chem. 581*, 258-264.

[14] Gerhardt, G. A., Oke, A. F., Nagy, G., Moghaddam, B., and Adams, R. N. (1984) Nafion-coated electrodes with high selectivity for CNS electrochemistry, *Brain Research 290*, 390-395.

[15] Hsueh, C., and Brajter-Toth, A. (1994) Electrochemical Preparation and Analytical Applications of Ultrathin Overoxidized Polypyrrole Films, *Analytical Chemistry 66*, 2458-2464.

[16] C. J. S. M. Silva *et al, Food Technol. Biotechnol. 42* (1) 51–56 (2004).v

[17] Shah, S., Sharma, A., and Gupta, M. N. (2006) Preparation of cross-linked enzyme aggregates by using bovine serum albumin as a proteic feeder, *Analytical Biochemistry 351*, 207-213.

[18] Rothwell, S. A., Killoran, S. J., and O'Neill, R. D. (2010) Enzyme Immobilization Strategies and Electropolymerization Conditions to Control Sensitivity and Selectivity Parameters of a Polymer-Enzyme Composite Glucose Biosensor, *Sensors (Basel, Switzerland) 10*, 6439-6462.

[19] Sasso, S. V., Pierce, R. J., Walla, R., and Yacynych, A. M. (1990) Electropolymerized 1,2-diaminobenzene as a means to prevent interferences and fouling and to stabilize immobilized enzyme in electrochemical biosensors, *Analytical Chemistry 62*, 1111-1117.

[20] Wahono, N., Qin, S., Oomen, P., Cremers, T. I. F., de Vries, M. G., and Westerink, B. H. C. (2012) Evaluation of permselective membranes for optimization of intracerebral amperometric glutamate biosensors, *Biosensors and Bioelectronics 33*, 260-266.

[21] Tolosa, V. M., Wassum, K. M., Maidment, N. T., and Monbouquette, H. G. (2013) Electrochemically deposited iridium oxide reference electrode integrated with an electroenzymatic glutamate sensor on a multielectrode array microprobe, *Biosens. Bioelectron. 42*, 256-260.

[22] Tsopela, A., Lale, A., Vanhove, E., Reynes, O., Séguy, I., Temple-Boyer, P., Juneau, P., Izquierdo, R., and Launay, J. (2014) Integrated electrochemical biosensor based on algal metabolism for water toxicity analysis, *Biosensors and Bioelectronics 61*, 290-297.

[23] Schuettler M et al, 10th Annual Conference of the International FES Society.

[24] Boehler, C., Stieglitz, T., and Asplund, M. (2015) Nanostructured platinum grass enables

superior impedance reduction for neural microelectrodes, *Biomaterials 67*, 346-353.

[25] Wassum, K., Vanessa, T.M, Wang, J.J, Walker, E., Monbouquette, H.M., Maidment, N.T., Silicon wafer-based platinum microeletrode array biosensor for near real-time measurement of gluatmate *in vivo*, Sensors 2008, 8 (8), 5023-5036.

[26] Guerrieri, A., De Benedetto, G. E., Palmisano, F., and Zambonin, P. G. (1995) Amperometric sensor for choline and acetylcholine based on a platinum electrode modified by a co-crosslinked bienzymic system, *Analyst 120*, 2731-2736.

[27] Anal. Chem. 2004, 76, 1098-1106.

[28] Gerhardt, *et al*., Eur. J. Neurosci. 2006, 24, 2749-2757.

[29] Shih T. and Hanin I., *Psychopharmacology* 58, 263-269 (1978).

Chapter 5: An electroenzymatic choline microsensor based on a nanostructured platinum microelectrode

Abstract

A microelectrode array microprobe with a choline sensing site and an on-probe reference electrode was constructed by depositing permselective polymer films and choline oxidase, and IrOx, respectively, on Pt microelectrodes coated with a nanostructured Pt deposit. The nanostructured Pt coating was deposited from a solution of H2PtCl6 and formic acid at reducing potential and the organized structure of the deposit, as observed by scanning electron microscopy, is referred to as Pt nanograss. Polyphenylenediamine (PPD) and Nafion were coated sequentially on the working (i.e., sensing) electrode surface to serve as permselective polymers. The choline sensor was tested at physiological concentrations of electroactive interfering species common to brain extracellular fluid (i.e., ascorbic acid, dopamine, DOPA, and DOPAC) and choline. The microsensor with on-probe IrOx reference showed high sensitivity (~123 μA mM-1 cm-2), low detection limit (~3 μM), fast response time (~3-5 s) and excellent selectivity. Selectivity likely was aided by the relatively low potential of 0.35 V vs. IrOx that was made possible by the apparently enhanced H2O2 electrooxidation activity of the underlying Pt nanograss-coated working electrode. Therefore, Pt nanograss appears to be an excellent Pt surface modification for creation of electroenzymatic biosensors for in vivo applications.

5.1 Introduction

Choline is a precursor and metabolite of the neurotransmitter acetylcholine. It can serve as a surrogate for acetylcholine measurement due to the rapid hydrolysis of acetylcholine to choline catalyzed by acetylcholine esterase in the brain. Therefore, the monitoring of choline is of importance to neuroscience, especially in the study of Alzheimer'sand Parkinson's diseases. Among the various methods available for choline sensing, amperometric choline oxidase (ChOx)-based biosensors have attracted considerable attention due to their simplicity, rapid response, high sensitivity and low cost. In these biosensors [1-4], choline detection is achieved by electrooxidation of the H2O2 produced during oxidation of choline catalyzed by choline oxidase:

$$\text{Choline} + 2O_2 + H_2O \xrightarrow{\text{ChOx}} \text{betaine} + 2H_2O_2$$

However, a drawback of this method is the high potential normally used for H2O2 electrooxidation. Many electroactive interfering substances present in brain extracellular fluid such as ascorbic acid (AA) dopamine (DA) can be electrooxidized at the potentials used to give false current signals. In order to solve this problem, several approaches have been explored to biosensor design for reduction of interference. Modification of the electrode surface by polymetric memberane permeable to H2O2 and impermeable to interfering species is one of the most effective methods to address this problem. For example, overoxidized polypyrrole (OPPy) could be used to reject DA. [5-6] The perfluoronated ionomer, Nafion, is commonly used to exclude anionic interferents.[7].

Alternative method that are not dependent on permseletive species had also been explored, such as operating at reducing potentials sufficient for H2O2 reduction using an extra

enzyme horseradish peroxidase or redox mediators.[8] However, the response of the mediated biosensors also faces challenges such as oxidation promotion of interferents by some mediators themselves.

By using some surface modification materials (such as Pt black) to enlarge the surface area may also result in potential reduction. Pt black has been shown to be one of the best electrode materials for oxidation of H_2O_2. [9] Hamdi et al. [10] demonstrated that by depositing Pt black on a Pt wire to be used for glutamate microsensor fabrication, the sensor working potential could be set at 0.45 V versus Ag/AgCl (as opposed to ~0.7 V in the usual case with polished Pt electrodes) without a loss in sensor performance. It was also mentioned that the good performance at reduced working potential is due at least partially to altered catalytic properties and is not merely the result of an increase in the electroative surface area. [11] However, practical applicability of Pt black is limited as a consequence of its low mechanical stability. [12-14] In addition, Pt black has been reported to cause a cytotoxic reaction presumably due to elution of traces of lead that were used in the fabrication of the deposit.[15]

Recently, Boehler et al. introduced a nanostructured Pt-coating. [16] In comparison to Pt black deposition, all chemicals used in this deposition process are non-cytotoxic. The grass-like nanostructure was found to reduce the impedance by almost two orders of magnitude compared to bare polished electrode surfaces. The Pt-grass coating method is performed via a simple electrochemical process that can be applied to virtually any possible electrode type and accordingly shows potential as a universal impedance reduction strategy. Their elution tests revealed non-toxicity of the Pt-grass and the coating was found to exhibit strong adhesion to the metallized substrate. Thus, the nanostructured Pt-coating could be an excellent replacement for Pt black provided it also enables operation of H2O2 sensing electrodes at reduced potential.

Smaller electrodes used for neurochemical monitoring in vivo cause reduced tissue damage and provide improved spatial and temporal resolution. However, in conjunction with the sensing electrode (the working electrode) a reference electrode (RE) must be provided to complete an electrochemical sensing system. Currently, a separate RE, typically Ag/AgCl is used in most in vivo studies.[17-21] However, Ag/AgCl is unstable, causes an inflammatory response and requires a separate penetration into the brain. Recently, Tolosa et al. reported the construction of a biocompatible iridium oxide (IrOx) RE on the same microprobe with the multielectrode sensing array. [22, 23-25] The reported multielectrode sensing device with on-probe reference showed reduced baseline noise, by an average of ~61% in vitro and ~71% in vivo with reduced tissue damage, which can result in improved detection limits.

Currently, we are fabricating an implantable, micromachined microprobe with a microsensor array for monitoring of multiple neurotransmitters, including glutamate (Glut), choline, and dopamine (DA), by constant potential amperometry. [26] This study focuses on the creation of an improved choline microsensor based on an underlying Pt electrode with a nanostructured Pt-coating. This Pt-coating also was used in the construction of a high surface area on-probe reference electrode. We demonstrate that this nanostructure Pt coating provides a feasible approach for construction of electoenzymatic microsensors operable at reduced potential and of biocompatible, on-probe REs that reduce noise and tissue damage.

5.2 Experimental Setup

5.2.1 Materials

Choline oxidase (Alcaligenes, 9028-67-5), m-phenylenediamine, Nafion® (5%), glutaraldehyde solution (25%), bovine serum albumin (BSA) lyophilized powder, 3,4-dihydroxyphenylacetic acid, 3,4-dihydroxy-DL-phenylalanine, (-)-epinephrine (+)-bitartrate

salt, DL-norepinephrine hydrochloride, serotonin hydrochloride, hydrogen peroxide solution (30%), choline hydrochloride, D-(+)-glucose, iridium tetrachloride hydrate, oxalic acid dehydrate (99%); L-ascorbic acid, dopamine hydrochloride, formic acid, chloroplatinic acid hexahydrate were purchased from Sigma-Aldrich (St. Louis, MO). Isopropyl alcohol and 1M sulfuric acid solution were obtained from Fisher Scientific (Pittsburgh, PA). Ag/AgCl glass-bodied reference electrodes with 3 M NaCl electrolyte, 0.5-mm-diameter Pt wire auxiliary electrodes and disk Pt electrodes (1.6 mm dia.) were purchased from BASi (West Lafayette, IN). Sodium phosphate buffer (PBS, pH 7.4) was composed of 50 mM sodium phosphate (dibasic) and 100 mM sodium chloride. Ultrapure water was generated using a Millipore Milli-Q Water System and was used for preparation of all solutions.

5.2.2 Instrumentation and electrochemical measurements

Electrochemical measurements were performed using a Versatile Multichannel Potentiostat equipped with the 'p' low current option and low current N0 stat box (VMP3, Bio-Logic USA LLC, Knoxville, TN, USA) or a multichannel FAST-16 potentiostat (Quanteon, LLC, Lexington, KY, USA). A standard three-electrode system was used with the VMP3 system, consisting of either an on-probe Pt site or a separate Pt-wire as a counter electrode; modified sites on our MEA as the working electrodes; and as RE, either an on-probe IrOx site or a separate AgCl-coated Ag wire (Bioanalytical Systems, Inc., West Lafayette, IN, USA. Constant potential amperometric measurements were conducted in PBS buffer either at 0.45 V vs. Ag/AgCl or 0.35 V vs. on-probe IrOx reference electrode at ambient laboratory temperature. Sufficient equilibration time in PBS buffer was required to achieve a stable current before adding analytes. A Nova 600 was used for SEM images. A Nova 600 was used for SEM images.

5.2.3 Microsensor preparation

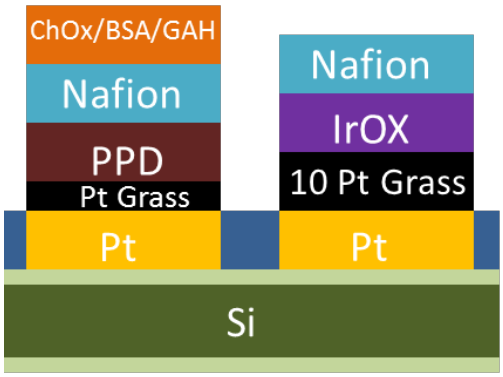

Figure 5.1 Schematic diagram of the choline sensor configuration. The left site is the choline working electrode coated with Pt nanograss, PPD, Nafion and enzyme layers. The right site is the IrOx reference electrode coated with Pt grass (10 times concentrated Pt nanograss solution was used), IrOx and Nafion.

The microelectrodes used in this work were silicon-based multielectrode arrays manufactured at UCLA using microelectro-mechanical-system (MEMS) technologies. The fabrication and array details are described in previous work.[27-28] The MEA consists of four ~6000 μm2 Pt sites, situated in pairs at the tip of a 9-mm-long shank. The pair nearest the shank tip is 100 μm from the pair farthest from the shank tip, and the paired sites are 40 μm apart. Each site was modified accordingly, to act either as a working, reference, or counter electrode.

The platinum nanograss was deposited in a chemical reduction reaction using an aqueous solution of 2.5 mM H2PtCl6 and 1.5 mM formic acid (1X solution) and 25 mM H2PtCl6 and 15 mM formic acid (10X solution). Pt-grass formation was conducted potentiostatically from the H2PtCl6 solution at -0.1 V vs Ag/AgCl for 300 s.[16] For the reference electrode, IrOx was electrodeposited following the method described by Yamanaka et al. and Tolosa et al. [22,29] after Pt nanograss deposition. [22] For Pt black deposition, a deposit was forced on the cleaned electrodes by cycling potential between 1.4 and 2.0 V at 500 mV/s for a total of 15 cycles in a

vigorously stirred plating solution. The plating solution consisted of 1% chloroplatinic acid, 0.0025% HCl, and 0.01% lead acetate in water, which was Ar-purged for 15 min prior to use. [10]

The choline sensing microelectrodes were created according to the general guidelines of our previously developed procedure except that PPD was electrodeposited instead of polypyrrole (PPy) from a solution of 5 mM PD in PBS (pH 7.4) by holding the voltage constant at 0.85 V for 5 min. The anionic polymer, Nafion, was deposited on all sites by rapid dip-coating of the probe tips in the Nafion solution and oven-casting at 175 °C for 4 min, followed by a 3-min cooling period in ambient air. After the polymer treatments, enzyme immobilization by chemical crosslinking was accomplished using a solution consisting of ChOx (0.33 unit/μL), BSA (20 μg/μL) and glutaraldehyde (5 × 10-3 μL/μL). While working under a microscope, a small drop of the solution was formed on a syringe tip and the drop was gently swiped across the bottom two microelectrode sites at the probe tip. Apply another swipe after the surface was dry. This swipe was repeated eleven more times. The resultant working electrodes (WEs) were used to sense choline by electroenzymatic amperometry.

Microelectrode sites coated with Pt grass, PPD, Nafion and ChOx are referred to here as the working electrode (WE). In contrast, microelectrode sites coated with Pt grass, IrOx and Nafion are referred to here as on-probe reference electrode (RE). The biosensors were sealed in a container with desiccant and stored dry at 4 °C for 48 h prior to testing. Fig. 5.1. is a schematic diagram showing the configuration of the working electrode and reference electrode.

5.3 Results and Discussion

5.3.1 Surface morphologies of Pt nanograss and Pt black

The surface morphologies of Pt nanograss and Pt black were imaged by SEM. As shown in Fig. 5.2 (a)-(d), Pt nanograss was grown from the surface and has a well-organized structure similar to that shown by Boehler et al. [16] Compared to 1X Pt nanograss (Fig. 5.2(a) and (b)), 10X Pt nanograss (Fig. 5.2(c) and (d)) appears thicker with a more uniform pillar-like structure. On the other hand, Pt black appears as an irregular, nonuniform deposit, Fig. 5.2(e) and (f). This difference in the structure could explain the superior mechanical stability of Pt nanograss compared to Pt black, whose practical applicability is limited as a consequence. Also, the random structure of Pt black could be a source of the excessive noise observed with electrodes coated with this material. In addition, Pt black-coated electrodes were reported to be cytotoxic due to traces of lead remaining from the deposition process.[15] In contrast the biocompatibility of the Pt-nanograss coating was validated by Boehler et al.[16]

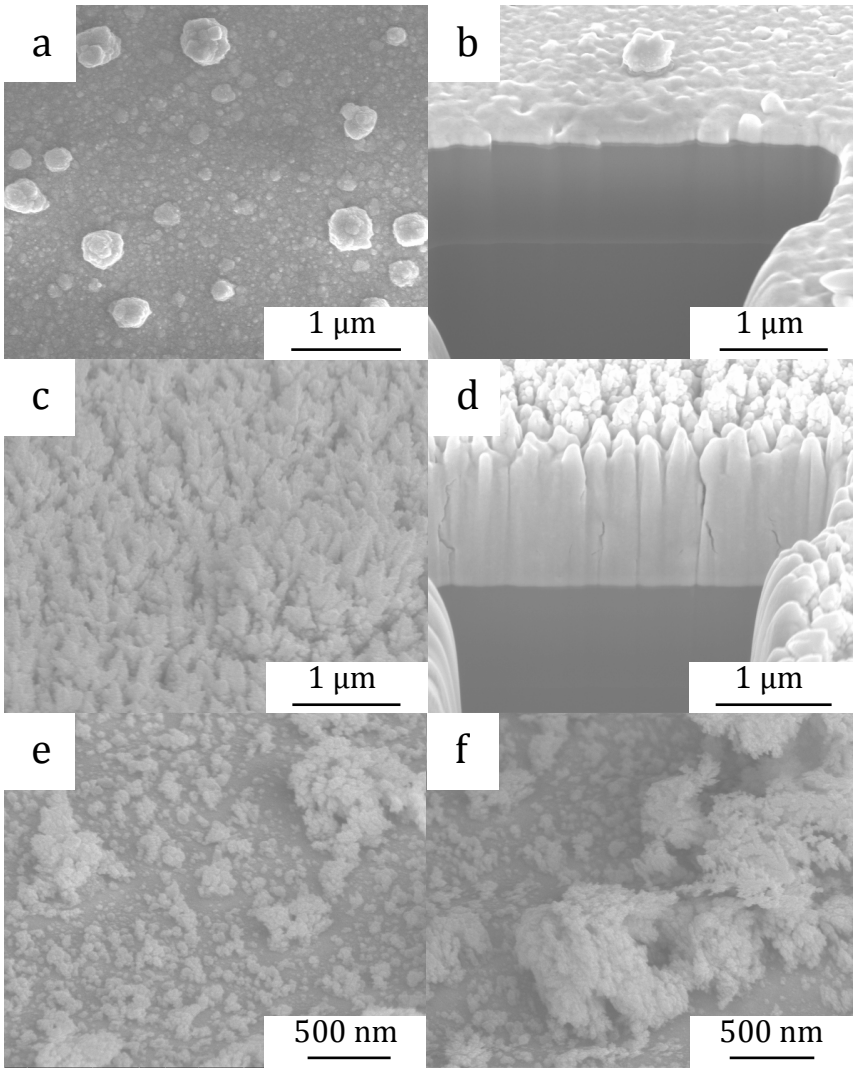

Figure 5.2. Scanning electron microscopic (SEM) images of (a) Top view of Pt/Pt-nanograss (1X), (b) Cross section view of Pt/Pt-nanograss (1X) (c) Angled top view of Pt/Pt-nanograss (10X), (d) Cross section view of Pt/Pt-nanograss (10X), and (e, f) Angled top view of Pt black.

5.3.2 Pt grass utilized for working electrode and Ag/AgCl as reference electrode

A working electrode was coated with 1X Pt nanograss, followed by PPD, Nafion and an enzyme coating. The enzyme mixture was prepared without choline oxidase for a control site. After testing choline microbiosensor with choline at different voltages, it was observed that at

potentials of 0.45 V and higher, the sensitivity remains essentially constant. At potentials lower than 0.45 V, the sensitivity decreased modestly. Thus, the working potential for further study was set at 0. 45 V.

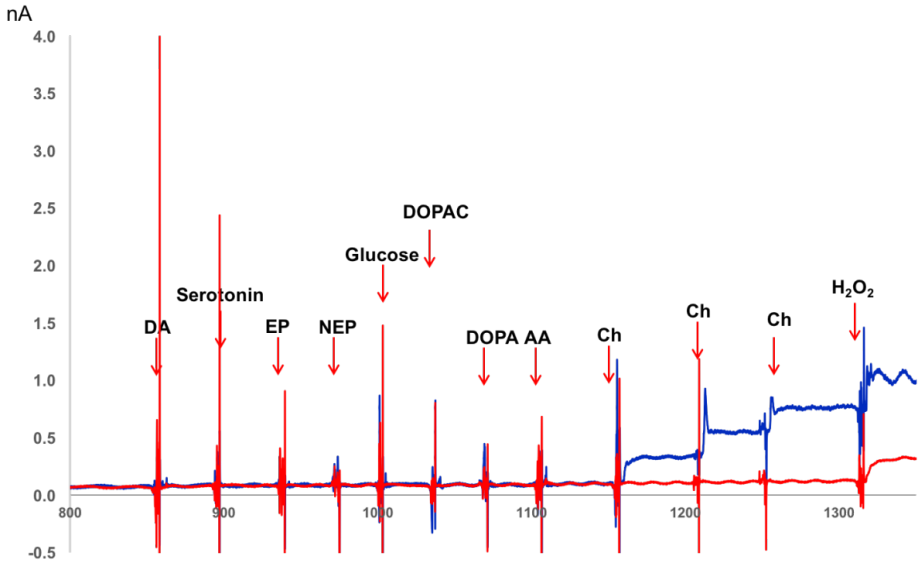

Figure 5.3. Current response of the choline biosensor to electroactive interferents, choline, and H2O2. The biosensor response at a constant potential of 0.45 V (vs. Ag/AgCl) was monitored in stirred solution upon sequential injections to give 12.5 µM DA, 5 µM Serotonin, 12.5 µM EP, 12.5 µM NEP, 0.8 mM Glucose, 50 µM DOPAC, 50 µM DOPA, 250 µM AA, followed by 20 µM, 40 µM and 60 µM of choline (Ch), and 20 µM of hydrogen peroxide (H2O2). Control site: red, Pt grass/PPD/Nafion/BSA; Choline sensor site: blue: Pt grass/PPD/Nafion/ChOx-BSA.

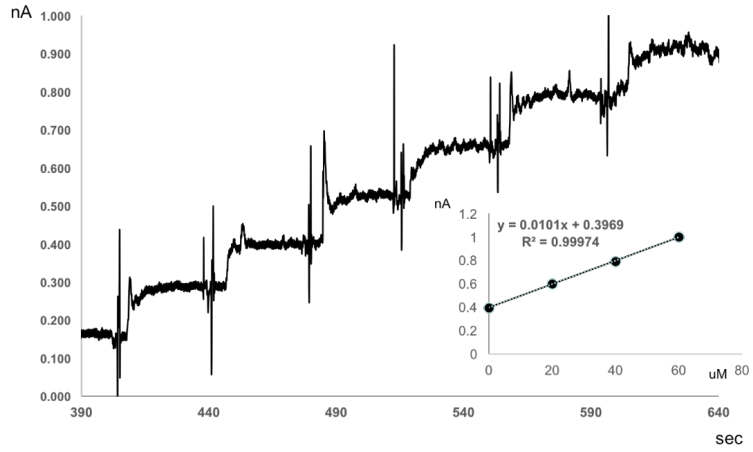

Figure 5.4. A calibration curve for choline sensor (Ag/AgCl as external RE). The biosensor response at a constant potential of 0.45 V (vs. Ag/AgCl) was monitored in stirred solution upon sequential injections to give 10 µM, 20 µM, 30 µM, 40 µM, 50 µM and 60 µM choline.

A typical calibration curves for the choline microsensor with underlying Pt nanograss coating is presented in Fig. 4. The choline sensor has a sensitivity of 196 ± 16 µA mM-1 cm-2 (n = 4) and a detection limit of 2 ± 0.3 µM (n = 4) at a signal-to-noise ratio of 3 for choline and a response time of 3-5 s. The sensor displayed a linear range up to 196 µM.

5.3.3 IrOx as reference electrode

In order to fabricate an all-in-one choline microbiosensor, which could be used conveniently without an external reference electrode (e.g. Ag/AgCl), IrOx was introduced as an on-probe reference electrode. Tolosa et al. recently reported an implantable micromachined multi-electrode array (MEA) microprobe modified for utilization as a complete electrochemical biosensor for rapid glutamate detection.[22] After 10X Pt nanograss deposition onto a Pt microelectrode surface, IrOx was deposited for making reference electrode. Pt nanograss coated at 1X concentration was found to REs with unsatisfactory performance including an unstable current response at the choline sensor site at higher analyte concentration.

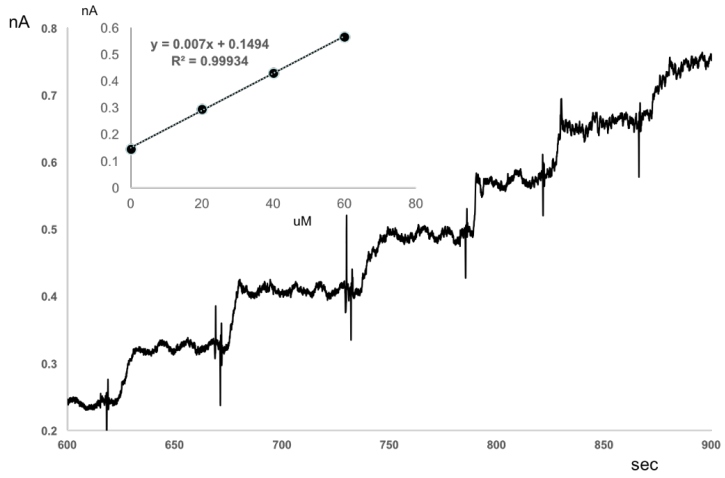

Figure 5.5. A calibration curve for choline sensor with an IrOx as on-probe RE. The biosensor response at a constant potential of 0.35 V (vs. IrOx) was monitored in stirred solution upon sequential injections to give 10 µM, 20 µM, 30 µM, 40 µM, 50 µM and 60 µM.

A calibration curve for the choline sensor with Pt nanograss-coated Pt used in constructing the working and reference electrodes are presented in Fig. 5. It should be noted that 0.35 V (vs. IrOx) corresponds to ~0.45 V (vs. Ag/AgCl). The choline sensor exhibited a 123 ± 11 µA mM-1 cm-2 (n = 4) and a detection limit of 3 ± 0.7 µM (n = 4) at a signal-to-noise ratio of 3. The sensor displayed a detection range up to 138 µM for choline and a response time of 3-5s.

5.3.4 Effect of interferents

The selectivity of the choline biosensors was evaluated. All fabricated biosensors (using external Ag/AgCl RE or on-probe IrOx RE) showed no response to common interferents of brain extracellular fluid at (or more than) physiological concentrations. The sensors were tested with 12.5 µM DA, 5 µM Serotonin, 12.5 µM EP, 12.5 µM NEP, 0.8 mM Glucose, 50 µM DOPAC, 50 µM DOPA, 250 µM AA at constant potential of 0.45 V vs. Ag/AgCl or 0.35 V vs. IrOx) and no obvious response was observed with the injections (see Fig. 3.). This indicates that PPD and

Nafion effectively block the access of electroactive interferents commonly encountered in brain extracellular fluid at the relatively low operating potentials used.

5.4 Conclusions

In summary, a high performance all-in-one electroenzymatic choline microsensor was fabricated by introducing nanostructured platinum as an underlying Pt coating. The working potential was adjusted to 0.45 V (vs. Ag/AgCl) instead of commonly used 0.7 V (vs. Ag/AgCl). The developed biosensor (either using external or on-probe reference IrOx electrode) demonstrated great performance in high sensitivity, low detection limit, fast response time and good selectivity. Pt nanograss coating was proved to be a perfect replacement for Pt black which is cytotoxic. The choline biosensor could be used for in vivo studies.

5.5 References

[1] Keihan, A. H.; Sajjadi, S.; Sheibani, N.; Moosavi-Movahedi, A. A. Sensor Actuat B-chem 204 (2014) 694-703.

[2] Baker, K. L.; Bolger, F. B.; Lowry, J. P. Analyst 140 (2015) 3738-3745.

[3] Mazurenko, I.; Tananaiko, O.; Biloivan, O.; Zhybak, M.; Pelyak, I.; Zaitsev, V.; Etienne, M.; Walcarius, A. Electroanal 27 (2015) 1685-1692.

[4] Santos, R. M.; Laranjinha, J.; Barbosa, R. M.; Sirota, A. Biosens Bioelectron 69 (2015) 83-94.

[5] Tseng, T. T. C.; Monbouquette, H. G. J Electroanal Chem 682 (2012) 141-146.

[6] Lowry, J. P.; Oneill, R. D. Electroanal 6 (1994) 369-379.

[7] Gerhardt, G. A.; Oke, A. F.; Nagy, G.; Moghaddam, B.; Adams, R. N. Brain Res 290 (1984) 390-395.

[8] Kulagina, N. V.; Shankar, L.; Michael, A. C. Anal Chem 71 (1999) 5093-5100.

[9] Khan, G. F.; Wernet, W. J Electrochem Soc 143 (1996) 3336-3342.

[10] Hamdi, N.; Wang, J. J.; Walker, E.; Maidment, N. T.; Monbouquette, H. G. J Electroanal Chem 591 (2006) 33-40.

[11] Ryan, M. R.; Lowry, J. P.; Oneill, R. D. Analyst 122 (1997) 1419-1424.

[12] Sharanya Arcot Desai, J. D. R., Liang Guo, and Steve M. Potter Front Neuroengineering 3 (2010) 1-5.

[13] Tang, R. Y.; Pei, W. H.; Chen, S. Y.; Zhao, H.; Chen, Y. F.; Han, Y.; Wang, C. L.; Chen, H. D. Science China-Information Sciences 57 (2014).

[14] ROBINSON, D. A. P IEEE 56 (1968) 1065-1071.

[15] Schuettler M, D. T., Wien SL, Becker S, Staiger A, Hanauer M, Kammer S, Stieglitz T 10th Annual Conference of the International FES Society, Montreal, Canada (2005).

[16] Boehler, C.; Stieglitz, T.; Asplund, M. Biomaterials 67 (2015) 346-353.

[17] Hu, Y. B.; Mitchell, K. M.; Albahadily, F. N.; Michaelis, E. K.; Wilson, G. S. Brain Res 659 (1994) 117-125.

[18] Lee, K. H.; Kristic, K.; van Hoff, R.; Hitti, F. L.; Blaha, C.; Harris, B.; Roberts, D. W.; Leiter, J. C. Brain Res 1162 (2007) 121-129.

[19] Thomas, T. C.; Grandy, D. K.; Gerhardt, G. A.; Glaser, P. E. A. Neuropsychopharmacol 34 (2009) 436-445.

[20] Walker, E.; Wang, J.; Hamdi, N.; Monbouquette, H. G.; Maidment, N. T. Analyst 132 (2007) 1107-1111.

[21] Wassum, K. M.; Tolosa, V. M.; Tseng, T. C.; Balleine, B. W.; Monbouquette, H. G.; Maidment, N. T. J Neurosci 32 (2012) 2734-2746.

[22] Tolosa, V. M.; Wassum, K. M.; Maidment, N. T.; Monbouquette, H. G. Biosens Bioelectron 42 (2013) 256-260.

[23] Yuen, T. G. H.; Agnew, W. F.; Bullara, L. A. Biomaterials 8 (1987) 138-141.

[24] Tivol, W. F.; Agnew, W. F.; Alvarez, R. B.; Yuen, T. G. H. J Neurosci Meth 19 (1987) 323-337.

[25] Dymond, A. M.; Kaechele, L. E.; Jurist, J. M.; Crandall, P. H. J Neurosurg 33 (1970) 574-&.

[26] Tseng, T. T.; Monbouquette, H. G. J Electroanal Chem (Lausanne Switz) 682 (2012) 141-146.

[27] Wassum, K. M.; Tolosa, V. M.; Wang, J.; Walker, E.; Monbouquette, H. G.; Maidment, N. T. Sensors 8 (2008) 5023-5036.

[28] Wassum, K. M.; Tolosa, V. M.; Wang, J. J.; Walker, E.; Monbouquette, H. G.; Maidment, N. T. Sensors 8 (2008) 5023-5036.

[29] Yamanaka, K. Jpn J Appl Phys 4 (1898) 632-637.

Chapter 6: Rapid glutamate signaling at AMPA receptors in the Basolateral amygdala mediates the biasing effect of reward-predictive cues on decision-making

Chapter 6 is a manuscript published under the following citation: Malvaez, M.; Greenfield, V. Y.; Wang, A. S.; Yorita, A. M.; Feng, L.; Linker, K. E.; Monbouquette, H. G.; Wassum, K. M. Sci. Rep. 2015, 5, 12511.

Lili Feng's contribution to this work focused on glutamate microsensor fabrication, from using MEMS technique to create 4-electrode micro probes to depositing permselective polymer, such as polyporrle and Nafion, to gain a good selectivity, as well as glutamate enzyme loading steps. Lili Feng also participated in the manuscript preparation.

Abstract

There is considerable evidence implicating the basolateral amygdala in reward-related decision-making and recent data suggests that glutamatergic signals in this region track reward seeking. The precise information conveyed by these glutamate release events, however, remains unknown. We monitored in near-real time basolateral amygdala glutamate concentration changes during instrumental conditioning, Pavlovian conditioning and a test of the ability of rewardpaired cues to cognitively bias action selection (Pavlovian-instrumental transfer). The data show that reward-predictive cues elicit an increase in the occurrence of transient glutamate release events and that these events precede and correlate with the ability of that cue to bias action selection. This effect was found to be mediated through the AMPA, but not NMDA glutamate receptor. These data suggest that transient glutamate release events acting at AMPA receptors in the

basolateral amygdala mediate the ability to extract predictive reward-specific information from the environment to guide decision-making.

6.1 Introduction

Adaptive reward seeking is critical to survival and is disrupted in a variety of neuropsychiatric disorders, including substance abuse, overeating and depression. The basolateral amygdala (BLA) has been implicated in these disorders [1-4] and is involved in reward processing [5-6], but much is unknown about its precise contribution. The BLA receives dense cortical and thalamic glutamatergic input [7-9]. Based on the results of BLA lesions [10-13], these excitatory chemical messages may be thought to convey a sustained emotional valence signal in response to reward-predictive stimuli. However, it is also possible that BLA signaling represents the motivational value of specific reward expectations generated by such cues. Here we investigate the latter.

Assessment of this hypothesis requires a method to selectively measure BLA glutamate signaling with fast temporal resolution in order to distinguish chemical messages related to individual reward-seeking behaviors. Microdialysis allows for selective measurement of extracellular neurochemical concentration changes, but the typical 10–20 min (or even rapid 14–20 s [14-16]) sampling window does not provide the appropriate temporal resolution and the spatial resolution is inadequate to record from BLA microenvironments. Single-unit electrophysiological recordings provide the required temporal and spatial resolution, but are nonselective and biased to record mostly from output neurons, precluding evaluation of glutamatergic input or local processing of such chemical messages within the BLA. Biosensor technologies [17-20] provide a solution. Using an electroenzymatic approach, this technique allows online, near-real time, sensitive and selective measurement of extracellular glutamate

concentration changes that result from neuronal release [21-25]. Recent biosensor data support the possibility that BLA glutamate release may convey information important for reward seeking; transient fluctuations in extracellular BLA glutamate concentration were detected immediately preceding reward-seeking actions [21], but the precise information encoded by these glutamate transients is unknown.

One major source of reward-seeking motivation is the cognitive expectation of specific available rewards, information that is often provided by environmental stimuli. Indeed, an environmental reward-predictive stimulus will selectively invigorate the performance of those actions that earn the same specific reward associated with the stimulus [26-29]. This capacity requires the BLA [11,13,30] and is thought to rely upon retrieval of a cognitive representation of the specific shared reward (i.e., outcome) encoded in both the Pavlovian stimulus-outcome and instrumental action-outcome association [31-32]. BLA neurons can fire in response to reward predictive cues [33-37] and in anticipation of reward [38], but the chemical message driving this neuronal activity and whether it encodes the motivational value of specific reward representations has yet to be clarified.

Therefore, we evaluated the role of BLA glutamate signaling in outcome-specific Pavlovian-instrumental transfer (PIT). In this task, rats are trained to associate two auditory Pavlovian stimuli (CS) with two distinct food rewards and then to respond on two independent levers to earn the same rewards. In the critical PIT test both levers are available and the CS will selectively enhance the response with which it shares a rewarding outcome [26-28,32]. Because the CSs are never directly associated with the instrumental actions, this test assesses the rats' ability to mentally represent each specific reward and to use this outcome-specific information to guide and motivate reward seeking. We reasoned that if BLA glutamate release is related to the

motivational influence of cue-induced, outcome-specific representations, then blocking ionotropic glutamate receptors (iGluRs) should disrupt the selective excitatory influence of the cue on reward seeking and, under normal conditions, glutamate release should precede and correlate with only those actions that are selectively invigorated by the CS.

6.2 Results

6.2.1 Experiment 1

In Experiment 1 (see Fig. 6.1A) we pharmacologically blocked either BLA AMPA (0, 1 or 3 μg/side of NBQX) or NMDA (0, 1 or 3 μg/side of AP5) glutamate receptors prior to the outcome-specific PIT test in order to assess their respective contributions to the selective invigorating influence of reward-predictive cues. During the PIT test both levers were simultaneously present, but pressing was never rewarded. Each CS was presented 4 times in alternating order, with intervening control CS-free periods (pre-CS). In this test the CS presentation provides the cognitive information (e.g., specific reward representation) that guides action selection and performance in the novel choice scenario.

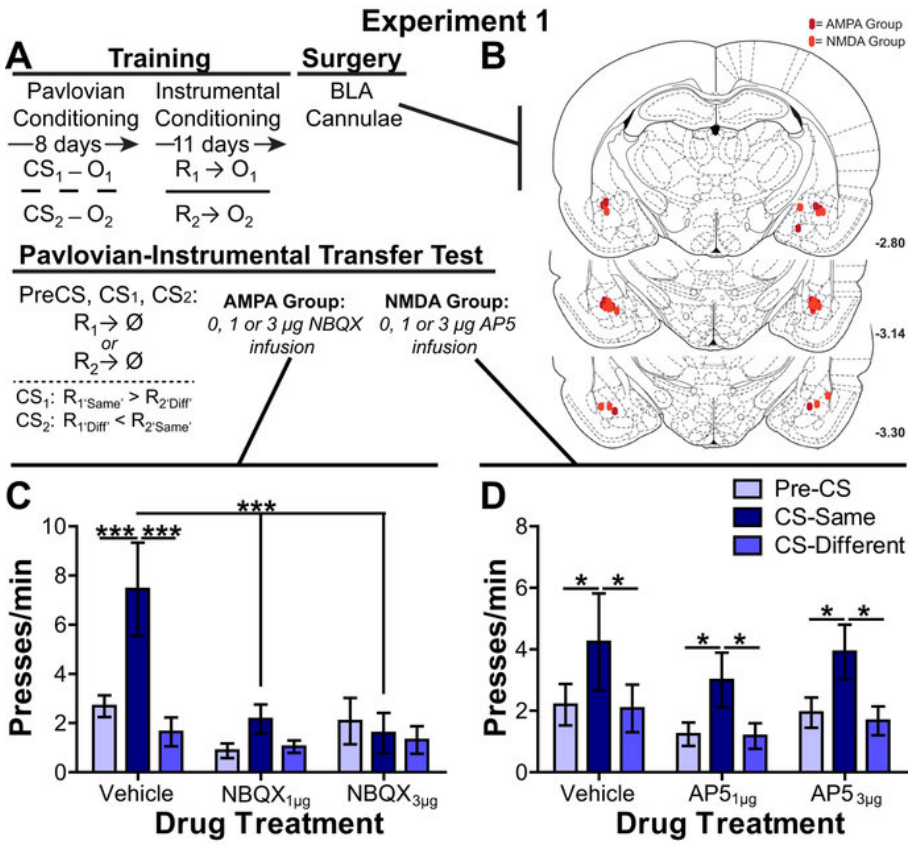

Figure 6.1. Effect of basolateral amygdala AMPA or NMDA receptor inactivation on Pavlovian-instrumental transfer. (A) Experimental procedure (see methods). CS, conditioned stimulus; O, outcome/reward; R, instrumental lever-press response; Ø, no reward delivery. During the PIT test both levers were available, but pressing was not reinforced and each CS was presented 4 times with intervening no-cue (Pre-CS) periods serving as a control. During CS presentation actions on the lever that, during training, earned the same outcome as the cue predicted were considered 'same' presses, while actions on the other available lever were considered 'different' (Diff) presses. (B) Schematic representation of microinfusion injector tips. Numbers to the lower right of each section represent the anterior-posterior distance (mm) from bregma of the section. Line drawings of coronal sections are taken from [73]. (C,D) The Pavlovianinstrumental

transfer effect; Lever-press rate (presses/min) averaged across levers during the control Pre-CS periods compared to pressing on lever that, in training, earned the same outcome as predicted by the CS (CS-Same) relative to pressing on the opposite lever (CS-Different) for the AMPA antagonist (C) or NMDA antagonist (D) group. Error bars +1 SEM. *p < 0.05, **p < 0.01, ***p < 0.001.

6.2.2 BLA AMPA and NMDA glutamate receptor involvement in the selective invigorating influence of reward-predictive stimuli over reward-seeking actions

As is clear from Fig. 6. 1C and D, we detected a differential effect of AMPA and NMDA iGluR receptor blockade on the selective-invigorating influence of reward-predictive stimuli over reward seeking during the outcome-specific PIT test. For the AMPA group there was a significant main effect of both CS ($F_{2,14} = 12.06$, $p < 0.001$) and NBQX dose ($F_{2,14} = 4.92$, $p = 0.02$) on lever pressing, as well as a significant interaction between these factors ($F_{4,28} = 5.26$, $p = 0.003$). Following a control vehicle infusion CS presentation selectively elevated press rate on the lever that, in training, earned the same reward as predicted by the CS (CS-Same) relative to both pre-CS press rate ($p < 0.001$) and pressing during the CS on the alternate available lever (CS-Different; $p < 0.001$). This selective elevation on the CS-Same action was blocked by BLA AMPA receptor inactivation ($p > 0.05$, for both doses) and, indeed, CS-Same responding was lower following intra-BLA NBQX infusion than vehicle control ($p < 0.001$, for both doses). Intra-BLA NBQX did not significantly alter pre-CS baseline or CS. Different response rates ($p > 0.05$), suggesting a specific effect of AMPA receptor blockade on the selective invigorating influence of cues over action performance. The low response rate during the pre-CS period may have, however, been close to the floor for detecting a significant decrease in responding. To

ensure AMPA receptor blockade did not alter baseline responding we isolated the first PIT trial for which the pre-CS response rate was higher (~5 presses/min) and in this case found identical results to the trial-averaged data; AMPA receptor blockade selectively attenuated CS-Same responding and did not significantly impact pre-CS response rate.

Blockade of BLA NMDA receptors was without effect on outcome-specific PIT (Fig. 6.1D). For the NMDA group there was a main effect of CS ($F_{2,16} = 18.68$, $p < 0.001$), with neither an effect of AP5 dose ($F_{2,16} = 0.46$, $p = 0.64$), nor AP5 dose x CS interaction ($F_{4,32} = 0.04$, $p = 0.99$). Under each drug dose treatment the CS elevated responding on the CSSame action relative to both the pre-CS period and to the CS-Different action ($p < 0.05$, in all cases). After both intra-BLA AMPA and NMDA receptor blockade rats were able to show a CSinduced elevation in Pavlovian conditioned food-port approach responding.

6.2.3 Experiment 2

The results of Experiment 1 suggest that BLA AMPA iGluR activation is necessary for reward-paired cues to selectively invigorate the performance of a specific reward-seeking action. We next used electroenzymatic biosensors to make sub-second measurements of extracellular glutamate concentration changes to interrogate the profile of BLA glutamate release during instrumental conditioning and PIT (see Fig. 6.2B). We reasoned that if BLA glutamate signaling is related to the motivational value of reward-specific representations, then such signaling might correlate with the performance of reward-seeking actions during instrumental conditioning. More importantly, during the critical PIT test BLA glutamate signaling should correlate with the performance of only those actions that are selectively motivated by the CS-generated reward representation (i.e., CS-Same pressing).

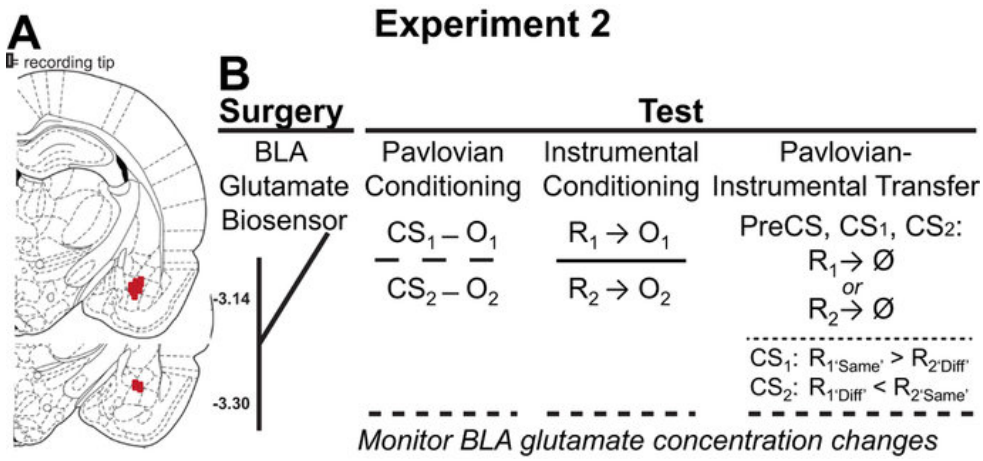

Figure 6.2. Experiment 2 Design. (A) Schematic representation of the placement of the microelectrode array biosensor tips. Numbers to the lower right of each section represent the anterior-posterior distance (mm) from bregma of the section. (B) Testing procedures (see methods). CS, conditioned stimulus; O, outcome/reward; R, instrumental lever-press response; Ø, no reward delivery. During the PIT test both levers were available, but pressing was not reinforced and each CS was presented 4 times with intervening no-cue (Pre-CS) periods. During the CS presentation actions on the lever that, during training, earned the same outcome as the cue predicted were considered 'same' presses, while actions on the other lever were considered 'different' (Diff) presses. BLA glutamate concentration changes were continuously monitored with constant potential amperometry at glutamate biosensors during each test.

6.2.4 BLA glutamate release during instrumental conditioning

As can be seen in the representative example presented in Fig. 6.3A, during the instrumental reward-seeking test there were rapid, short-duration increases in glutamate concentration (i.e., glutamate transients) that were increased in both frequency (Fig. 6.3B; $t7 = 2.34, p = 0.05$) and amplitude (Fig. 6.3C; $t7 = 2.85$, $p = 0.02$) during instrumental performance, relative to the pre-test baseline period. Interestingly, the frequency of these glutamate release

events positively correlated (r16 = 0.58, p = 0.02; Fig. 6.3E) with lever-press rate (see Fig. 6.3D), such that higher press rates were associated with more frequent BLA glutamate transients.

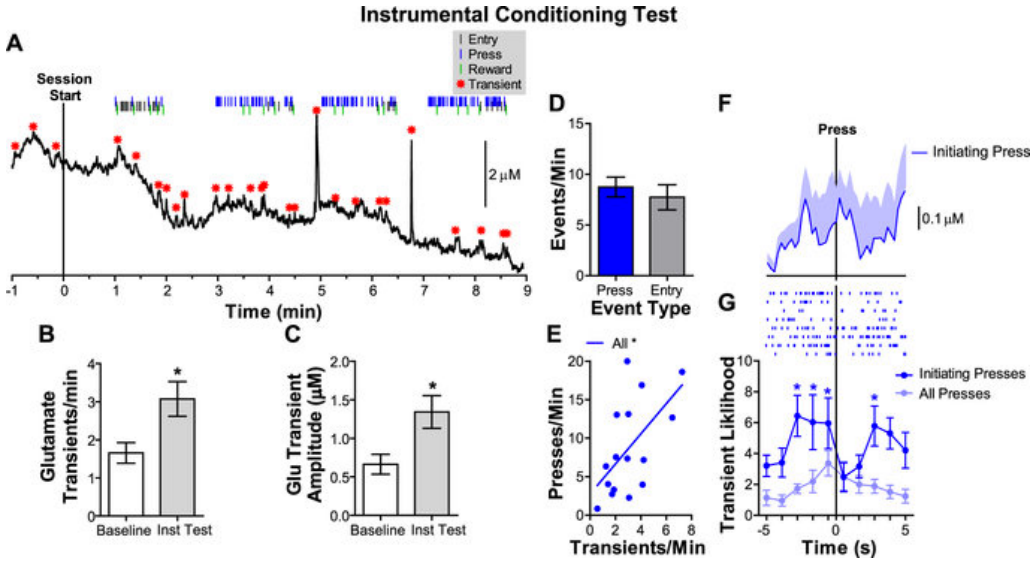

Figure 6.3. Basolateral amygdala glutamate release during instrumental conditioning. (A) Representative glutamate concentration v. time trace during instrumental conditioning. Instrumental session started with lever insertion at time 0 s. Red asterisks represent significant transient glutamate concentration fluctuations above baseline (transients). Behavioral events are marked above the trace. (B) BLA glutamate transients that reached threshold were counted and averaged for each rat across the 2-min pre-test baseline period and the instrumental (inst) test sessions. (C) Glutamate transient amplitude (µM) was calculated as the peak amplitude of the transient minus the baseline concentration (first minima 0.5–5 s before the peak). (D) Lever press and food-port entry rate collapsed across the instrumental conditioning tests. (E) Betweensubject correlation between glutamate transient frequency (Transients/min) and lever-press rate (Presses/min). Each rat is represented twice, once for each instrumental test. (F) Glutamate concentration v. time trace around initiating lever presses (occurring at time 0 s) averaged across all initiating presses in the session for a representative subject. Shading reflects +1 SEM across trials. (G) The likelihood of a glutamate transient in 10, 1-s bins, evenly distributed around presses divided by initiating presses (first press after the collection of an earned reward or after a >6 s pause in pressing, excluding presses that occurred within a pressing bout) or all lever

presses combined (including both initiating and intra-bout presses), averaged across the two instrumental tests. The press occurs at time 0 s. Likelihood of a glutamate transient is defined as the percentage of presses (or initiating presses) that had a glutamate transient in the represented 1-s time bin. Asterisks represent significance relative to the control 1-s time bin, 5 s prior to the press. The raster plot shows the corresponding raw data with each subject represented on an individual line on the y-axis, tick marks represent the peak time of each significant glutamate transient surrounding initiating presses. Error bars +1 SEM. *p < 0.05, ***p < 0.001.

As can also be seen in Fig. 6.3A, the frequency of glutamate transients fluctuated throughout the instrumental conditioning test and appeared to share a tight temporal relationship to lever-press actions, especially those actions initiating bouts of reward seeking (see representative trial-averaged glutamate concentration v. time trace in Fig. 6.3F). To specifically evaluate the relationship between glutamate release events and instrumental reward seeking we calculated the likelihood of a glutamate transient in the time immediately surrounding lever presses. Because rats tended to organize their lever pressing into clusters we divided our analysis for those presses that initiated reward seeking (i.e., 'initiating presses') excluding presses that occurred within a pressing bout and compared this to all lever presses (including both initiating and intra-bout presses). Initiating presses were defined as the first press after collection of an earned reward or the first press after a >6 s pause in pressing. During the instrumental test rats showed on average 34.25 (sem = 5.53) total reward-seeking bouts per session, with 23.68% (1.77) of total presses being considered 'initiating presses'. Reward-seeking bouts had an average duration of 8.20 s (1.33), and contained on average 5.84 (1.03) presses. The average reward receipt to next initiating press latency was 23.10 s (7.47). To isolate the initiation of instrumental reward seeking and avoid the presence of contaminating events (e.g., reward receipt, termination

of previous bout, etc.) in the reward-seeking initiation analysis window we calculated the change in likelihood of a glutamate transient by counting the glutamate transients in 10, 1-s bins evenly distributed around presses.

The raw glutamate transient counts around initiating presses for each subject are displayed in the raster plot shown in Fig. 6.3G. Statistical analysis of the data collapsed over 1-s intervals (to match biosensor response time) and averaged across subjects (Fig. 6.3G- bottom) found a marginally insignificant effect of Time surrounding the press ($F_{9,63} = 1.79$, $p = 0.08$), a significant effect of Type of press (Initiating press v. All presses, $F_{1,7} = 61.42$, $p = 0.0001$) and a Time x Type of press interaction ($F_{9,63} = 2.67$, $p = 0.01$; Fig. 6.3G). Glutamate transients were more likely (when controlling for number of presses) to occur time-locked to those initiating presses that followed either reward delivery or a pause in pressing than all presses combined. The likelihood of a glutamate transient was elevated (relative to the control 1-s time bin, 5 s prior to the press, which itself did not differ from the baseline likelihood of a glutamate transient in similar epochs without lever pressing during the pre-test period: $t7 = 2.12$, $p = 0.07$) between 3 and 1 s prior to initiating lever presses ($p < 0.05$). The likelihood of a glutamate transient became elevated again in the 3-s window after the initiating press, which corresponded to the average time at which the next press within a bout occurred (average 2.02 s, sem = 0.12). Given that the average latency between an initiating press and reward delivery was 44.4 s (sem = 10.0; max = 160.6, min = 7.76m), it is unlikely that the glutamate release events that occurred during the 5 s following initiation of reward seeking activity were related to reward receipt. These results corroborate our previous report21 and suggest that BLA glutamate release events are increased in frequency and amplitude during instrumental reward seeking, are tightly timelocked to the initiation of instrumental action and positively correlate with instrumental performance.

6.2.5 BLA glutamate release during Pavlovian-instrumental transfer

We next measured BLA glutamate concentration changes during PIT to evaluate how BLA glutamate release relates to the cognitive, reward-specific representations generated by reward-predictive cues that allow them to selectively invigorate reward-seeking actions. As can be seen in the group-averaged glutamate concentration v. time trace presented in Fig. 6.4A, presentation of a Pavlovian CS did not induce any apparent robust or sustained increase in glutamate concentration, although there was a slight overall drift in the baseline current. The reward-predictive cues did, however, elevate the frequency of discrete glutamate release events (Fig. 6.4B; main effect of Period: $F_{2,14} = 4.25, p = 0.04$), but the amplitude of these transients was, on average, not significantly altered by CS presentation (Fig. 6.4C; main effect of Period: $F_{2,14} = 1.72$, $p = 0.22$). Glutamate transients were more frequent than the pre-test (no behavior or cues) baseline period during the CS ($p < 0.05$), but not pre-CS period ($p > 0.05$) in a manner similar to that seen during Pavlovian conditioning (no effect of Extinction: Pavlovian conditioning v. PIT test $F_{1,5} = 0.74$, $p = 0.43$ or Extinction x CS interaction: $F_{2,10} = 0.11, p = 0.89$).

That there was not a significant difference in glutamate transient frequency during the CS relative to the pre-CS period is likely due to the reward-predictive nature of the operant box context because of its pairing with reward during instrumental conditioning. Indeed, rats were exploring the chamber, entering the food-delivery port and lever pressing during this period.

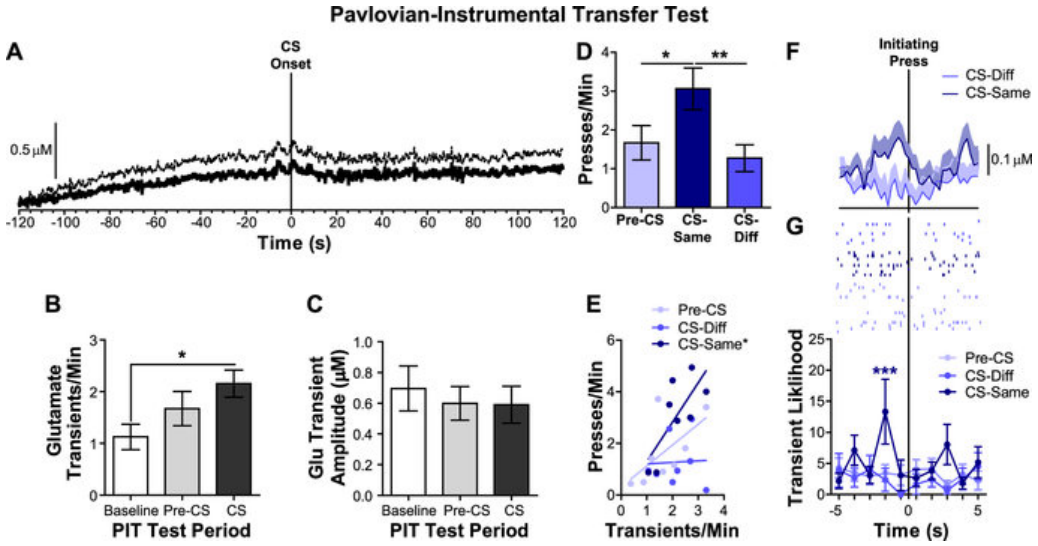

Figure 6.4. Basolateral amygdala glutamate release during Pavlovian-instrumental transfer. (A) Average glutamate concentration change (µM) during the 2-min conditioned stimulus (CS) presentation (beginning at time 0 s) and immediately preceding 2-min pre-CS period averaged across trials during the PIT test for each rat and then averaged across rats. Dashed lines represent the between-subjects +1 SEM. (B) Glutamate transients that reached threshold were counted and averaged for each rat across the 2-min pre-test baseline period, the 2- min pre-CS periods and the 2-min CS periods. (C) Glutamate transient the amplitude (µM) was calculated as the peak amplitude of the transient minus the baseline glutamate concentration. (D) Lever-press rate (Presses/min) averaged across levers during the control Pre-CS periods compared to pressing during CS presentation distinguished by whether it was on lever that, in training, earned the same outcome as predicted by the presented CS (CS-Same Actions) relative to pressing on the opposite lever (CS-Diff Actions). Main effect of CS: $F_{2,14} = 8.85$, $p = 0.003$. (E) Glutamate transient frequency (Transients/min) v. lever-press rate (Presses/min) betweensubjects correlation. (F) Glutamate concentration v. time traces for the 5 s prior to and after initiating presses (occurring at time 0 s) during the CS averaged across all initiating presses for a representative subject. Shading reflects +1 SEM across trials. (G) The likelihood of a glutamate transient distributed in 1-s bins, 5 s prior to and after initiating presses (occurring at time 0 s; first press after a >6 s pause in pressing). Glutamate transient likelihood is defined as the percentage of initiating presses with a glutamate transient in the

represented 1-s time bin. Asterisks represent significance relative to the first 1-s time bin. Raster plot displays corresponding raw data; each subject is represented on an individual line on the y-axis with tick color reflecting trial type. Tick marks represent the peak time of each glutamate transient that reached threshold surrounding initiating presses. Error bars +1 SEM. *p < 0.05, **p < 0.01, ***p < 0.001.

As during instrumental conditioning, BLA glutamate transient frequency correlated with lever pressing, but only during the CS and with only those actions for which performance was selectively invigorated by the CS, i.e., CS-Same actions (see behavioral results in Fig. 6.4D). During the pre-CS period the positive correlation between glutamate transient frequency and lever pressing was weakened, relative to instrumental conditioning as a result of extinction; there was a positive, but non-significant between-subjects relationship between pre-CS lever-press rate and pre-CS glutamate transient frequency ($r8 = 0.61$, $p = 0.11$; Fig. 6.4E). The significant positive correlation reemerged when the CS was present, but only for the CS-Same action ($r8 = 0.75$, $p = 0.03$), such that those rats for which the CSs caused a stronger selective invigoration of responding it also induced a higher frequency of BLA glutamate transients. Glutamate transient frequency did not significantly correlate with the performance of actions during the CS that, during training, earned an outcome different from that predicted by the CS (CS-Different actions; $r8 = 0.04$, $p = 0.92$).

More importantly, examination of the representative example in Fig. 4Fand raster plot displaying raw glutamate transient peak times for all subjects in Fig. 4G suggests that BLA glutamate transients were time-locked to the initiation of reward-seeking activity (see Table 1) specifically on the CS-Same action. There was an overall effect of CS (Pre-CS v. CS-Same v. CS-Different initiating presses; $F2,14 = 6.00$,$p = 0.01$) on the likelihood of glutamate transients

(normalized to number of initiating pressing) distributed around initiating lever presses, with no significant effect of Time ($F_{9,63} = 1.21$, $p = 0.31$) and a marginally insignificant Time x CS interaction ($F_{18,126} = 1.50$, $p = 0.10$; Fig. 6.4G- bottom). The likelihood of a glutamate transient was only significantly elevated during the CS prior to initiating presses on the CS-Same action (1-s bin, 2 s prior to CS-Same initiating presses, $p < 0.001$ relative to the control, 1-s bin 5 s prior to the initiating press). Initiation of CS-Same pressing was significantly more likely than initiation of CS-Different pressing to be preceded (within 5 s) by a glutamate transient (average percentage of CS-Same initiating presses preceded by glutamate transient: 28.87%, sem = 6.09; CS. Different initiating presses: 12.96%, sem = 5.39; $t_7 = 2.78$, $p = 0.04$). These data suggest that extinction of the press-reward and context-reward associations during the PIT test disrupted the normal temporal relationship between glutamate release and reward seeking, but this was restored when action performance was motivated by outcome-specific information provided by reward-paired cues.

	Pre-CS	CS: Same	CS: Diff
Total Bouts	11.63	17.125*	10.38
	3.50	3.60	2.95
Average Presses/Bout	2.69	3.77	2.12
	0.38	1.31	0.18
Average Bout Duration (s)	3.61	5.03	2.58
	0.54	1.73	0.51
% Presses = Bout Initiating	57.00	40.03	46.06
	9.93	6.82	6.45

Table 6.1. Pavlovian-instrumental transfer test lever pressing bouts. As in the instrumental conditioning test, rats organized their reward seeking in bouts of lever pressing during the PIT test. Because no rewards were delivered during this test an initiating press was defined as the first press after a pause in pressing of >6 s. Pressing bout information is presented in this table. Numbers represent average values, with values in italics below representing the between-subject SEM. During the PIT test rats showed significantly more lever-pressing

bouts on the CS- Same action relative to both the CS-Different action and to the pre-CS period (*p < 0.05, in both cases; main effect of CS period $F_{2,4} = 5.81$, p = 0.01). Main effects for all other measures were non-significant.

Interestingly, on the macro scale glutamate transient frequency positively correlated with the ratio of responding between actions during the CS ($r_8 = 0.71$, p = 0.049; Fig. 6A), but did not significantly correlate with all non-discriminate CS responding ($r_8 = 0.22$, p = 0.60). This correlation with the CS response ratio was significant even when controlling for overall response rate during instrumental conditioning (partial correlation: $r_8 = 0.81$, p = 0.03) or during the pre-CS period (partial correlation: $r_8 = 0.83$, p = 0.02) and when controlling for the CSs' ability to non-discriminately elevate reward seeking (partial correlation: $r_8 = 0.75$, p = 0.05). These data suggest that BLA glutamate transients may be related to the motivational influence of outcome specific representations.

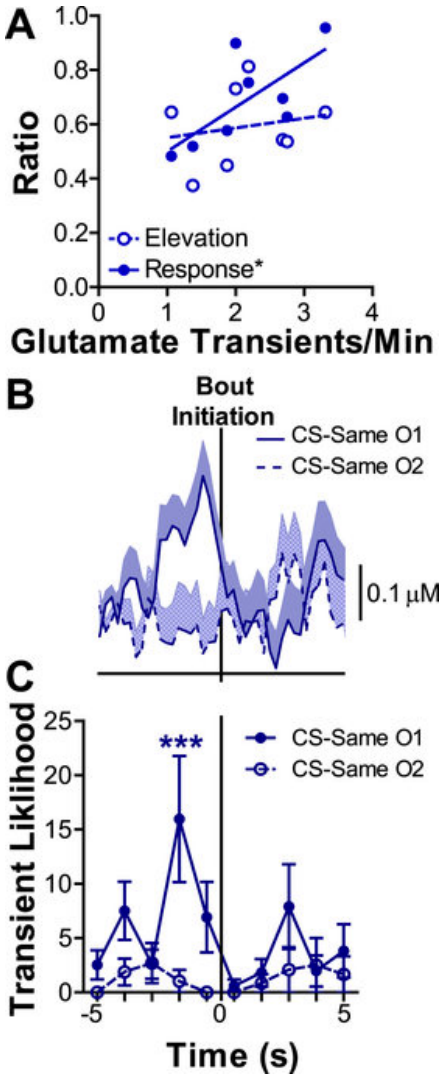

Figure 6.5. Outcome specificity of basolateral amygdala glutamate release during Pavlovian-instrumental transfer. (A) Between-subjects correlation between glutamate transient frequency (Transients/min) and elevation [CS pressing/(CS + Pre-CS pressing)] v. response [CSSame/(CS-Same + CS-Different)] ratio. (B) Glutamate concentration v. time traces for the 5 prior to and after initiating presses (occurring at time 0 s) was averaged across all CS-Same initiating presses during the PIT test for the same representative subject as in 4F. Traces are divided by the type of outcome the action earned. Shading reflects the +1 SEM across trials. (C) The likelihood of a glutamate transient distributed in 1-s bins, 5 s prior to and after CS-Same initiating presses (occurring at time 0 s). Data are divided by the two CS-Same trial types. O1: Outcome 1 is defined as the outcome earned by the action that was exclusively (for 6/8 subjects) or preferentially (for 1/8 subjects)

preceded by transient glutamate release. For the single subject in which he glutamate signal did not distinguish between outcome types outcome 1 was randomly assigned to the grain pellet outcome. Likelihood of a glutamate transient is defined as the percentage of initiating presses that had a glutamate transient in the represented 1-s time bin. Asterisks represent significance relative to the control 1-s time bin 5 s prior to the press. *p < 0.05, ***p < 0.001.

To further support this interpretation we exploited the utility of the two different specific PIT trial types (one for each predicted outcome). If BLA glutamate transients reflect outcome specific motivational information then, because glutamate biosensors record from BLA microenvironments, recorded glutamate transients for a given subject/recording location should be specific to CS-Same responding for only one outcome type. If however, glutamate transients are simply related to all motivated lever pressing then they should occur prior to CS-Same actions regardless of expected outcome. The data provide evidence in support of the former. For 6/8 subjects glutamate transients were time-locked to initiating presses on the CS-Same action exclusively for only one outcome type (defined as outcome 1). Which outcome served as outcome 1 was not a function of outcome type (pellets v. sucrose), lever, action-outcome arrangement, CS type, outcome preference, or PIT effect magnitude. In the other 2 subjects glutamate transients showed an outcome-selectivity ratio of 0.57 and 0.50, respectively. Fig. 6.5B displays a representative trial-averaged glutamate concentration v. time trace around initiating presses on the CS-Same action divided by each outcome type. As is clear from this figure, glutamate concentration increased prior to initiating presses on the CS-Same action, but only for one outcome type. The data averaged across subjects support this observation. There was a main effect of Outcome type ($F_{1,7} = 6.54$, $p = 0.04$), and of Time ($F_{9,63} = 2.48$, $p = 0.02$), as well as a Time x Outcome type interaction ($F_{9,63} = 2.27$, $p = 0.03$) on the likelihood of a

glutamate transient in the 10-s period around initiating presses on the CS-Same action. Together these results suggest that BLA glutamate transients encode outcome-specific motivational information provided by reward-predictive cues.

6.3 Discussion

The data collected here indicate that transient fluctuations in BLA glutamate release are time-locked to and correlate with instrumental reward seeking and that during PIT these glutamate transients are time-locked to and correlate with only those actions invigorated by outcome-specific motivational information provided by a reward-predictive stimulus. This correlational relationship was bolstered by evidence that blockade of AMPA, but not NMDA iGluRs attenuates the selective invigorating influence of reward-predictive stimuli over reward seeking.

That transient BLA glutamate release events were related to instrumental reward seeking replicates previous results demonstrating a similar relationship [21] and extends this to show that BLA glutamate transients were associated with the actions that initiated reward seeking following reward delivery or a pause in activity, rather than actions occurring within a bout of reward seeking. This release may drive the previously-reported increases in BLA cell body activity that occur prior to instrumental action [38-39] and have been hypothesized to encode outcome expectations [38]. The results here suggest that BLA glutamate input may encode information vital for motivating goal-directed action, because after a task is well-learned such information is only necessary for initial actions within a chunk [40-42]. Indeed, these results corroborate evidence that amygdala neurons in primates show prospective activity that reflects internally-generated plans towards future goals [43]. Of course BLA glutamate release is not exclusively related to instrumental action; glutamate transients were more likely to occur around

instrumental actions, but release events were detected throughout the instrumental test, including especially large events during reward receipt.

The temporal relationship between BLA glutamate transients and reward-seeking was tight, but it was not one-to-one and glutamate release events that reached the detection threshold occurred at a rate lower than might be expected for the major excitatory neurotransmitter and primary input signal to the amygdala. The recording technique employed here measures changes in extrasynaptic glutamate concentration, which, because these signals are abolished by tetrodotoxin [21], are a proxy measure for the tightly-regulated44 synaptic overspill [44-45]. Glutamate release within the synapse might, therefore, be expected to relate to a much larger percentage of, if not all, initiating lever presses.

This study provided a novel evaluation of the profile of BLA glutamate release during appetitive Pavlovian conditioning. Although the baseline drift in electrochemical measurements do not allow for a definitive answer, the data showed no indication that Pavlovian reward predictive cues elicited an overall elevation in glutamatergic tone, contrary to what might be expected if BLA glutamate signaling conveys a sustained, cue-induced, emotional valence or motivational signal. This finding is interesting in light of the wealth of data from single-unit electrophysiological recordings showing that reward-predictive stimuli increase BLA cell body firing [35-36,38,46-47]. Single-unit recordings are biased towards monitoring mostly from output neurons and the glutamate release recorded here reflects input and local activity, but it is this glutamate input from thalamic [46,48-49] or cortical afferents6 that is thought to drive the cell body excitation. There are three potential explanations for this discrepancy. First, for the reasons mentioned above it is possible that glutamate biosensors do not provide the adequate

sensitivity to measure glutamate that is being released to drive BLA activity upon CS presentation.

Secondly, the aforementioned CS-induced BLA neural activity may not be driven by glutamate. We find this unlikely given data demonstrating strengthened glutamatergic thalamic-BLA synapses during Pavlovian conditioning [46], but dopamine release has been shown to directly excite BLA projection neurons [50]. Thirdly, key task differences may explain the discrepancy between the current glutamate input recordings and the previously reported cue-evoked cell body firing. In the previous reports BLA cell body firing was robustly elicited by short-duration (2– 5 s) CSs that predicted immediate reward with strong certainty. The long-duration (2-min) CS probabilistically paired with reward in our task provides more a context for reward and may not induce a robust increase in BLA cell body firing. In support of this, preliminary evidence suggests that a longer duration (30-s) CS that predicts reward at a variable latency is more likely to induce an inhibition in BLA cell body firing [51], which corroborates our current glutamate release results. Clearly, further interrogation of both glutamate release and cell body activity in similar Pavlovian tasks is necessary. Such investigation may lead to important information regarding potential differences between excitatory BLA input and output activity and of the role of such signaling in Pavlovian reward prediction.

Importantly, although there was no detected sustained CS-induced increase, glutamate release did show transient elevations during the PIT test. Following extinction of the responsereward (and context-reward) association the relationship between BLA glutamate transients and instrumental reward seeking was degraded. During the CS, however, this relationship was restored; glutamate transients were significantly more likely to occur

time-locked to rewardseeking activity selectively on the action that shared the same rewarding outcome as the CS. That this relationship was restored despite the fact that the CS induced only a modest (relative to the pre-CS period) increase in the frequency of glutamate transients suggests it was not merely a coincidence of both elevated responding (which the analysis controlled for) and elevated glutamate transients. These data lend support to the hypothesis that BLA glutamate transients encode the outcome-specific motivational information provided by reward-predictive stimuli. In further support of this, cue-induced transient glutamate release only correlated with the ratio of responding during the CS, which is thought to reflect the CS's cognitive, outcome-specific motivational influence. This accords with the relationship between BLA activity and biasing influence of cues over instrumental action in humans [52]. Moreover, for each subject/recording location glutamate transients encoded only one specific outcome type. Because biosensors record glutamate in BLA microenvironments, the presumption is that for each subject glutamate input signals related to the other outcome were released in a microenvironment outside the sampling space. In the one subject for which glutamate release did not show outcome specificity the biosensor was likely receiving intermixed glutamate input for both outcome types. This specificity in the glutamate input signal suggests that rather than relating simply to motivated lever pressing, the BLA glutamate release detected here encoded outcome-specific information. BLA glutamate release events were shown to relate to the outcome-specific motivational influence of Pavlovian stimuli, but it is unlikely that these signals participate in the decisionmaking process itself. If the BLA, and glutamate release therein, was required for the decision process then blockade of BLA AMPA receptors should have not only attenuated actions on thelever that earned the same outcome as the CS, but also increased responding on the alternate lever, indicating an inability to select between actions on the basis of

the CS-provided outcome expectation. Instead, BLA AMPA receptor inactivation (Experiment 1) and BLA lesions [11,13] only attenuate the selective invigorating influence of CSs. Lesions to either the orbitofrontal cortex or mediodorsal thalamus do, however, cause such non-discriminate CS-induced response invigoration [11,53]. Both of these regions send excitatory projections to the BLA [7-9] and unilateral, ipsilateral orbitofrontal cortex inactivation abolishes reward seeking-related BLA glutamate transients [21]. Therefore, the glutamate signals detected here likely arise directly from the orbitofrontal cortex, or, given that our sensor placements are located primarily in the basal amygdala, indirectly from this region via projections from the lateral amygdala [54]. BLA glutamate release may, therefore, be vital for invigorating the performance of actions planned in the orbitofrontal cortex by incorporating outcome-specific motivational value. Indeed, the BLA isvital for outcome-specific representations of motivationally significant, but not valueless events [55]. Correlates of the latter have, however, been identified in the orbitofrontal cortex [56]. This interpretation is also supported by the myriad data suggesting the BLA is required for other behaviors that rely on outcome-specific value information [10,57-60] and evidence that BLA neural activity can be outcome specific [33,36,38,47] and may encode such value in the rodent [33,38,61], primate [36,62,63-64], and even human BLA65.

In summary, the findings here support a role for rapid BLA glutamate signaling in the motivating influence of outcome-specific representations, in this case provided by a Pavlovian reward-predictive stimulus. These results lay the groundwork for further exploration of the role of BLA excitatory glutamatergic signaling and modulation of such signaling in the variety of reward-seeking behaviors that require retrieval of reward-specific information and are relevant to understanding the neuropsychological disorders marked by a disruption in such cognitive processing.

6.4 Methods

6.4.1 Subjects

Male Long Evans rats (Experiment 1: n = 17, Experiment 2: n = 8; Charles River Laboratories, Wilmington, MA) weighing between 280–340 g were group housed and were handled for 3–5 days prior to training. Training and testing took place during the dark phase of the 12:12 h reverse dark:light cycle. Rats were maintained on a food-deprived schedule whereby they received 10–12 g of their maintenance diet daily in order to maintain 85% free-feeding body weight. All procedures were conducted in accordance with the NIH Guide for the Care and use of Laboratory Animals and approved by the UCLA Institutional Animal Care and Use Committee.

6.4.2 Apparatus

Training took place in 16 Med Associates operant boxes (East Fairfield, VT). The chambers contained 2 retractable levers that could be inserted to the left and right of a recessed food delivery port in the front wall. A photobeam entry detector was positioned at the entry to the food port. The chambers were also equipped with syringe pump to deliver 20% sucrose solution in 0.1 ml increments through a stainless steel tube into a custom-designed well in the food port and a pellet dispenser to deliver a single 45-mg grain pellet (Bio-Serv, Frenchtown, NJ). Both a tone and white noise generator were attached to individual speakers on the wall opposite the lever and magazine. A 3-watt, 24-volt house light mounted on the top of the back wall opposite the food cup provided illumination. For experiment 2 all testing was conducted in a single Med Associates operant box housed within a continuously-connected, copper mesh-lined sound attenuating chamber and outfitted with an electrical swivel (Crist Instrument Co,

Hagerstown, MD) connecting a headstage tether that extended within the operant chamber to the potentiostat recording unit (Fast-16 mkIII, Quanteon, LLC, Lexington, KY) positioned outside the operant chamber.

6.4.3 Behavioral training and surgery

Rats were first given Pavlovian training (see below and Fig. 6.1A), to associate two distinct 2-min duration auditory stimuli (CSs) each with a different palatable food reward, delivered into a single food port on a random-time 30 s schedule. Rats were then separately trained to instrumentally earn these same food rewards by responding on independent levers on a random ratio (RR) 20 schedule (see below). During training the CSs and levers were never presented together. Following training rats underwent surgery using standard aseptic stereotaxic procedures described previously [66]. In Experiment 1 rats were implanted with guide cannula (22-gauge stainless steel, Plastics One, Roanoke, VA) targeted bilaterally 1 mm above the BLA. In Experiment 2 rats were implanted with a unilateral pre-calibrated glutamate biosensor (see below) into the BLA (AP −3.0 mm, ML +5.1, DV −8.0) and a Ag/AgCl reference electrode (200 μm diameter) into the contralateral cortex (histological verification of placements shown in Figs 6.1B and 6.2A). Following surgery rats were individually housed and allowed to recover.

6.4.4 Pavlovian training

Rats received 1 Pavlovian training session/day for 8 days. Each session consisted of 8 tone and 8 white noise (75 db, 2-min duration) presentations, during which either 20% sucrose solution or grain pellets, as appropriate, were delivered on a 30-s random-time schedule into a single food-delivery port, resulting in an average of 4 stimulus-outcome pairings per trial (CSreward relationship counterbalanced). CSs were delivered in pseudo-random order with no

more than 2 successive presentations of the same CS and a variable inter-trial interval between 2–4 min (3-min mean). The rate at which rats entered the food port was recorded for the 2-min pre-CS period, for the CS-probe period (interval between CS onset and first US delivery) and for the CS-reward period (interval after first US delivery to CS offset). No levers were present during these Pavlovian conditioning sessions.

6.4.5 Instrumental training

Rats were then given 11 days of instrumental training, receiving 2 separate training sessions per day, one with the lever to the left of the food-delivery port and one with the right lever. Each action was reinforced with a different outcome- either grain pellets or sucrose solution (counterbalanced with respect to the Pavlovian training contingencies). Each session was terminated after 30 outcomes had been earned or after 30 min had elapsed. Actions were continuously reinforced (CRF) for the first day of instrumental conditioning, on days 2-3 rewards were delivered on a random ratio (RR)-2 schedule, increasing to RR-5 for days 4-5, RR-10 for days 6–7 and ending with RR-20 for days 8-11. Importantly, neither CS was present during this instrumental training. The rate of responding on each lever was measured throughout training.

6.4.6 Experiment 1: Outcome-specific Pavlovian-instrumental transfer tests

After 5 days of recovery, rats were given 2 retraining sessions for each instrumental association (2 sessions/day for 2 days) and then one Pavlovian retraining session. On the day prior to each PIT test rats were given a single 30-min extinction session where both levers were available, but pressing was not reinforced to establish a low level of responding.

Rats were split into two drug groups, one (n = 8) group receiving bilateral infusions of 0, 1 or 3 μg/side of the selective α-amino-3-hydroxy-5-methyl-4-isoxazolepropionic acid

(AMPA)/kainate receptor antagonist NBQX into the BLA and another (n = 9) receiving 0, 1 or 3 μg/side of the selective N-methyl-D-aspartate (NMDA) receptor antagonist AP5 10 min prior to the onset of the PIT test. Each rats was given 3 total PIT tests to allow within-subject drug dose comparisons (test order counterbalanced). During this test both levers were continuously present, but pressing was not reinforced. After 10 min of extinction to re-establish a low level of responding each 2-min CS was presented separately 4 times each in pseudorandom order, separated by a fixed 4-min inter-trial interval. No rewards were delivered during CS presentation. The 2-min prior to each CS presentation served as the 'pre-CS' control period. Ratswere retrained as above between each PIT test.

6.4.7 Drug administration

AP5 (D-(-)-2-Amino-5-phosphonopentanoic acid) and NBQX (2,3-Dioxo-6-nitro-1,2,3,4-tetrahydrobenzo[f]quinoxaline-7-sulfonamide disodium salt) were obtained from Tocris Bioscience (Bristol, UK) and were dissolved in sterile saline vehicle. Drugs were infused bilaterally into the BLA in a volume of 0.5 μl over 1 min via an injector inserted into the guide cannula fabricated to protrude 1 mm ventral to the tip using a microinfusion pump. Injectors were left in place for at least 1 additional min to ensure full infusion. Rats were placed in the operant chamber for the PIT test 10 min after infusion to allow sufficient time for the drug to become effective. The dose range for each drug (1 or 3 μg/side for both AP5 and NBQX) was selected based on previous research showing intra-BLA infusion of these doses to be effective in a variety of Pavlovian and reward-related tasks [67-69]. Drug test order was counterbalanced across rats. On 2 of the retraining days prior to the first PIT test rats were given mock infusions to habituate them to the infusion procedures; injectors were inserted into the cannula and the pump was turned out, but no fluid was infused.

6.4.8 Experiment 2: Electroenzymatic glutamate sensing

Microelectrode array (MEA) probes were fabricated in the Nanoelectronics Research Facility at UCLA and modified for glutamate detection as described previously [17,21]. Briefly, these biosensors use glutamate oxidase as the biological recognition element and rely on electrooxidation, via constant-potential amperometry (0.7 V versus a Ag/AgCl reference electrode), of enzymatically-generated hydrogen peroxide (reporter molecule) to provide a current signal. This current output is recorded and converted to glutamate concentration using a calibration factor determined in vitro. Interference from both electroactive anions and cations is effectively excluded from the amperometric recordings, while still maintaining a <1-s response time, by application of Nafion and polypyrrole (PPY) films to the electrode sites prior to enzyme immobilization [17]. Additionally, incorporation of a non-enzyme-coated sentinel electrode on the MEA enabled removal of correlated noise from the glutamate sensing electrode output by signal subtraction (see Data Analysis), as described previously [21]. The average in vivo limit of glutamate detection of the sensors used in this study was 0.38 μM (sem = 0.04, range 0.2–0.7 μM), which is an improvement over our previous reports [17,21] and allowed detection of lower amplitude glutamate release events.

6.4.9 Reagents

Nafion (5 wt.% solution in lower aliphatic alcohols/H2O mix), bovine serum albumin (BSA, min 96%), glutaraldehyde (25% in water), pyrrole (98%), L-glutamic acid, L-ascorbic acid, 3-hydroxytyramine (dopamine) were purchased from Aldrich Chemical Co. (Milwaukee, WI, USA). L-Glutamate oxidase (GluOx) from Streptomyces Sp. X119-6, with a rated activity of 24.9 units per mg protein (U mg−1, Lowry's method), produced by Yamasa Corporation (Chiba, Japan), was purchased from US Biological (Massachusetts MA). Phosphate buffered saline (PBS)

was composed of 50 mM Na2HPO4 with 100 mM NaCl (pH 7.4). Ultrapure water generated using a Millipore Milli-Q Water System (resistivity = 18 MΩ cm) was used for preparation of all solutions used in this work.

6.4.10 Instrumentation

Electrochemical preparation of the sensors was performed using a Versatile Multichannel Potentiostat (model VMP3) equipped with the 'p' low current option and low current N' stat box (Bio-Logic USA, LLC, Knoxville, TN). In vitro and in vivo measurements were conducted using a low-noise multichannel Fast-16 mkIII potentiostat (Quanteon), with reference electrodes consisting of a glass-enclosed Ag/AgCl wire in 3 M NaCl solution (Bioanalytical Systems, Inc., West Lafayette, IN) or a 200 μm diameter Ag/AgCl wire, respectively. All potentials are reported versus the Ag/AgCl reference electrode.

6.4.11 In vitro biosensor characterization

All biosensors were calibrated in vitro to test for sensitivity and selectivity of glutamate measurement. A constant potential of 0.7 V was applied to the working electrodes against a Ag/AgCl reference electrode in 40 mL of stirred PBS at pH 7.4 and 37 °C within a Faraday cage. Data were collected at 80 kHz and averaged over 1-s intervals. After the current detected at the electrodes equilibrated to baseline (approx. 30–45 min), aliquots of glutamate were added to the beaker to reach final glutamate concentrations in the range 5–60 μM. A calibration factor based on analysis of these data was calculated for each electrode. Additionally, aliquots of ascorbic acid (250 μM final concentration) and dopamine (5–10 μM final concentration) were added to the beaker as representative examples of readily oxidizable potential anionic and cationic interferent neurochemicals, respectively, to confirm selectivity for glutamate. For the sensors

used in these studies no current changes above the level of the noise were detected to the addition of cationic (dopamine) or anionic (ascorbic acid) interferents, as reported previously [17,21]. In order to assess the sensitivity and response time to peroxide at sites uncoated with enzyme, aliquots of H2O2 (10 μM) were also added to the beaker. Importantly, electrodes coated with PPy, Nafion and BSA/glutaraldehyde, but not GluOx, showed no detectable response to glutamate, despite being sensitive to H2O2. Indeed, there was less than a 10% statistically insignificant ($t8 = 1.28$, $p = 0.24$) difference in the H2O2 sensitivity on control electrode sites relative to enzyme-coated sites, indicating that any changes detected in vivo on the enzyme coated sites could not be attributed to endogenous H2O2.

6.4.12 Online, near-real time glutamate detection during reward seeking

Prior to the start of each test session (see Fig. 2B) rats were placed in the recording operant chamber and the biosensor was tethered to the potentiostat via the electrical swivel for application of the 0.7 V potential. Oxidative current was recorded at 80 kHz and averaged over 0.25-s intervals. The recorded amperometric signal was allowed to stabilize prior to session onset (approx. 45 min). The 2-min period immediately prior to the onset of the behavioral session was used as the baseline period for comparison of glutamate concentration changes in the absence of any reward-related behavior to those induced by responding during test. On the first test day rats received a single Pavlovian conditioning test that was identical to Pavlovian training described above. On the second day of testing rats were given instrumental conditioning sessions as described above, but with the ratio requirement progressively increasing from fixed ratio-1 to RR-20 after each 5th outcome earned. On the last test day rats received a single PIT test, identical to that described for Experiment 1.

6.4.13 Data analysis

Unless otherwise mentioned, all data were processed using Microsoft Excel (Redmond, WA), then compiled and statistically analyzed with GraphPad Prism (La Jolla, CA) and SPSS (IBM Corp, Chicago, IL). For all hypothesis tests, the α level for significance was set to $p < 0.05$. The data were analyzed with paired t-tests, repeated-measures ANOVAs (with post hoc analysis correcting for multiple comparisons), correlation and regression, where appropriate.

6.4.14 Behavioral analysis

Lever-press rate was the primary behavioral output measure. During the PIT test lever pressing for the 2-min pre-CS period was compared to that during the CS period, which was divided for presses on the lever that, during training, earned the same outcome as the cue predicted (i.e., CS-Same presses) versus those on the other available lever (i.e., CS-Different presses).

Because rats tended to organize their instrumental lever-pressing activity into clusters of many lever presses in quick succession, we focused on those presses that initiated reward seeking (i.e., 'initiating presses') excluding presses that occurred within a pressing bout when analyzing the temporal relationship between glutamate release and instrumental activity. For the instrumental conditioning test an 'initiating press' (23.68% of total presses, sem = 1.77) was defined as the first press after collection of an earned reward or, because rats often disengaged from the lever and then reinitiated reward seeking, the first press after >6 s pause in pressing. Similar definitions of initiation of reward seeking and instrumental bouts defined by pauses in activity have been described previously [70-72]. The average reward receipt to next initiating press latency was 23.10 s (sem = 7.47) for the instrumental tests, indicating that those glutamate release events that occurred within 5 s prior to initiating presses were related to the performance of this action and not to consumption of the previously earned reward. For the instrumental test

we compared the temporal relationship between glutamate and these initiating presses to that with all presses (including both initiating and intra-bout presses) in order to determine if BLA glutamate release was related to individual actions or initiation of reward-seeking activity. For the 2 instrumental conditioning tests data were collapsed across sessions, because there was neither a significant main effect of Earned outcome type ($F_{1,7} = 0.14$, $p = 0.72$), nor Outcome type x Time interaction ($F_{9,63} = 0.86$, $p = 0.56$) on the temporal relationship between glutamate and instrumental activity.

Because no rewards were delivered during the PIT test an initiating press was defined as the first press after a pause in pressing of >6 s. On average 57.00% (sem = 9.30) of all presses during the pre-CS period were initiating presses, with 40.03% (sem = 6.82) of CS-Same presses and 46.06% (sem = 6.45) of CS-Different presses considered initiating presses.

6.4.15 Neurochemical recording analysis

Analysis details and characterization of glutamate release events have been described previously [21]. Each electrode's baseline current was subtracted from its current output after equilibration (average current over 10-s period, 2 min prior to test onset). The current changes from baseline on the PPY/Nafion-coated sentinel electrode were subtracted from current changes on the PPY/Nafion/GluOx glutamate biosensor electrode to remove noise correlated among the electrodes on the MEA. The glutamate biosensor response then was converted to glutamate concentration using an electrode-specific calibration factor obtained in vitro, which averaged 152.86 μM/nA.

Because the baseline current detected at the glutamate sensing electrodes drifted over minutes during the course of the test session (see examples in Fig. 3A), as is typical for

electrochemical recordings, we focused our analysis on transient glutamate concentration changes. Mini Analysis (Synaptosoft, Decatur, GA) was used to determine the frequency, and amplitude of these rapid changes. A fluctuation in the glutamate trace was deemed a glutamate transient if it was at >2.5x the RMS noise sampled from the pre-test baseline period. To determine the transient amplitude a baseline was taken by averaging 3 sample bins around the first minima located 0.5–5 s before the peak and this baseline was subtracted from the peak amplitude. If one peak followed another within 5 s the baseline was taken after the first peak to distinguish these events. Peaks with a total duration below 0.5 s or with an immediately preceding or following negative deflection greater than half the peak amplitude were considered noise spikes and were omitted from the analysis. The frequency and amplitude of glutamate transients were averaged across the 2-min pre-test baseline period and compared to that averaged across the instrumental conditioning test, or that averaged across the 2-min pre-CS or 2-min CS periods for the PIT test. These variables were correlated against instrumental press rate during each test.

We also evaluated the precise temporal relationship between transient glutamate release events and behavioral output by assessing the likelihood of a glutamate transient in the time immediately surrounding a lever press. The likelihood of a glutamate transient was defined as the percentage of lever presses that had a glutamate transient in each of 10, 1-s time bins distributed evenly around the event. This time window was selected to ensure release events in the 5 s prior to an initiating presses were specifically related to that particular initiating press and not to contaminating events (e.g., reward delivery during the instrumental test, termination of a previous bout, head entries into the food-delivery port etc.). During the instrumental test the average reward collection to next initiating press latency was 23.10 s (SEM = 7.47), and by

definition an initiation press must have been preceded by a >6 s pause in pressing. Values were normalized as a percentage of presses, as opposed to number or percentage of transients, to control for the variation in pressing that resulted from experimental manipulation (e.g., CS presentation), which could confounded interpretation. In all cases the 1-s time bin 5 s prior to the event served as the control bin for statistical comparison because in this time bin glutamate transient likelihood did not differ from the baseline likelihood of a glutamate transient in similar epochs without lever pressing during the pre-test period ($t7 = 2.12$, $p = 0.07$). Raw glutamate transient peak times for each subject in the 5 s prior to and after initiating press are displayed in the raster plots shown in Figs 3G and4G.

6.4.16 Histology

At the conclusion of each experiment rats were anesthetized with Nembutal and transcardially perfused with 0.9% saline followed by 10% formalin saline. The brains were removed and post-fixed in formalin, then cryosectioned into 60 μm slices, mounted onto slides and stained with cresyl violet. Light microscopy was used to examine sensor or cannula placement in the BLA. Histological data are presented in Fig. 1B(Experiment 1) and 2A (Experiment 2). Four rats were removed from Experiment 1 due to cannula misplacement or bilateral BLA tissue damage.

6.5 References

[1] See, R. E., Fuchs, R. A., Ledford, C. C. & McLaughlin, J. Drug addiction, relapse, and the amygdala. Ann N Y Acad Sci 985, 294–307 (2003).

[2] Koob, G. F. & Volkow, N. D. Neurocircuitry of addiction. Neuropsychopharmacology 35, 217–238, doi: 10.1038/npp.2009.110 (2010).

[3] Belzung, C., Willner, P. & Philippot, P. Depression: from psychopathology to pathophysiology. Curr Opin Neurobiol 30C, 24–30, doi: 10.1016/j.conb.2014.08.013 (2014).

[4] Boyle, L. M. A neuroplasticity hypothesis of chronic stress in the basolateral amygdala. Yale J Biol Med 86, 117–125 (2013).

[5] Balleine, B. W. & Killcross, S. Parallel incentive processing: an integrated view of amygdala function. Trends Neurosci 29, 272–279 (2006).

[6] Janak, P. H. & Tye, K. M. From circuits to behaviour in the amygdala. Nature 517, 284–292, doi: 10.1038/nature14188 (2015).

[7] Ray, J. P. & Price, J. L. The organization of the thalamocortical connections of the mediodorsal thalamic nucleus in the rat, related to the ventral forebrain-prefrontal cortex topography. J Comp Neurol 323, 167–197, doi: 10.1002/cne.903230204 (1992).

[8] Carmichael, S. T. & Price, J. L. Limbic connections of the orbital and medial prefrontal cortex in macaque monkeys. J Comp Neurol 363, 615–641, doi: 10.1002/cne.903630408 (1995).

[9] Ghashghaei, H. T. & Barbas, H. Pathways for emotion: interactions of prefrontal and anterior temporal pathways in the amygdala of the rhesus monkey. Neuroscience 115, 1261–1279, doi: S0306452202004463 (2002).

[10] Balleine, B. W., Killcross, A. S. & Dickinson, A. The effect of lesions of the Basolateral amygdala on instrumental conditioning. J Neurosci 23, 666–675 (2003).

[11] Ostlund, S. B. & Balleine, B. W. Differential involvement of the basolateral amygdala and mediodorsal thalamus in instrumental action selection. J Neurosci 28, 4398–4405 (2008).

[12] Ostrander, S. et al. Orbitofrontal cortex and basolateral amygdala lesions result in suboptimal and dissociable reward choices on cue-guided effort in rats. Behav Neurosci 125, 350–359, doi: 10.1037/a0023574 (2011).

[13] Corbit, L. H. & Balleine, B. W. Double dissociation of basolateral and central amygdala lesions on the general and outcomespecific forms of pavlovian-instrumental transfer. J Neurosci 25, 962–970 (2005).

[14] Venton, B. J., Robinson, T. E. & Kennedy, R. T. Transient changes in nucleus accumbens amino acid concentrations correlate with individual responsivity to the predator fox odor 2,5- dihydro-2,4,5-trimethylthiazoline. J Neurochem 96, 236–246 (2006).

[15] Venton, B. J., Robinson, T. E., Kennedy, R. T. & Maren, S. Dynamic amino acid increases in the basolateral amygdala during acquisition and expression of conditioned fear. Eur J Neurosci 23, 3391–3398 (2006).

[16] Bowser, M. T. & Kennedy, R. T. In vivo monitoring of amine neurotransmitters using microdialysis with on-line capillary electrophoresis. Electrophoresis 22, 3668–3676, doi: 10.1002/1522-2683(200109)22:173.0.CO;2-M (2001).

[17] Wassum, K. M. et al. Silicon Wafer-Based Platinum Microelectrode Array Biosensor for Near Real-Time Measurement of Glutamate In Vivo. Sensors 8, 5023–5036 (2008).

[18] Burmeister, J. J. et al. Improved ceramic-based multisite microelectrode for rapid measurements of L-glutamate in the CNS. J Neurosci Methods 119, 163–171 (2002).

[19] Rutherford, E. C., Pomerleau, F., Huettl, P., Stromberg, I. & Gerhardt, G. A. Chronic secondby-second measures of L-glutamate in the central nervous system of freely moving rats. J Neurochem 102, 712–722 (2007).

[20] Walker, E., Wang, J., Hamdi, N., Monbouquette, H. G. & Maidment, N. T. Selective detection of extracellular glutamate in brain tissue using microelectrode arrays coated with overoxidized polypyrrole. Analyst 132, 1107–1111 (2007).

[21] Wassum, K. M. et al. Transient Extracellular Glutamate Events in the Basolateral Amygdala Track Reward-Seeking Actions. J Neurosci 32, 2734–2746, doi: 32/8/2734 (2012).

[22] Hascup, K. N., Hascup, E. R., Pomerleau, F., Huettl, P. & Gerhardt, G. A. Second-by-second measures of L-glutamate in the prefrontal cortex and striatum of freely moving mice. J Pharmacol Exp Ther 324, 725–731 (2008).

[23] Belay, A. et al. Redox hydrogel based bienzyme electrode for L-glutamate monitoring. J Pharm Biomed Anal 19, 93–105 (1999).

[24] van der Zeyden, M., Oldenziel, W. H., Rea, K., Cremers, T. I. & Westerink, B. H. Microdialysis of GABA and glutamate: analysis, interpretation and comparison with microsensors. Pharmacol Biochem Behav 90, 135–147 (2008).

[25] Hascup, E. R. et al. Rapid microelectrode measurements and the origin and regulation of extracellular glutamate in rat prefrontal cortex. J Neurochem 115, 1608–1620 (2010).

[26] Colwill, R. M. & Motzkin, D. K. Encoding of the unconditioned stimulus in Pavlovian conditioning. Animal Learning & Behavior 22, 384–394 (1994).

[27] Kruse, H., Overmier, J., Konz, W. & Rokke, E. Pavlovian conditioned stimulus effects upon instrumental choice behavior are reinforcer specific. Learn Motiv 14, 165–181 (1983).

[28] Holmes, N. M., Marchand, A. R. & Coutureau, E. Pavlovian to instrumental transfer: a neurobehavioural perspective. Neurosci Biobehav Rev 34, 1277–1295, doi: S0149-7634(10)00081-3 (2010).

[29] Colwill, R. M. & Rescorla, R. A. Associations between the discriminative stimulus and the reinforcer in instrumental learning. Journal of Experimental Psychology: Animal Behavior Processes 14, 155–164 (1988).

[30] Blundell, P., Hall, G. & Killcross, S. Lesions of the basolateral amygdala disrupt selective aspects of reinforcer representation in rats. J Neurosci 21, 9018–9026 (2001).

[31] Corbit, L. H. & Janak, P. H. Posterior dorsomedial striatum is critical for both selective instrumental and Pavlovian reward learning. Eur J Neurosci 31, 1312–1321, doi: 10.1111/j.1460- 9568.2010.07153.x (2010).

[32] Dickinson, A. & Balleine, B. W. in Learning, Motivation and Emotion, Volume 3 of Steven's Handbook of Experimental Psychology Vol. 3 (ed C. R. Gallistel) 497–533 (John Wiley & Sons, 2002).

[33] Schoenbaum, G., Chiba, A. A. & Gallagher, M. Neural encoding in orbitofrontal cortex and basolateral amygdala during olfactory discrimination learning. J Neurosci 19, 1876–1884 (1999). [34] Uwano, T., Nishijo, H., Ono, T. & Tamura, R. Neuronal responsiveness to various sensory stimuli, and associative learning in the rat amygdala. Neuroscience 68, 339–361 (1995).

[35] Tye, K. M. & Janak, P. H. Amygdala neurons differentially encode motivation and reinforcement. J Neurosci 27, 3937–3945, doi: 10.1523/JNEUROSCI.5281-06.2007 (2007).

[36] Paton, J. J., Belova, M. A., Morrison, S. E. & Salzman, C. D. The primate amygdala represents the positive and negative value of visual stimuli during learning. Nature 439, 865–870 (2006).

[37] Ambroggi, F., Ishikawa, A., Fields, H. L. & Nicola, S. M. Basolateral amygdala neurons facilitate reward-seeking behavior by exciting nucleus accumbens neurons. Neuron 59, 648–661, doi: 10.1016/j.neuron.2008.07.004 (2008).

[38] Schoenbaum, G., Chiba, A. A. & Gallagher, M. Orbitofrontal cortex and Basolateral amygdala encode expected outcomes during learning. Nat Neurosci 1, 155–159, doi: 10.1038/407 (1998).

[39] Carelli, R. M., Williams, J. G. & Hollander, J. A. Basolateral amygdala neurons encode cocaine self-administration and cocaineassociated cues. J Neurosci 23, 8204–8211 (2003).

[40] Dezfouli, A. & Balleine, B. W. Actions, action sequences and habits: evidence that goaldirected and habitual action control are hierarchically organized. PLoS Comput Biol 9, e1003364, doi: 10.1371/journal.pcbi.1003364 (2013).

[41] Ostlund, S. B., Winterbauer, N. E. & Balleine, B. W. Evidence of action sequence chunking in goal-directed instrumental conditioning and its dependence on the dorsomedial prefrontal cortex. J Neurosci 29, 8280–8287 (2009).

[42] Graybiel, A. M. The basal ganglia and chunking of action repertoires. Neurobiol Learn Mem 70, 119–136 (1998).

[43] Hernádi, I., Grabenhorst, F. & Schultz, W. Planning activity for internally generated reward goals in monkey amygdala neurons. Nat Neurosci 18, 461–469, doi: 10.1038/nn.3925 (2015).

[44] Bergles, D. E., Diamond, J. S. & Jahr, C. E. Clearance of glutamate inside the synapse and beyond. Curr Opin Neurobiol 9, 293–298, doi: nb9304 (1999).

[45] Diamond, J. S. A broad view of glutamate spillover. Nat Neurosci 5, 291–292, doi: nn0402- 291(2002).

[46] Tye, K. M., Stuber, G. D., de Ridder, B., Bonci, A. & Janak, P. H. Rapid strengthening of thalamo-amygdala synapses mediates cue-reward learning. Nature 453, 1253–1257, doi: 10.1038/nature06963 (2008).

[47] Shabel, S. J. & Janak, P. H. Substantial similarity in amygdala neuronal activity during conditioned appetitive and aversive emotional arousal. Proc Natl Acad Sci USA 106, 15031–15036, doi: 10.1073/pnas.0905580106 (2009).

[48] LeDoux, J. E. & Farb, C. R. Neurons of the acoustic thalamus that project to the amygdala contain glutamate. Neurosci Lett 134, 145–149 (1991).

[49] Quirk, G. J., Armony, J. L. & LeDoux, J. E. Fear conditioning enhances different temporal components of tone-evoked spike trains in auditory cortex and lateral amygdala. Neuron 19, 613–624 (1997).

[50] Kröner, S., Rosenkranz, J. A., Grace, A. A. & Barrionuevo, G. Dopamine modulates excitability of basolateral amygdala neurons in vitro. J Neurophysiol 93, 1598–1610, doi: 10.1152/jn.00843.2004 (2005).

[51] Vitale, K. R. & Janak, P. H. in Society for Neuroscience Annual Meeting 462.412 (Washington D.C., USA, 2014).

[52] Prévost, C., Liljeholm, M., Tyszka, J. M. & O'Doherty, J. P. Neural correlates of specific and general Pavlovian-to-Instrumental Transfer within human amygdalar subregions: a highresolution fMRI study. J Neurosci 32, 8383–8390, doi: 10.1523/ JNEUROSCI.6237-11.2012 (2012).

[53] Ostlund, S. B. & Balleine, B. W. Orbitofrontal cortex mediates outcome encoding in Pavlovian but not instrumental conditioning. J Neurosci 27, 4819–4825 (2007).

[54] Sah, P., Faber, E. S., Lopez De Armentia, M. & Power, J. The amygdaloid complex: anatomy and physiology. Physiol Rev 83, 803–834, doi: 10.1152/physrev.00002.2003 (2003).

[55] Dwyer, D. M. & Killcross, S. Lesions of the basolateral amygdala disrupt conditioning based on the retrieved representations of motivationally significant events. J Neurosci 26, 8305–8309 (2006).

[56] McDannald, M. A. et al. Orbitofrontal neurons acquire responses to 'valueless' Pavlovian cues during unblocking. Elife 3, e02653, doi: 10.7554/eLife.02653 (2014).

[57] Hatfield, T., Han, J. S., Conley, M., Gallagher, M. & Holland, P. Neurotoxic lesions of basolateral, but not central, amygdala interfere with Pavlovian second-order conditioning and reinforcer devaluation effects. J Neurosci 16, 5256–5265 (1996).

[58] Pickens, C. L. et al. Different roles for orbitofrontal cortex and basolateral amygdala in a reinforcer devaluation task. J Neurosci 23, 11078–11084 (2003).

[59] Wellman, L. L., Gale, K. & Malkova, L. GABAA-mediated inhibition of Basolateral amygdala blocks reward devaluation in macaques. J Neurosci 25, 4577–4586 (2005).

[60] Johnson, A. W., Gallagher, M. & Holland, P. C. The basolateral amygdala is critical to the expression of pavlovian and instrumental outcome-specific reinforcer devaluation effects. J Neurosci 29, 696–704 (2009).

[61] Fontanini, A., Grossman, S. E., Figueroa, J. A. & Katz, D. B. Distinct subtypes of Basolateral amygdala taste neurons reflect palatability and reward. J Neurosci 29, 2486–2495 (2009).

[62] Belova, M. A., Paton, J. J., Morrison, S. E. & Salzman, C. D. Expectation modulates neural responses to pleasant and aversive stimuli in primate amygdala. Neuron 55, 970–984 (2007).

[63] Salzman, C. D., Paton, J. J., Belova, M. A. & Morrison, S. E. Flexible neural representations of value in the primate brain. Ann N Y Acad Sci 1121, 336–354 (2007).

[64] Belova, M. A., Paton, J. J. & Salzman, C. D. Moment-to-moment tracking of state value in the amygdala. J Neurosci 28, 10023–10030 (2008).

[65] Jenison, R. L., Rangel, A., Oya, H., Kawasaki, H. & Howard, M. A. Value encoding in single neurons in the human amygdala during decision making. J Neurosci 31, 331–338, doi: 10.1523/jneurosci.4461-10.2011 (2011).

[66] Wassum, K. M., Cely, I. C., Balleine, B. W. & Maidment, N. T. Mu opioid receptor activation in the basolateral amygdala mediates the learning of increases but not decreases in the incentive value of a food reward. Journal of Neuroscience 31, 1583–1599 (2011).

[67] Zimmerman, J. M. & Maren, S. NMDA receptor antagonism in the basolateral but not central amygdala blocks the extinction of Pavlovian fear conditioning in rats. Eur J Neurosci 31, 1664– 1670, doi: 10.1111/j.1460-9568.2010.07223.x (2010).

[68] Walker, D. L., Paschall, G. Y. & Davis, M. Glutamate receptor antagonist infusions into the basolateral and medial amygdala reveal differential contributions to olfactory vs. context fear conditioning and expression. Learn Mem 12, 120–129, doi: 10.1101/lm.87105 (2005).

[69] Feltenstein, M. W. & See, R. E. NMDA receptor blockade in the basolateral amygdala disrupts consolidation of stimulus-reward memory and extinction learning during reinstatement of cocaine-seeking in an animal model of relapse. Neurobiol Learn Mem 88, 435–444, doi: 10.1016/j.nlm.2007.05.006 (2007).

[70] Wassum, K. M., Ostlund, S. B., Loewinger, G. C. & Maidment, N. T. Phasic Mesolimbic Dopamine Release Tracks Reward Seeking During Expression of Pavlovian-to-Instrumental Transfer. Biol Psychiatry 73, 747–755, doi: 10.1016/j.biopsych.2012.12.005 (2013).

[71] Shull, R. L., Gaynor, S. T. & Grimes, J. A. Response rate viewed as engagement bouts: resistance to extinction. J Exp Anal Behav 77, 211–231, doi: 10.1901/jeab.2002.77-211 (2002).

[72] Mellgren, R. L. & Elsmore, T. F. Extinction of operant behavior: An analysis based on foraging considerations. Animal Learning & Behavior 19, 317–325 (1991).

[73] Paxinos, G. & Watson, C. The rat brain in stereotaxic coordinates. 4th edn (Academic Press, 1998).

Chapter 7: Recommendations for Future Work

7.1 NADH sensing

Future work on NADH sensing should focus on improving the current coating methods. As mentioned before, the usage of CNT has two positive effects. First, the overpotential of NADH can be reduced with CNT, which can avoid the fouling effect on platinum electrode. Second, CNT is a material with large surface area, and CNT-coating allows more chemical reactions on the electrode. Thus, sensitivity of the NADH biosensor can be further improved. Nevertheless, there is one limitation of CNT-coated electrodes. In our current protocol, single-wall or multiple-wall CNT are coated to the electrode manually, which takes a long time and the stability of sensor performance cannot be guaranteed. If the coating process can be done by electrodeposition, the efficiency, accuracy and robustness of producing NADH biosensors will be significantly enhanced.

Graphene is another nanomaterial with excellent electron transfer properties that has been demonstrated to be very effective as catalysts. Similar to SWCNT and MWCNT, graphene also has large surface area for chemical reactions. In addition, as two-dimensional material, graphene has been reported[1] to be electrochemically deposited onto electrodes. Moreover, graphene has less metallic impurities than CNT. These impurities might dominate the electrochemistry of CNTs, reduce the signal-to-noise ratio and poison the electrode. Subbiah Alwarappan et al. [2] have shown many advantages of graphene-based electrode over MWCNT-based electrode. In their work, it is shown that graphene has more sp2 planes than MWCNT using Raman spectroscopy. The presence of more sp2 planes also leads to many positive results. First, it is observed that graphene has more than 60 times more conducting than MWCNT. Second,

electrochemical experiments found that graphene possesses greater surface negative charge than SWCNTs. Third, graphene exhibited better stability and signal-to-noise ratio than SWCNTs in ascorbic acid (AA), serotonin (ST) and dopamine (DA) sensing. It is thus promising to use electrochemically deposited-graphene to replace CNT in coating electrodes for NADH sensing.

7.2 Estradiol sensing

Further work on estradiol sensing could also focus on coating graphene on working electrode using electrochemical deposition methods. In NADH sensing, the working electrode size can be as large as 2 mm^2 to benefit the manual coating of CNT. However, in estradiol sensing, the electrode size must be kept very small. This is because that the enzyme used in EMIT is extremely expensive and sensing estradiol using the working electrode of the similar size with the one in NADH sensing is impractical. In our protocol, the size of working electrode in estradiol sensing is 40×120 μm^2. This size would make manual coating of CNT impossible. Also, the microsensor dip coating method would cause all four of the sensing sites to be coated.

The use of electrochemically deposited graphene could solve the dilemma between the size restriction of working electrode and difficulties of CNT-coating on microsensors. It was previously reported[3] that graphene oxide-platinum nanoparticles composites could sense estradiol at a level of 2 nM using ELISA. Our preliminary results of sensing estradiol on bare platinum electrode using EMIT has an even lower detection limit (1 nM). Therefore, it is promising to use graphene or graphene oxide-platinum nanoparticles composites on our working electrode to further improve the sensitivity and decrease the detection limit.

7.3 Enzyme stamp printing on microelectrode

In choline sensing, there exists a similar issue with NADH sensing. In NADH sensing, CNT are coated onto the working electrode manually. In choline sensing, choline oxidase is also loaded onto platinum electrode manually. Both steps need very careful operation and the stability of sensor is limited. It is desirable to have automatic, machine-based enzyme loading method to increase the accuracy and robustness of choline sensor.

Recently, several printing techniques have been reported to address the issue mentioned above. S. Liébana et al. designed a novel screen-printing method for mass production of biosensors[4]. In their protocol, enzymes and mediators are directly incorporated into screen printing ink followed by laser ablation procedures. Efrat Gdor et al. reported a multienzyme inkjet printing method to produce enzyme-incorporated 2D arrays[5]. Cheng-Kuan Su et. al reported an enzyme-immobilized 3D-printed reactor for glucose and lactate detection in rat brain[6]. Therefore, further work of choline sensing also includes using existing techniques to printing enzymes on microelectrode, as well as developing new stamp printing techniques for enzyme loading.

7.4 References

[1] Keun Soo Kim, et al., Large-scale pattern growth of graphene films for stretchable transparent electrodes, *Nature* 457, 706-710 (5 February 2009). Liuyun Chen, Direct electrodeposition of reduced graphene oxide on glassy carbon electrode and its electrochemical application, *Electrochemistry Communications*, Volume 13, Issue 2, February 2011, Pages 133–137.

[2] Subbiah Alwarappan, Arzum Erdem, Chang Liu and Chen-Zhong Li, Probing the Electrochemical Properties of Graphene Nanosheets for Biosensing Applications, *J. Phys. Chem. C*, 2009, 113 (20), pp 8853–8857

[3] Tingting Wen, et al. Reduced graphene oxide-platinum nanoparticles composites based imprinting sensor for sensitively electrochemical analysis of 17β-estradiol, *Journal of Electroanalytical Chemistry*, Volume 682, 15 August 2012, Pages 121–127

[4] S. Liébanaa, L.J. Jonesa, G.A. Dragoa, R.W. Pittsona, b, D. Liuc, d, W. Perriec, J.P. Hart, Design and development of novel screen-printed microelectrode and microbiosensor arrays fabricated using ultrafast pulsed laser ablation, *Sensors and Actuators B: Chemical*, Volume 231, August 2016, Pages 384–392

[5] Gdor E1, Shemesh S1, Magdassi S1, Mandler D, Multienzyme Inkjet Printed 2D Arrays, *ACS Appl Mater Interfaces.* 2015 Aug 19;7(32):17985-92

[6] Cheng-Kuan Su, Shuo-Chih Yen, Tzu-Wen Li, and Yuh-Chang Sun, Enzyme-Immobilized 3D-Printed Reactors for Online Monitoring of Rat Brain Extracellular Glucose and Lactate, *Anal. Chem*. 2016, 88, 6265−6273

Appendix A: Microprobe Fabrication Process Traveler

Updated at September 9th, 2016

Process	Step	Name	Description	Remarks
I. Field oxide formation process				
	1	Label	Label wafer backside on top/bottom/left/right edges	1. Use diamond pen 2. Inscribe on the back unpolished side
Cleaning Steps	2	Piranha bath	Remove organic contaminants: 1. H_2SO_4:H_2O_2 = 17:1 2. T=70°C; time=10min	1. Use wafer carrier 2. Refresh solution with 250mL H_2O_2 if hasn't been used that day
	3	Rinse	Time = 2min	Use rinse cycle in PFC hood
	4	HF bath	Remove native oxide: 5 sec. HF dip (DIW:HF = 10:1)	Caution. Very corrosive.
	5	Rinse	Time = 2min., N_2 blow dry after	1. Gentle water stream 2. Don't use spin dryer (wafers will break)
Furnace	6	Oxide furnace	Thermally grow 1μm SiO_2 1. Wet recipe (WET1100.001) 2. T=1100°C, time=2.5hr	1. Keep everything clean (gloves/mask on) 2. High temperature (use caution) 3. Use quartz boat. Load wafers ASAP/
	7	Nanospec	Measure SiO_2 thickness (Silicon dioxide on silicon)	Measure center/top/bottom/left/right, average it
Cleaning Steps	8	Piranha bath	Remove organic contaminants: 3. H_2SO_4:H_2O_2 = 17:1 T=70°C; time=10min	1. Use wafer carrier 2. Refresh solution with 250mL H_2O_2 if hasn't been used that day
	9	Rinse	Time = 2min	Use rinse cycle in PFC hood
II. Electrode sites, channels, and bonding pads formation				
Lithography I	10	Dehydration bake	T=150°C Time ≥ 5 min	Drive off moisture, and improve PR adhesion
	11	HDMS coat	Improve PR adhesion	1. HMDS: hexamethyldisilazane

			Time ≥ 5 min	2. Place wafer into HDMS container while it is still hot 3. Toxic (operate underneath hood) 4. Do not place wafer in the middle of metal container. Handle dips down and will break wafer when putting cover on.
	12	Photoresist spin coat	PR: AZ5214-EIR Thickness: ~1.6μm 2500 RPM, Ramp = 1000, time = 30sec	Clean wafer chuck with acetone Make sure PR covers at least 2/3 of the wafer surface prior to spin
	13	Soft bake	T=100°C, time = 1 min. (critical) Place at the center of hotplate	Make sure wafer is flat on hotplate
	14	Exposure	Karl Suss alignment: Soft contact, expose for 18 sec (when power = 8 mW/cm^2)	If power varies, use this formula to correct exposure time: t (sec) = 18*(8/actual power in mW/cm^2)
		Relax for 5 mins		
	15	Development	Remove exposed PR 5:1 :: DIW:AZ400K developer 19 sec. swishing back and forth	1. 1500mL DIW : 300mL AZ400K 2. Use single wafer holder 3. Rinse with DIW for 2 min. 4. Dry with N_2
	16	Microscope	Inspection	Make sure wafer is fully developed. Do NOT hardbake after this step (for better lift-off results) Remove 100A PR for the whole wafer to prevent metal from being washed off during Lift-off
		Remove 100A PR	Tegal	
Metal Deposition	17	Metal deposition	Old CHA (evaporated metal deposition) Cr/Pt 200Å/1000Å	1. Deposit metal within 2 weeks after Litho I 2. Total deposition time: ~3hrs

			(respectively) Deposition rate: 1Å/sec	
	18	Lift-off	Metal etch: sonicate in acetone (in 2L beaker)	1. Use 3 beakers of acetone in series to clean each wafer 2. Do not sonicate wafer for more than 10s in acetone for each time 3. Keep wafers wet by rinsing with acetone 4. Rinse with DIW and dry with N_2
	19	Microscope	Inspection	Check for broken leads, chipped sites
III. Insulation layer deposition				
Oxide/Nitride Deposition	20	PECVD oxide	STS PECVD: 7500Å Recipe: HFSIOST Time: ~30min	Blowdry wafer with N_2 prior to placing in machine
	21	Nanospec	Measure SiO_2 thickness (Silicon dioxide on silicon) Goal: 7500Å	Measure center/top/bottom/left/right Subtract field oxide thickness to calculate deposited thickness
	22	PECVD nitride	STS PECVD: 7500Å Recipe: HFSINST Time: ~50min	
	23	Nanospec	Measure Si_3N_4 thickness (silicon nitride on silicon dioxide) Goal: 7500Å	Measure center/top/bottom/left/right For previous oxide thickness, type in average from step #21
IV. Open electrodes/soldering pads				
Lithography II	24	Dehydration bake	T=150°C Time ≥ 5 min	Drive off moisture
	25	HDMS coat	Improve PR adhesion Time ≥ 5 min	1. HMDS: hexamethyldisilazane 2. Toxic (operate underneath hood) 3. Do not place wafer in the middle of metal container. Handle dips down and will break wafer when putting

				cover on.
	26	Photoresist spin coat	PR: AZ5214-EIR Thickness: ~1.6μm 2500 RPM, Ramp = 1000, time = 30sec	Clean wafer chuck with acetone Make sure PR covers at least 2/3 of the wafer surface prior to spin
	27	Soft bake	T=100°C, time = 1 min. (critical) Place at the center of hotplate	Make sure wafer is flat on hotplate
	28	Exposure	Karl Suss alignment: Soft contact, expose for 18 sec (when power = 8 mW/cm^2)	If power varies, use this formula to correct exposure time: t (sec) = 18*(8/actual power in mW/cm^2)
	29	Development	Remove exposed PR 5:1 :: DIW:AZ400K developer 19 sec. swishing back and forth	1. 1500mL DIW : 300mL AZ400K 2. Use single wafer holder 3. Rinse with DIW for 2 min. 4. Dry with N_2
	30	Microscope	Inspection	Make sure wafer is fully developed.
	31	Hard bake	T = 150°C, 5min. Place at center of hotplate	1. Do not post bake before inspection 2. Let cool before storing
Nitride/Oxide Etch	32	Si wafer carrier	Apply moist cooling grease on 500μm Si wafer carrier Bake 3min @ 75°C on hotplate	1. Use q-tips to apply grease in circles over entire surface of carrier wafer 2. Make sure wafer backside is clean of grease 3. Stick wafer onto carrier wafer tightly by placing onto wafer and rotating until flats are aligned
	33	Nitride and oxide etch	AOE (recipe: OXIDAPIC) Etch time: ~4 min. (this etch time may be longer or shorter depending on the status of the AOE)	1. Remove 1.5μm of nitride and oxide insulation layer 2. Do not run the etching more than 2 min for each time
	34	Inspection	Voltmeter or Nanospec	Voltmeter: check if resistance between test metal is zero

				Nanospec: check if thickness of oxide ≤field oxide thickness (oxide thickness<10,000A)
Cleaning Steps	35	PR strip	Matrix stripper "3 min strip" recipe	Make sure to keep wafer stuck to carrier wafer until after this step
	36	Release carrier	Slide wafer off carefully	Clean wafer backside and carrier wafer with acetone
V. Define probe outline				
Lithography III	37	Dehydration bake	T=150°C Time ≥ 5 min	Drive off moisture
	38	Photoresist spin coat	PR: AZ4620 Thickness: ~7μm 3000RPM, Ramp: 1000, Time: 30sec	1. Clean chuck with acetone 2. Make sure PR covers at least 2/3 of wafer surface
	39	Soft bake (prebake)	T=100°C, 1'30". (critical) Place at center of hotplate	Make sure wafer is flat on hotplate
	40	Exposure	Karl Suss alignment: Soft contact, exposure time: 18 sec (power: 8mW/cm^2)	If power varies, use this formula to correct exposure time: t (sec) = 18*(8/actual power in mW/cm^2)
	41	Relax	Ambient 5 min	
	43	Development	Remove exposed PR DIW:AZ400K = 4:1 developer 4-10 mins.	Rinse with DI water for 2 min. post development Blow dry with N_2
	44	Microscope	Inspection	Make sure wafer is fully developed
		Hard bake	150°C for 5 mins	
Si Wafer Etch-Through	45	Si wafer carrier	Apply moist cooling grease on 500μm thick Si carrier wafer Bake 3 min. @ 75°C	1. Use q-tips to apply grease in circles over entire surface of carrier wafer 2. Make sure wafer backside is clean of grease 3. Stick wafer onto carrier wafer

				tightly by placing onto wafer and rotating until flats are aligned
	46	Nitride/oxide etch	AOE (recipe: OXIDAPIC) Etch time: ~7-8 min. (this etch time may be longer or shorter depending on the status of the AOE)	1. Remove all nitride and oxide from exposed areas
	47	Inspection	Voltmeter: Si test square at bottom	1. Resistance is ~16MΩ if all oxide and nitride is removed
	48	Si etch through	FDRIE (deep reactive ion etch): Recipe FN-DY ~20 min. total etch time (this etch time may be longer or shorter depending on the status of the FDRIE)	1. Do not run DRIE for more than 5 minutes at a time (could overheat the wafer) 2. If getting pressure error, run an O_2 plasma clean for 30 min
	49	Inspection	Microscope	Do not release wafer from carrier until etch through of silicon is confirmed. Should be able to see cooling grease through the outlines for silicon etch through
Stripping PR	50	Release carrier	Slide wafer off carefully	Clean carrier with acetone
	51	PR strip	PR stripper sink (ALEG 355) T=75°C, at least 30 min.	Rinse with DI water for 2 min. after Blow dry with N2

Appendix B: CNT Coatings Preparation on Disk Electrode

B.1 Materials

- IsoNanotube-M, a single-walled, metallic carbon nanotubes (SWCNTs) (NanoIntegris, Inc.)
- FloTube™ 9000, a multiwalled carbon nanotube (MWCNT) powder of 95% purity (Cnano, Inc.).
- N,N-dimethylformamide (DMF) (Sigma Aldrich).
- Beta Nicotinamide adenine dinucleotide (NADH), reduced disodium salt hydrate, ≧97% (Sigma Aldrich)
- Phosphate buffer solution (PBS; pH 7.4), prepared with 50 mM sodium phosphate dibasic (Sigma) and 100 mM sodium chloride (Fisher)
- Acetic acid, 99.7% (Fisher, ACS certified reagent grade)
- Sulfuric acid, 73–98% (Fisher, ACS certified reagent grade)
- Nitric acid, 50%–70% (Fisher, ACS certified reagent grade)
- Isopropyl alcohol (Fisher, ACS certified reagent grade)

B.2 Pre-procedure

B.2.1 Preparation of metallic SWCNT-coated electrodes

1. Clean Scan: Bare platinum electrodes were cleaned chemically with isopropyl alcohol and then treated electrochemically in 1 M sulfuric acid by cycling from−0.25 V to 1.65 V at a scan rate of 50 mV s−1 for 3 cycles. Following cleaning, the electrodes were dried with Ar.
2. The metallic SWCNT coated electrodes were prepared by casting 2 μL aliquots of a 0.1 mg SWCNT in 10 mL aqueous suspension on the surfaces of 1.6-mm-diameter Pt disk electrodes and by drying for 30 min in air at room temperature between applications.
3. After application and drying of each layer, three droplets (50–100 μL) of a nitric and sulfuric acid mixture (1:3 ratio, of 70% and 98% acid, respectively) were applied to the electrode surfaces.
4. After 10 min, the electrodes were rinsed with ultrapure water and dried with Ar.
5. Repeat step 2-4 if more layers need to be loaded

B.2.2 Preparation of MWCNT-coated electrodes

1. Clean Scan: Bare platinum electrodes were cleaned chemically with isopropyl alcohol and then treated electrochemically in 1 M sulfuric acid by cycling from−0.25 V to 1.65 V at a scan rate of 50 mV s−1 for 3 cycles. Following cleaning, the electrodes were dried with Ar.
2. The MWCNT powder was dispersed in 1 mL DMF solvent and sonicated for 1 h.

3. 2 μL volumes of these multiwall MWCNT-DMF solutions were cast on Pt disk electrodes and dried for 1 h at room temperature.
4. After application and drying of each layer, three droplets (50–100 μL) of a nitric and sulfuric acid mixture (1:3 ratio, of 70% and 98% acid, respectively) were applied to the electrode surfaces.

B.3 Procedure

B.3.1 Cyclic Voltammetry Test

1. Make a 10mL10 mM NADH solution in PBS buffer, pH 7.4.
2. Set the potentiostat settings over a potential range of−0.4–1.0 V (vs. Ag/AgCl) at a potential sweep rate of 5 mV s^{-1} for totally 3 cycles.
3. Record the value of potential corresponding to peak currents..

B.3.2 Constant Potential Amperometry Test

1. Make a 1mL 25 mM NADH stock solution in PBS buffer, pH 7.4.
2. For metallic SWCNT-coated electrodes, apply 0.7v potential to run the amperometry test in 10 mL of PBS buffer. For MWCNT-coated electrodes, apply peak potential from cyclic voltammograms to run the amperometry test in 10 mL of PBS.
3. Successively add 10 μL of 25 mM NADH stock solution into PBS.

Appendix C: Ag/Ag Cl Wire Reference Electrode Preparation

C.1 Materials

- Silver wire (A-M systems)
- Hydrochloride Acid (Fisher)
- Sodium Chloride (Fisher)
- 9V battery and alligator clips

C.2 Procedures

1. Slice off coating of silver wire (200 microns of one end and about 1 cm of other)
2. Using alligator clips, clamp the 1 cm end to the + lead of a 9V battery
3. Place this and the silver wire attached to the – lead in a small vial of 2mM HCl saturated with NaCl for 15 minutes (bubbles should form immediately)
4. When done, place in 3M NaCl solution to cure before used in electrochemical measurement.

(This procedure is based on the protocol from Eric Walker)

Appendix D: Estradiol ElectroEMIT Detection-Immunoassay Preparation and Electrochemical Measurement

D.1 Materials

- β-Ethyl-6-one 6-(O-carboxymethyloxime) (E2-6-CMO, Sigma K2126)
- N-hydroxysuccinimide (NHS, Pierce 24500)
- 1-Ethyl-3-[3-dimethylaminopropyl]carbodiimide hydrochloride (EDC, Pierce 22980)
- Glucose-6-phosphate dehydrogenase from Leuconostoc mesenteroides (G6PDH, Sigma G5885)
- N,N-Dimethylformamide, anhydrous, 99.8% (DMF, Sigma 227056),
- Zeba™ desalt spin columns, 0.5mL, (Pierce 89883)
- Microcon Y-M30 (Millipore 42410), β-Estradiol (E2, Sigma E8875)
- D-Glucose 6-phosphate sodium salt, (G6P, Sigma G7879)
- Nicotinamide adenine dinucletide hydrate (NAD+, Sigma N7004)
- Filtered PBS buffer (pH = 7.3)
- Trizma
- Gelatin
- Sodium chloride (Fisher)

D.2 Pre-procedures

1. Make stock solutions
   a. 150mM E2-6-CMO stock: dissolve E2-6-CMO (5 mg/bottle, in fridge) solid in 93 uL DMF. Store in 4 °C fridge before use.
   b. 4 mg,protein/mL G6PDH stock: dissolve G6PDH in DI water. The volume of DI water added depends on the specific activity of the enzyme. Store the solution at 4 °C before use. The reconstituted solution is good ~1 month.
   c. EDC stock: dissolve 10 mg EDC solid (in -20°C freezer) in 500uL DMF. Prepare freshly.
   d. NHS stock: dissolve 10 mg EDC solid (in 4 °C fridge) in 500uL DMF. Prepare freshly.
   e. PBS buffer: 100 mM Sodium phosphate buffer at pH 7.3. Use filter to filtrate it.
   f. Gelatin storage solution: 50mM Trizma, 0.1M NaCl, 1% gelatin solution heat up to 60°C to dissolve gelatin and cool down to room temperature and adjust PH to 8. The solution should prepare freshly or aliquoted in freezer.
   g. Tris-buffer: 30mM MgCl2, 50mM Trizma, pH = 7.8.
   h. Estradiol antibody (E2AB) aliquots: dissolve lyophilized E2AB in 1.5 mL gelatin storage buffer in the vial. Dispense the solution into microcentrifuge tubes and store at -20 °C before use.
2. E2-6-CMO activation solution
   a. Put a micro stir bar into a micro-centrifuge tube, and turn on the stirrer.

b. Add 23uL DMF, 10.36uL NHS stock, 3uL E2-6-CMO stock solution and 8.63uL EDC stock in sequence to make a final concentration 40 mM NHS, 20 mM EDC, and 10 mM E2-6-CMO in 100% DMF
c. Stir for 1h for activation solution preparation at room temperature.

3. G6PDH conjugation solution
   a. Put another micro stir bar into another micro-centrifuge tube, and turn on the stirrer (mild).
   b. Add 100uL filtered SPB,14.95uL DMF, 3.94Ul G6PDH stock and 11.05uL E2-6-CMO (step addition, 5 times, 2.21uL each time) activation solution in sequence to make a final concentration 100 U/mL G6PDH, 20% DMF, and 0.85 mM E2-6-CMO (corresponding to 9 E2/lysine) in SPB
   c. Mildly stir 40 min for enzyme conjugation at room temperature.

4. Exchange desalt spin column buffer
   a. Place the column in a microcentrifuge tube, centrifuge at 4500 rpm for 1 min to remove storage solution,
   b. Add 300 uL filtered SPB and centrifuge at 4500 rpm for 1 min
   c. Repeat exchanging buffer for two more times.

5. Enzyme Conjugate Purification
   a. Load 130uL G6PDH conjugation solution on top of the compact resin bed of desalt column and centrifuge at 4500 rpm for 2 min. Discard the desalt column after use.
   b. Transfer the 130uL filtrate to microcon reservoir and add 370uL filtered SPB to make the total volume equals to 500uL. Centrifuge at 6000 rpm for 10 min.
   c. Discard the filtrate and repeat two more times
   d. Collect the purified G6PDH conjugation solution by invert the membrane reservoir into another clean microcentrifuge tube and spin at 3500 rpm for 3 min.
   e. Dilute the recovered G6PDH conjugation solution 50 times in gelatin storage solution and store at 4°C prior use.

D.3 Procedures

1. Dilute 2.25 mM 17beta-estradiol (E2) stock solution with Tris-buffer to make a 30uM, 3uM, 300nM, 30nM, 3nM E2.
2. Put microsensors, Ag/AgCl wires, platinum counter electrode into a very small vial and connect the electrodes into electro system.
3. For the unrepressed test (Negative):
   a. Prepare 100 mM G6P (28.2mg) solution in 1mL DI water and 60 mM NAD+ (39.8 mg) solution in 1mL DI water. Store at 4 °C before use (good for ~1 week). Mix G6P solution and NAD+ solution in 1:1 volumetric ratio (G6P/NAD+ solution: 50 mM

G6P and 30 mM NAD+) right before performing enzyme assay (discard the mixture after performing the assay).

b. Inject 70uL Tris-buffer and 14uL gelatin solution into the small vial, mix them well.
c. Start the potentiostat, 0.7v constant amperometry, and wait for 5min.
d. Inject G6P/NAD+ mixture 14uL into the small vial and use pipet to mix the solution well, and wait for 1min.
e. Inject 7uL E2-G6PDH enzyme conjugation solution (50x or 100x diluted in gelatin solution) and use pipet to mix the solution well and wait for over 30min.

4. For the full repressed test (Positive):
   a. Inject 70uL Tris-buffer and 14uL E2AB solution into the small vial, mix them well.
   b. Start the potentiostat, 0.7v constant amperometry and wait for 5min.
   c. Inject G6P/NAD+ mixture 14uL into the small vial and use pipet to mix the solution well and wait for 1min.
   d. Inject 7uL E2-G6PDH enzyme conjugation solution (50x or 100x diluted in gelatin solution) and use pipet to mix the solution well and wait for over 30min.

5. For various concentration of free estradiol test
   a. Inject 70uL free estradiol solution and 14uL E2AB solution into the small vial, mix them well.
   b. Start the potentiostat, 0.7v constant amperometry and wait for 5min.
   c. Inject G6P/NAD+ mixture 14uL into the small vial and use pipet to mix the solution well and wait for 1min.
   d. Inject 7uL E2-G6PDH enzyme conjugation solution (50x or 100x diluted in gelatin solution) and use pipet to mix the solution well and wait for over 30min.

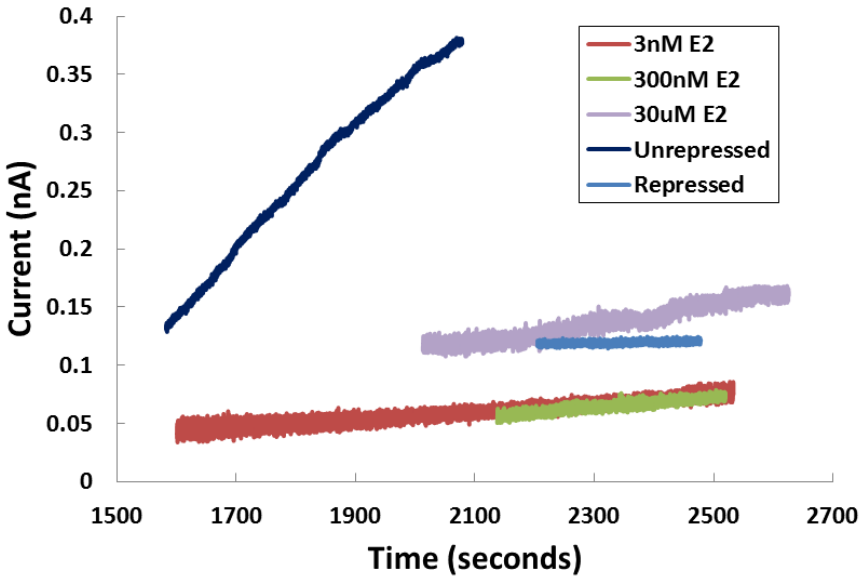

Estradiol detection with potentiostat, current vs. time

This is the figure that should be observed after injection of E2-G6PDH enzyme conjugate.

50X Estradiol	**Regression**
Negative Equation	y=0.0005x-0.6727
Positive Equation	y=0.000008x+0.0998
3 nM	y=0.00003x-0.0129
300 nM	y=0.00004x-0.0389
30 uM	y=0.00008x-0.0551

The slope of the regression equation could be used to calibrate and quantify the estradiol concentration.

Appendix E: Choline Microsensor Preparation

E.1 Materials

- Choline Oxidase from Anthrobacter globiformis. (C5896, Sigma). Dilute ChOx to 0.5 units/uL in DI water, mix well (for 100 units, add 200 uL H_2O). Divide into 4ul (2U) aliquots. Store in freezer
- glutaraldehyde solution (25%) (Sigma)
- bovine serum albumin (BSA) lyophilized powder (Sigma)
- m-phenylenediamine, Nafion® (5%, Sigma P23954)
- hydrogen peroxide solution (30%), formic acid, chloroplatinic acid hexahydrate, chloroplatinic acid, and lead acetate (Sigma)
- Iridium tetrachloride hydrate, anhydrous potassium carbonate, oxalic acid dehydrate (99%) (Sigma)
- choline hydrochloride, L-ascorbic acid, dopamine hydrochloride, 3,4-dihydroxyphenylacetic acid, 3,4-dihydroxy-DL-phenylalanine, uric acid (Sigma)
- Isopropyl alcohol and hydrochloric acid (Fisher Scientific)
- Ag/AgCl glass-bodied reference electrodes with 3 M NaCl electrolyte and a 0.5 mm diameter platinum (Pt) wire auxiliary electrode (BASi)
- Sodium phosphate buffer (PBS) was composed of 50 mM sodium phosphate (dibasic) and 100 mM sodium chloride (pH 7.4). Deionized water was generated using a Millipore Milli-Q Water System and was used for preparation of all solutions.

E.2 Procedures

E.2.1 Probe Assembly

- Detach each probe off of wafer (press on corner w/ fine forceps); record wafer ID and region of wafer. Check (under microscope) for surface scratches that have compromised insulation, or nicks along platinum leads
- Secure probe on plastic backing: Cut plastic square coverslips into strips (width equal to probe width) Use quick stick epoxy (1:1 ratio, mix) on back end of swab to dab on one end of plastic strip. Use fine forceps to place probe on plastic (plastic backing should not extend past contact pads). Allow to dry for at least 10min.
- Cut 2 red and 2 white insulated wires (~250-75 mm) per probe, strip one end ~1cm, another end ~2 mm
- Solder (@ 510°C) wires to probe head (one color of wire for Ch. 1&2; another color of wire for Ch. 3&4) with metal Lead. Apply dab of soldering flax to probe head using back of swab. Roll large bead of platinum over contact pads to create individual beads on each

pad. Place 2 mm stripped end on platinum bead, using additional solder on tip to melt wire into platinum bead.

- Clean probe for 2 min in 2-propanol (IPA) at RT in beaker floating in sonicator. Submerge entire probe in first beaker of IPA first and submerge only tip of probe in second beaker of **clean** IPA. Rinse with DI water and dry with argon gas
- Insulate probe head with quick stick epoxy (1:1 ratio, mix). Dab on with back end of swab, allow to cure 10 min. Reapply to ensure there is no open wire/solder, especially around corners
- Label probe (attach label to Ch. 1)

E.2.2 Bare sensor test

- Make 1:1000 H_2O_2 dilution solution
- Apply 0.7v potential to do the amperometric test in PBS buffer, wait 2min
- Inject 20uL of H2O2 solution and record the current increase. The probe could be used only if the current increase is over 1nA.

E.2.3 PPY or PPD deposition and Nafion coating

Protocol 1: PPY+Nafion

Pyrrole (Py) Deposit – Dopamine exclusion layer

1. Prepare 200mM Py in 1X PBS (140ul Py + 10mL 1X PBS) in 15mL falcon tube, shake vigorously
    - Solution should be very faint yellow and uniform; if yellow, it may be too old
    - Pour 200mM Py solution in small glassware with mini stir bar, set to high stirring
2. Connect reference electrode and counter electrode to corresponding clips
    - Ensure stir bar is not hitting either, or you will get noisy data
3. Secure probe on holder, submerge half of probe shaft in 200mM Py and connect each Ch. 1-4 to corresponding clip
4. Use EC-Lab software to load Py depositing settings to desired channels (hold Shift + Ch#)
    - Apply 0.85V, 5min; record current, I (nA), and charge, Q (nA*h)
    - Current and total charge is a good indicator of pyrrole layer thickness and uniformity (High I & Q indicates thick Py, low sensitivity. Noise usually indicates uneven coating. I should be <5nA, ideally ~2nA. Q should be <1nA*h, ideally ~0.5nA*h. Copy final I and Q data to Biosensor worksheet

5. Disconnect probe, raise probe, remove from holder, Rinse with DI water and dry gently with Argon gas

6. Check under microscope for uniformity of Py deposit on each site

- Angle probe under scope, such that light reflects maximally off probe surface
- Good deposit will appear as shiny, smooth, gold
- Bad deposit will appear gold with black puncta (grainy), uneven/clumps, or large black areas
- No deposit will look metallic (bare Platinum), usually resulting from disrupted leads

Nafion (Nf) Coating – Ascorbic Acid exclusion layer

1. Set Oven to 180°C (~30 min before coating)

- Good idea to set 30min before experiments to reduce waiting

2. Dip-coat the probe sites in 2% Nf solution in hood very slowly.

- Ensure Nf solution being used is 2% concentration (200uL 5%Nf + 300uL DI water) and that it is not too old (will start to look dark).
- Secure on aluminum tray, with tip of probe tilted up (not touching tray) to avoid scorching

3. Place tray with secured probed in oven for 3 min on upper shelf (bottom shelf in much hotter).

- Remove tray from oven with forceps and allow to cool >2min

4. Repeat steps 2-3, one time for a total of two 2% Nf layers.

Protocol 2: PPD+Nafion

PPD Deposit – Ascorbic and Dopamine exclusion layer

1. Prepare 5mM PPD in 1X PBS (5.4mg PPD powder + 10mL 1X PBS) in 15mL falcon tube, shake vigorously

- Pour 5mM PPD solution in small glassware with mini stir bar, set to high stirring

2. Connect reference electrode and counter electrode to corresponding clips

- Ensure stir bar is not hitting either, or you will get noisy data

3. Secure probe on holder, submerge half of probe shaft in 5mM PPD and connect each Ch. 1-4 to corresponding clip

4. Use EC-Lab software to load PPD depositing settings to desired channels (hold Shift + Ch#)

    - Apply 0.85V, 5min; record current, I (nA), and charge, Q (nA*h)
    - Current and total charge is a good indicator of pyrrole layer thickness and uniformity. (High I & Q indicates thick PPD, low sensitivity. Noise usually indicates uneven coating. Q should be <0.3nA*h, ideally ~0.1-0.2nA*h. Most common value 0.13 nA*h)
    - Copy final I and Q data to Biosensor worksheet

5. Disconnect probe, raise probe, remove from holder, Rinse with DI water and dry gently with Argon gas

6. Check under microscope for uniformity of PPD deposit on each site

    - Angle probe under scope, such that light reflects maximally off probe surface
    - Good deposit will appear as shiny, smooth, gold
    - Bad deposit will appear gold with black puncta (grainy), uneven/clumps, or large black areas
    - No deposit will look metallic (bare Platinum), usually resulting from disrupted leads

Nafion (Nf) Coating – Ascorbic Acid exclusion layer

1. Set Oven to 175°C (~30 min before coating)

    - Good idea to set at start of Py deposit to reduce waiting

2. Dip-coat the probe sites in 1% Nf solution in hood very slowly.

    - Ensure Nf solution being used is 1% concentration (100uL 5%Nf + 400uL DI water) and that it is not too old (will start to look dark).
    - Secure on aluminum tray, with tip of probe tilted up (not touching tray) to avoid scorching

3. Place tray with secured probed in oven for 4 min on upper shelf (bottom shelf in much hotter).

    - Remove tray from oven with forceps and allow to cool >3min

Protocol 3: PPD only without Nafion

PPD Deposit – Ascorbic and Dopamine exclusion layer

1. Prepare 5mM PPD in 1X PBS (5.4mg PPD powder + 10mL 1X PBS) in 15mL falcon tube, shake vigorously

- Pour 5mM PPD solution in small glassware with mini stir bar, set to high stirring

2. Connect reference electrode and counter electrode to corresponding clips

   - Ensure stir bar is not hitting either, or you will get noisy data

3. Secure probe on holder, submerge half of probe shaft in 5mM PPD and connect each Ch. 1-4 to corresponding clip

4. Use EC-Lab software to load PPD depositing settings to desired channels (hold Shift + Ch#)

   - Apply 0.85V, 10min; record current, I (nA), and charge, Q (nA*h)
   - Current and total charge is a good indicator of pyrrole layer thickness and uniformity. (High I & Q indicates thick PPD, low sensitivity. Noise usually indicates uneven coating Q should be <0.3nA*h, ideally ~0.1-0.2nA*h. Most common value 0.16 nA*h)
   - Copy final I and Q data to Biosensor worksheet

5. Disconnect probe, raise probe, remove from holder, Rinse with DI water and dry gently with Argon gas

6. Check under microscope for uniformity of PPD deposit on each site

   - Angle probe under scope, such that light reflects maximally off probe surface
   - Good deposit will appear as shiny, smooth, gold
   - Bad deposit will appear gold with black puncta (grainy), uneven/clumps, or large black areas
   - No deposit will look metallic (bare Platinum), usually resulting from disrupted leads

E.2.4 Enzyme Immobilization

1. Thaw 4 uL ChOx Enzyme aliquot (2 units), and allocate sensors under microscope and make it visible under microscope.

2. Prepare fresh protein matrix (60mg BSA + 1000ul DI water, dissolve; then add 15uL 25% glutaraldehyde), mix well. Immediately add 2 uL the BSA/GAH mixture into 4uL enzyme aliquot, mix well.

3. Immediately (because the mixture could turn into get in 2 min) coat control channels (Ch. 1 and 2) with BSA/GAH mixture (4 coats). Special pipet tip (thin and long) should be used here to load enzyme.

4. After at least 5 minute of incubation in room temperature, the BSA/GAH/ChOx mixture should be loaded on 2 sites (Ch. 3, and 4) with12 coats each.

5. Label the sensors and carrying box and allow them to cure 48 hours in fridge with desiccants.

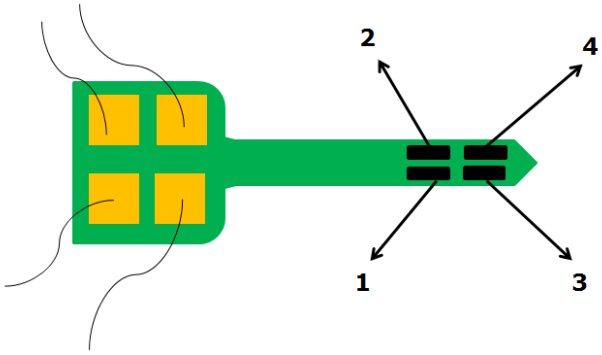
2
4
1
3

Appendix F: IrOx/ PtBLK / Pt Grass Deposition Solution Preparation

F.1 IrOx deposition

1. Iridium tetrachloride (IrCl4) solution

    a. Dissolve 15 mg of iridium tetrachloride in 10 mL of water then stir solution for 30 min. Purge the IrCl4 bottle then store in container with dessicant in 4°C.
    b. Add 0.1 mL of aqueous 30% hydrogen peroxide solution then stir for 10 min.
    c. Add 50 mg of oxalic acid dihydrate to solution and stir for 10 min.
    d. Adjust pH of solution to 10.5 by adding small portions of anhydrous potassium carbonate.
    e. Allow the resulting solution to sit quiescently for 48 h before electrodeposition. (When colors changed to purple)

2. Iridium oxide electrodeposition

    a. Cycle 100 times between 0.0 V and 0.6 V at 50 mV/s while stirring on lowest setting. Film should be a purple or blue color when inspected under the microscope.

3. Store sensor

    a. Place ~200 uL of PBS in microcentrifuge tube. Insert probe such that only shaft is submerged in PBS. Do not let head touch PBS. Hold probe in place and seal top with putty. *Sensor should be stored in this manner ~2 days prior to further sensor modifications (i.e. for glutamate sensor).

Reference

Yamanaka, K. "Anodically Electrodeposited Iridium Oxide Films (AEIROF) from Alkaline Solutions for Electrochromic Display Devices," Japanese J. of Applied Physics, April 1989.

F.2 PtBLK deposition

1. PtBlk plating solution

    a. Dissolve 0.1g chloroplatinic acid, 0.001g lead acetate in 9.9mL DI water.
    a. Dilute pure HCL 10 times and then get out 2.1uL and inject to a mixture to make final concentration 1% chloroplatinic acid, 0.0025% HCl, and 0.01% lead acetate in water

2. PtBLK electrodeposition

a. Use CV deposition method: –1.4 to –2.0V at 500 mV/sec for a total of 15 cycles in the vigorously stirred PtBlk plating solution
b. Rinse electrode in 30% H2O2 to remove any weakly bound Pt particles.

If PtBLK is used as a pre-coating material of reference electrode, then after PtBLK electrodeposition, IrOX should be electrodeposited over the PtBLK, following Appendix F.1 .

F.3 Pt Grass deposition

1. Pt grass deposition solution

    a. Make 2.5 mM H2PtCl6 and 1.5 mM formic acid (1x concentrated for working electrode use or reference electrode use)
    b. Make 25 mM H2PtCl6 and 15 mM formic acid (10x concentrated for reference electrode use)

2. Pt grass electrodeposition

    a. Conduct constant potential amperometry in Pt grass deposition solution at a potential of -0.1 V vs Ag/AgCl for 300 s

If Pt grass is used as a pre-coating material of reference electrode, then after Pt grass electrodeposition, IrOX should be electrodeposited over the Pt grass, following Appendix F.1 .

Appendix G: Noise filtering protocol for the VMP3 potentiostat

The following protocols can filter background noise generated in constant potential amperometry test using VMP3 potentiostat. Platinum black (Pt-black) is used as example here.

1. The original current vs. time figure is like the following two, where the second one is the enlargement of part of the first figure.

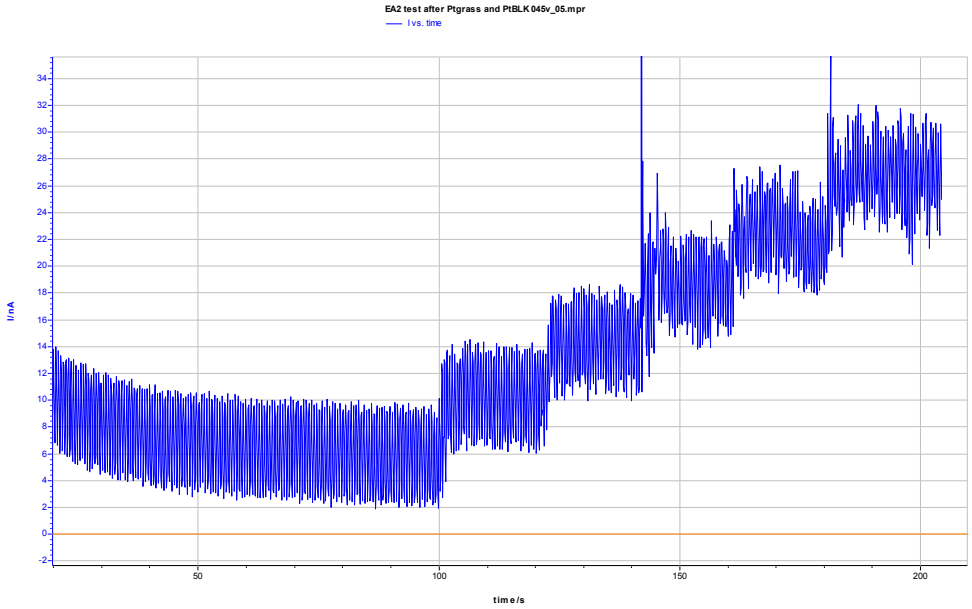

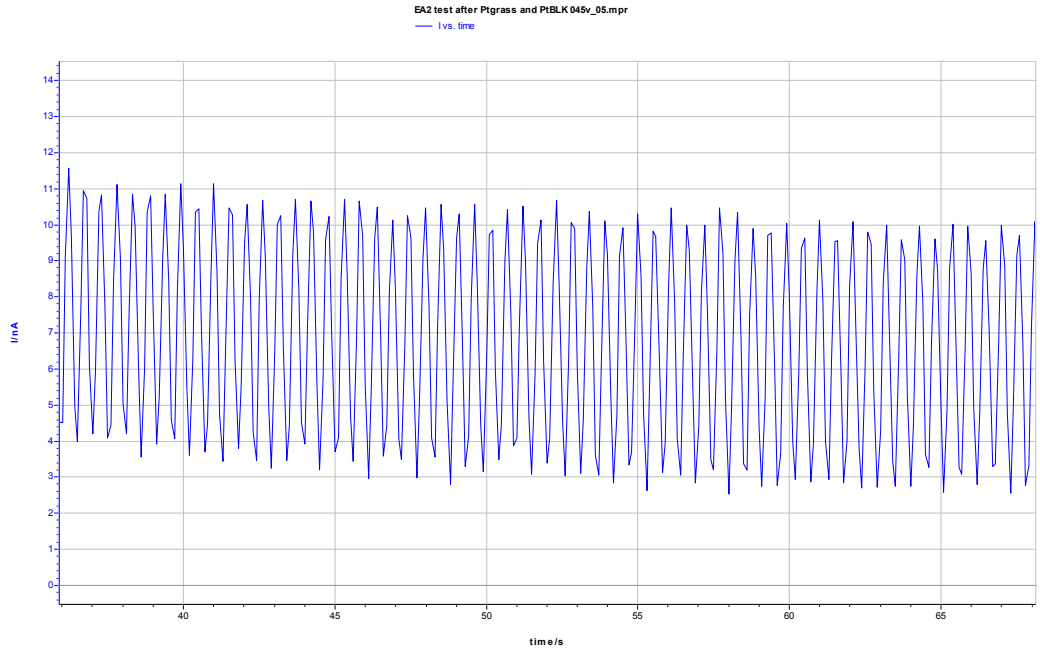

2. Do the Fourier Transformation to find the frequency band of the noise, choose ‘Fourier Transformation’ button.

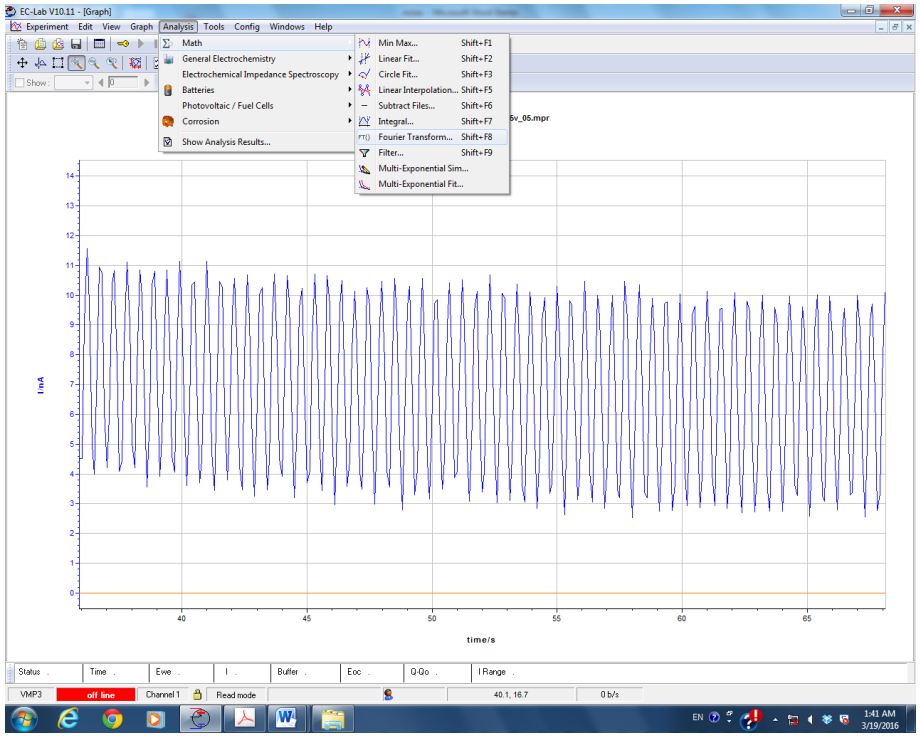

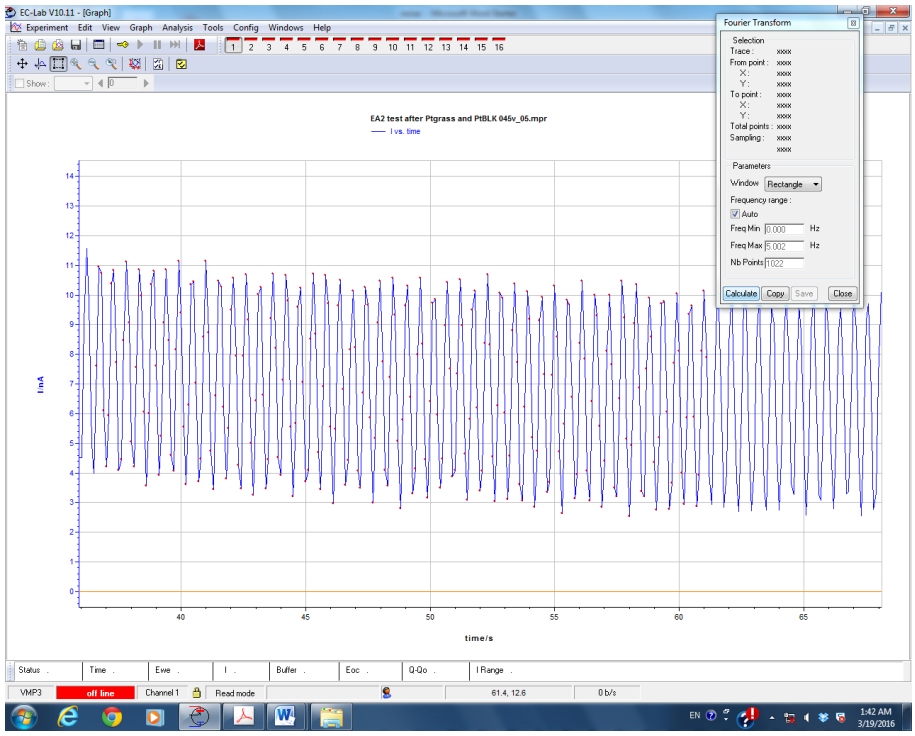

3. Click Calculate, then we get the following figure:

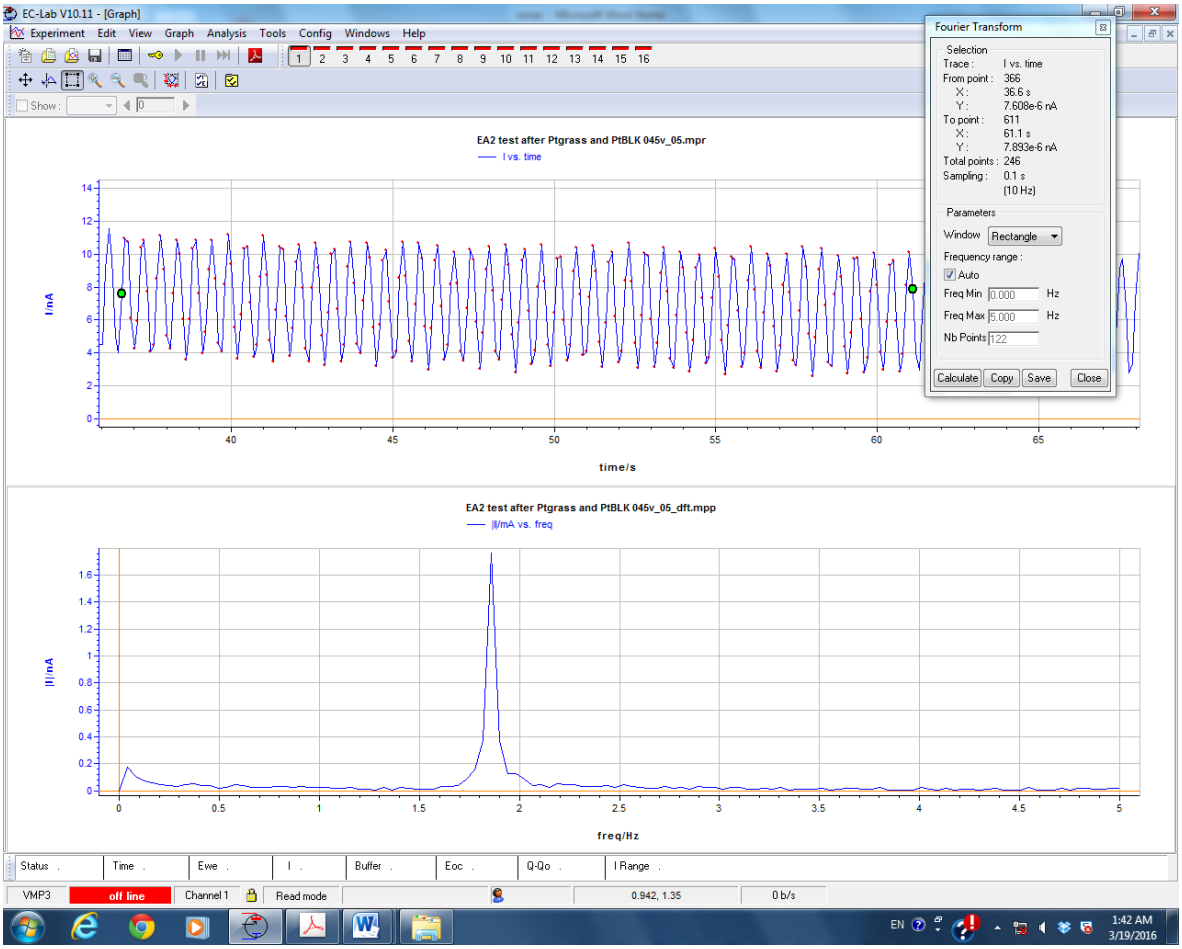

From the lower figure (|I| vs Frequency) we can see there is a peak between 1.6Hz to 2.2Hz. We will apply a filter to the data to eliminate this frequency range.

4. Next step is to do the noise filter.

click ‘Analysis’->’Math’->’Filter’, choose ‘Band Reject’ and fill the blank with ‘1.6’ and ‘2.2’. Use the ‘Black man’ mode.(I have tried the results of all the five mode: ‘Rectangle’, ‘Barlett’, ‘Hann’, ‘Hanming’, ‘Blackman’ and ‘Welch’, it seems the ‘Blackman’ have the least noise and cleanest figure, but the other four modes may be useful in other situations)

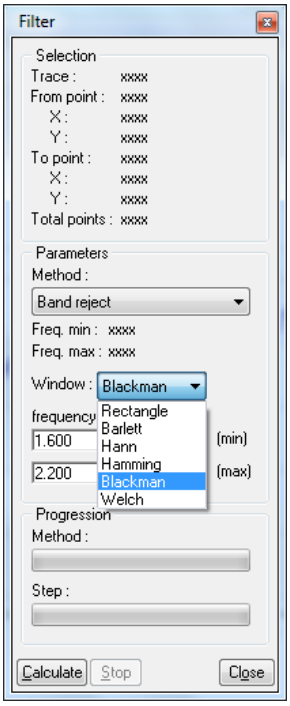

5. Click ‘Calculate’ to perform the filtering process. The result is shown as below.

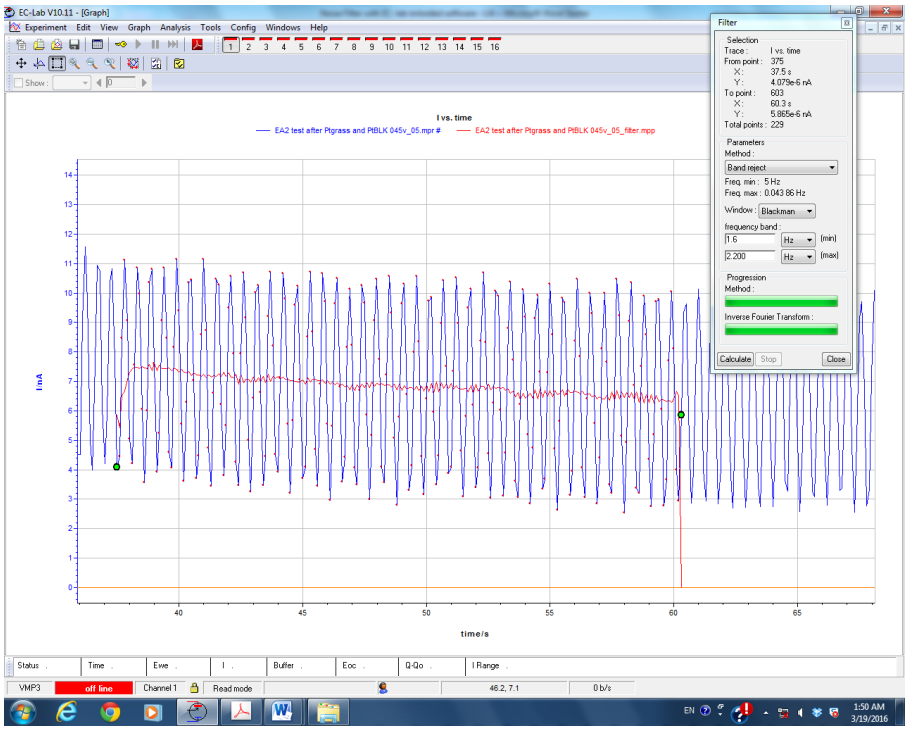

6. We can further apply this method to the whole data range. We get the filtered result (red line) vs original data (blue line) figure shown as below. The filtered data will automaticlly saved in the same folder as the original data.

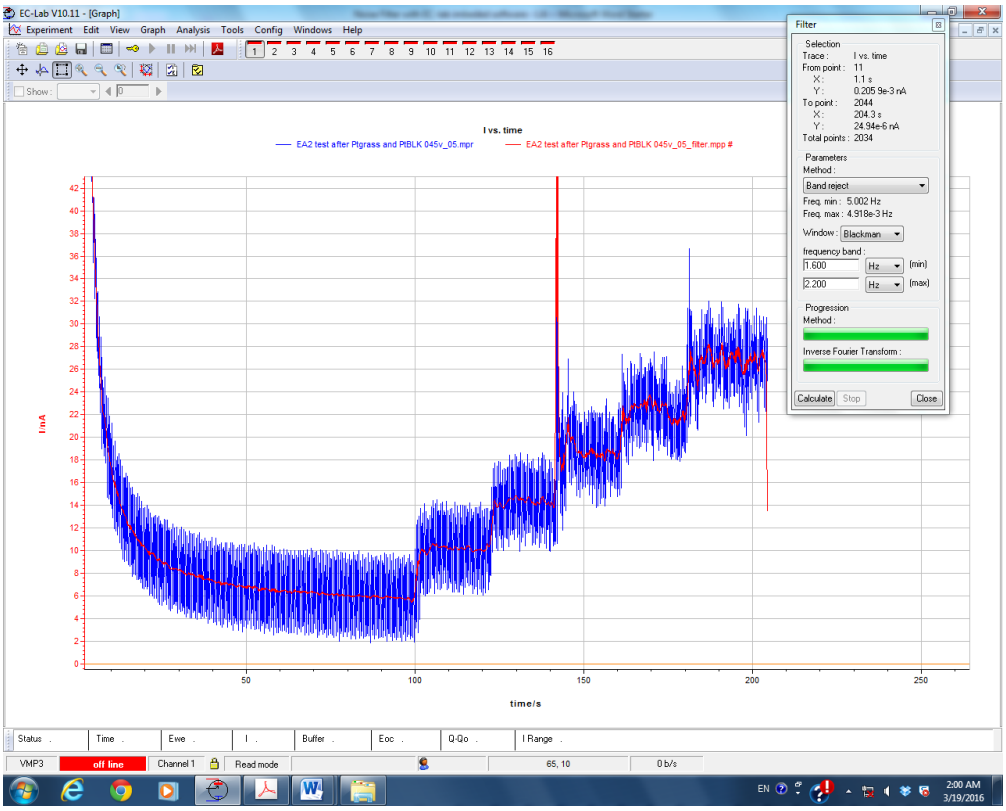

7. After the noise filter, we see a huge improvement of the figure quality and less noise.

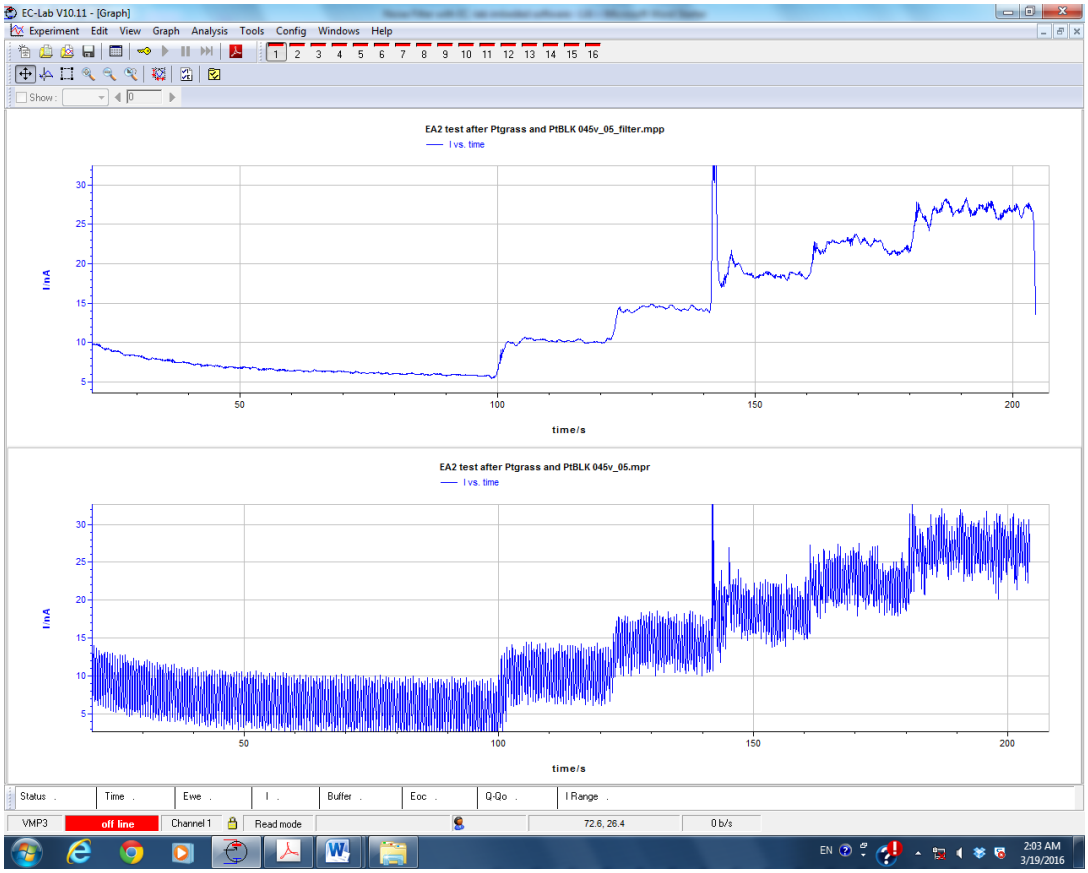

To summarize, two major steps to filter the noise are:

1. Find the frequency band with Fourier Transformation
2. Use band reject to filter the frequency range corresponding to the peak in the frequency band

The red colored sentences above are the detailed steps to do the noise filtering.